THE ROLE OF CD248^{+} STROMAL CELLS IN THE PATHOGENESIS OF RENAL FIBROSIS

By

STUART WILLIAM SMITH

A thesis submitted to the
University of Birmingham
for the degree of
DOCTOR OF PHILOSOPHY

Inflammatory Renal Research Group
School of Immunity and Infection
College of Medical and Dental Sciences
University of Birmingham
November 2011

ABSTRACT

Chronic kidney disease affects 10-13% of the population. The dominant processes that promote kidney disease, irrespective of the trigger, occur in the stromal compartment where fibrosis is considered the hallmark of progressive renal disease. Recent studies have highlighted the importance of the vasculature and the role of the renal pericyte as a progenitor of activated matrix-depositing stromal myofibroblasts, cells that drive the development of renal fibrosis.

CD248 is a 175 KDa type I transmembrane glycoprotein expressed at low levels in non-inflamed kidney by resident renal stromal cells (pericytes and myofibroblasts). In this thesis I demonstrate that CD248 expression is increased in a cohort of patients with progressive renal fibrosis (n=93). Furthermore, increased CD248 expression in the kidney stroma is an independent risk factor for the progression of renal disease. I have then used an established murine model of renal fibrosis (unilateral ureteric obstruction) to characterise the origin, phenotype and function of $CD248^{+}$ cells *in vitro* and *in vivo*. A transgenic mouse, with a targeted disruption to the CD248 gene has been used to assess the causal role that CD248 plays in the pathogenesis of renal fibrosis. Mice deficient in CD248 are protected against myofibroblast accumulation, tissue fibrosis and microvascular rarefaction following renal injury. *In vitro* data suggests that this phenotype may be due to a defect seen exclusively in stromal cell, but not epithelial cell, function as a consequence of the loss of CD248. Taken together these studies suggest that CD248 represents a novel stromal cell specific target for the treatment of chronic kidney disease.

ACKNOWLEDGEMENTS

I would like to thank my supervisors Professor Caroline Savage and Professor Christopher Buckley for their help and support throughout my PhD. Thank you to all the members of the Renal and Rheumatology research groups at the University of Birmingham for their advice and guidance over the last 3 years. Thank you also to Spike Clay, Dr Jeremy Hughes and Dr Tim Johnson who trained me in the animal surgical techniques used in this thesis, and to Professor Clare Isacke who developed the CD248 antibodies used in this work. Finally, I would like to acknowledge the support I have received from the Wellcome Trust who funded this project by providing me with a Clinical Training Fellowship.

CONTENTS

Page number

LIST OF FIGURES

LIST OF TABLES

ABBREVIATIONS

ACR	Albumin creatinine ratio
Ang 1	Angiopoietin 1
Ang 2	Angiopoietin 2
ANOVA	Analysis of variance between groups
αSMA	Alpha smooth muscle actin
BMP-7	Bone morphogenic protein 7
BrdU	Bromodeoxyuridine
BSAO	Bovine serum albumin overload
CKD	Chronic kidney disease
CTGF	Connective tissue growth factor
DC	Dendritic cells
DMEM	Dulbecco's Modified Eagle Medium
DMSO	Dimethyl sulfoxide
ECM	Extracellular matrix
EGF	Epidermal growth factor
eGFR	Estimated glomerular function
EM	Electron microscopy
EMT	Epithelial mesenchymal transformation
EndMT	Endothelial mesenchymal transformation
ESRF	End stage renal failure
FCS	Foetal calf serum
FGF-2	Fibroblast growth factor 2
GEC	Glomerular endothelial cell
GMCSF	Granulocyte macrophage colony stimulating factor
HBSS	Hank's Balanced Salt Solution
HGF	Hepatocyte growth factor
HIF	Hypoxia inducible factor
HSC	Haemopoetic stem cell
HUVEC	Human umbilical vein endothelial cells
ICD	Index of chronic damage
IFNg	Interferon gamma
IL-10	Interlukin 10
IL-13	Interlukin 13
IL-4	Interlukin 4
IL-6	Interlukin 6
IL1β	Interlukin 1 beta
K/DOQI	Kidney disease outcome quality initiative
MCP-1	Monocyte chemotactic protein 1
MEFs	Murine embryonic fibroblasts
MMP	Matrix metalloproteinase
MSC	Mesenchymal stem cell
MTT	3-(4,5-Dimethylthiazol-2-yl)-2,5-diphenyltetrazolium bromide
PAI-1	Plasminogen activator inhibitor 1

PCR	Protein creatinine ratio
PDGF	Platelet derived growth factor
PDGFRβ	Platlet derived growth factor beta receptor
POD	Podocyte
PTEC	Proximal tubular epithelial cell
RCC	Renal cell carcinoma
ROS	Reactive oxygen species
RRT	Renal replacement therapy
SCID	Severe combined immunodeficiency
SDF-1	Stromal cell-derived factor-1
TEC	Tubular epithelial cells
TGFβ	Transforming growth factor beta
Thy1	Thymocyte differentiation antigen 1
Tie 2	Tyrosine kinase with immunoglobulin-like and EGF-like domains 2
TIMP	Tissue inhibitor of metalloproteinases
TNFα	Tumour necrosis factor alpha
tPA	Tissue plasminogen activator
TTG	Tissue transglutaminase
uPA	Urokinase type plasminogen activator
UUO	Unilateral ureteric obstruction
VEGF	Vascular endothelial growth factor
VHL	Von Hippel–Lindau
VSMC	Vascular smooth muscle cell

CHAPTER 1

BACKGROUND AND LITERATURE REVIEW

CHAPTER 1

BACKGROUND AND LITERATURE REVIEW

1.1 Introduction

Globally chronic kidney disease (CKD) affects 1 person in 8 of the population and contributes considerably to premature morbidity and mortality (1). Only a small, yet significant proportion of patients with CKD will progress to end stage renal failure (ESRF) requiring Renal Replacement Therapy (RRT) in the form of dialysis or transplantation. It is becoming increasingly recognised that even relatively mild renal impairment is a significant independent risk factor for cardiovascular disease and stroke (2, 3). Unfortunately current therapeutic options to arrest disease progression in patients with moderate to severe renal disease are limited. This has significant cost implications and the management of renal disease and its associated complications account for nearly 5% of the total National Health Service annual expenditure (4). The dominant processes that promote progressive kidney disease, irrespective of the trigger, occur in the renal stromal compartment where fibrosis is considered the hallmark of progressive disease (5).

This thesis seeks to identify the role of the novel stromal fibroblast and pericyte marker CD248 in renal fibrosis. In this chapter the structure and function of the renal stroma in health and disease is first discussed and then framed within its clinical context. The cellular and non-cellular mediators in the evolution of fibrosis are then described. Finally, the literature detailing our current understanding of CD248 is reviewed.

1.2 Overview of renal anatomy

The mechanisms and processes of the human kidney involved in regulating blood pressure, clearing toxins and secreting a number of hormones are important to health. Humans have 2 kidneys. Each weighs approximately 150 grams and measures 12 cm in length (6). The outer most layer of the kidney is transparent and is referred to as the capsule. Inside the kidney capsule two further layers are recognised. The first of these is referred to as the cortex and the second is known as the medulla. Each kidney has approximately 1 million functional units distributed through its structure known as nephrons. Individual ephrons consist of a glomerulus and a tubule (6). The glomerulus filters toxins and fluid from the blood. The tubules modify the filtrate through reabsorption and secretion to form urine. The renal microvasculature is organised into two sequential capillary beds (see Figure 1.1) thus allowing exquisite balance between glomerular filtration and tubular reabsorption and secretion (7). The stroma of the kidney comprises the extravascular inter-tubular spaces of the renal parenchyma (8).

Figure 1.1

Schematic diagram of a nephron and its vasculature

Nephrons consist of a glomerulus and a tubule. The renal microvasculature is organised into two sequential capillary beds [adapted from (9)].

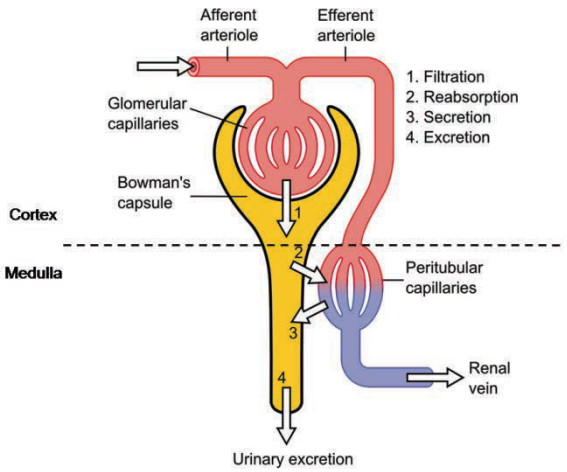

1.3 The renal stroma (interstitium)

The renal stroma, more commonly referred to as the renal interstitium or tubulointerstitial space, makes up 90% of total kidney volume (5). In healthy resting tissue the stroma serves two main roles; the provision of structural support, and the maintenance of homeostasis in the associated parenchyma (10).

The stroma is derived from the embryonic mesoderm (11) and is situated in the space between the basement membrane of the epithelial cells that form the renal tubules and the peri-tubular capillaries. The stromal space contains cells, extracellular fibrillary structures, proteoglycans, glycoproteins and interstitial fluid (8). Stromal fibroblasts within the interstitium provide a framework which helps to maintain the three dimensional architecture of the tissue and also produce homeostatic regulatory substances such as erythropoietin and adenosine (12, 13). The stromal space is also part of the mononuclear phagocytic system with dendritic cells forming a tightly enlaced network with stromal renal fibroblasts. Pericytes are found in the stromal compartment, located between the cortical efferent arterioles and the peri-tubular capillaries, where they are enclosed by a basement membrane (12). Otherwise in the normal healthy renal stroma, aside from the occasional macrophage, other cell types are rarely seen (8, 12, 13).

Fibrosis is the formation of excess amounts of fibrous connective tissue resulting from chronic inflammation of the tissue (5). The extent of tubulointerstitial fibrosis seen at kidney biopsy has been repeatedly demonstrated to be a rigorous, reliable

predictor of renal disease progression (14). The stroma supports the evolution of fibrosis. This occurs directly, by depositing pathological amounts of matrix, destabilising the renal vasculature and secreting pro-fibrotic cytokines, and indirectly by supporting the survival of infiltrating leucocytes. Consequently, a detailed process map of the biological mechanisms of the microenvironment in which inflammation takes place is crucial to help understand the pathogenesis of renal fibrosis.

1.4 Glomerular versus tubulointerstitial injury

The stroma is the stage on which the final act of progressive renal fibrosis is played out, but as highlighted by Schlondorff (7), it is also important to consider the underlying anatomy of the kidney when considering how injury is initiated. The arrangement of the glomerular and peri-tubular vasculature (see section 1.2) and the passage of the glomerular ultrafiltrate downstream to the tubules render the kidney vulnerable, not only to vascular compromise but also to the spreading of inflammation throughout the renal compartment. Glomerular and tubulointerstitial injury are therefore considered interdependent.

Damage to a single glomerulus may lead to peri-tubular inflammation and tubular atrophy that can progress to loss of the whole nephron (15). Secondary localised tubulointerstitial inflammation can equally spread to adjacent tubules and cause further damage and nephron loss. Remaining glomeruli develop capillary hypertension to maintain function, and as a result secondary glomerulosclerosis develops. Damaged glomeruli can also leak pro-inflammatory molecules downstream

to the tubulointerstitium (16). Thus regardless of the originating compartment (glomerular or tubulointerstitial) chronic inflammation develops and progresses to stromal fibrosis through a final common pathway, ultimately producing the single indistinguishable pathological renal phenotype of chronic kidney disease. Histologically this phenotype is characterised macroscopically by small, scarred, shrunken fibrotic kidneys due to the replacement of functioning parenchyma by organised contracted matrix. Microscopically there is glomerulosclerosis, vascular sclerosis and tubulointerstitial fibrosis (5)

1.5 Chronic kidney disease

1.5.1 Epidemiology

CKD, defined as the presence of a marker of kidney damage such as protein or blood in the urine or a reduction in kidney function for 3 or more months (17), is a major public health problem affecting 10-13% of the population (1). In the Western world the major causes of CKD are diabetes mellitus, hypertension and glomerulonephritis (18).

The number of patients with CKD is rising and this is mirrored in the increase in ESRF requiring RRT globally (4). In the UK the annual incidence of ESRF has doubled over the last decade (4). Figures taken from the UK Renal Registry show that in 2008 there were 47,525 adult patients receiving RRT equating to a UK prevalence of 774 per million population, an annual increase in prevalence of 4.4% (19). The UK increase in prevalence, as in other countries, is projected to continue at

a rate of 5-8% per year (20). Quantifying the number of patients with ESRF alone probably underestimates the population burden of CKD as only a small proportion of patients with stage 3 to 4 CKD (see below) progress to RRT (21). Despite this, even the early stages of CKD are associated with an increased risk of developing vascular and cardiovascular disease (22, 23). Consequently preventing or ameliorating CKD and its pathological phenotype of stromal fibrosis is desirable regardless of the underlying mechanism of renal injury or disease stage.

1.5.2 Classification of CKD

In 2002 the Kidney Disease Outcomes Quality Initiative (K/DOQI) published clinical practice guidelines to identify and classify patients with kidney disease (17). These guidelines use a previously described mathematical formula (24) to calculate an estimate of an individual's renal function from plasma creatinine, age, sex and ethnic origin. This is known as the estimated glomerular filtration rate (eGFR). The eGFR is widely used to triage patients into distinct stages of renal disease (Table 1.1)

Table 1.1 Chronic kidney disease staging [Adapted (17)]

Stage	eGFR ml/min/1.73m^2	Description
1	$\geq$ 90	Normal kidney function but with the presence of urine abnormalities or a structural/genetic defect.
2	60-89	Mild renal impairment
3A **3B**	45-59 30-44	Moderate renal impairment
4	15-29	Severely reduced renal function
5	<15 or on dialysis	Very severe approaching or already established on renal replacement therapy

Following the publication of these guidelines there has been increasing interest within the renal community in screening sections of the population to identify and treat patients with CKD who also exhibit additional known clinical determinants of progression to ESRF.

1.5.3 Determinants of disease progression

Multiple predictors of renal progression are now recognised (25). However, combining these factors is likely to be more effective when developing scoring systems to identify patients at high risk of disease progression (1, 21, 26). To simplify discussion, the most common clinically recognised determinants of disease progression are individually discussed below.

1.5.3.1 Proteinuria

In health, negligible amounts of protein are found in the urine as large molecular weight proteins are not filtered through the intact glomerular basement membrane; any low molecular weight proteins that are filtered are reabsorbed by the renal tubules. In disease states these mechanisms are impaired and clinically urinary protein loss can be measured using either the protein creatinine ratio (PCR) or the albumin creatinine ratio (ACR). In adults it is preferable to measure the urinary ACR, as this is a more sensitive marker, than total urine protein loss (PCR), for chronic kidney disease (17). Individuals who have renal disease and an ACR greater than 100 mg/mmol are known to be at significantly higher risk of progressing to ESRF (1). Population based studies have previously demonstrated proteinuria to be a predictor

of future decline in renal function and the development of ESRF (27, 28). In addition to being a determinant of renal progression, proteinuria is also a target for treatment as urinary protein loss drives cytokine release, damage to tubulointerstitial cells and localised fibrosis (29).The blockade of the renin angiotensin system has been demonstrated to reduce proteinuria and improve outcome in multiple clinical cohorts (30).

In our group we have previously demonstrated a close association between albuminuria, urinary cytokines (MCP-1/CCL2), and interstitial macrophage infiltration with i*n situ* renal fibrosis and clinical outcomes (31, 32). These studies also demonstrated that although proteinuria is important in early disease as renal scarring evolves, alternative pathways relating to progressive tissue ischemia secondary to microvascular rarefication (see below) might be more important. The clinical importance of proteinuria is emphasised by the modification of the K/DOQI clinical practice guidelines to include the suffix ‘P’ to denote significant proteinuria (33, 34)

1.5.3.2 Hypertension

Systemic hypertension, which can be both a cause and a consequence of renal disease, leads to intraglomerular hypertension with subsequent hypertrophy and damage. Hypertensive patients when compared to normotensive patients with CKD progress to ESRF faster (35-37).

1.5.3.3 Estimated glomerular filtration rate (eGFR)

A reduction in eGFR is not only a marker of CKD, it is a determinant of renal progression (1, 38) and reflects functioning nephron mass at the time of diagnosis. Tsuboi *et al* have shown in a wide range of glomerulonephropathies that assessing glomerular density in renal biopsy sections, as a proxy measure of functional nephron mass, is a useful tool to help determine disease outcome (39-41). Although eGFR is strongly associated with progressive disease it is now recognised that all levels of reduced eGFR should be complemented by quantification of proteinuria to optimally predict progression to ESRF(1).

1.5.3.4 Histology

To investigate the underlying aetiology of a patient's renal disease, a renal biopsy is often performed. This involves removing a small sample of kidney using a needle under local anaesthetic. Renal biopsy samples can also be used to assess the degree of stromal fibrosis at presentation and this can then be used to predict renal progression. Multiple methodologies exist within the literature for this purpose but broadly two main features are examined either individually or in combination:

1. **Chronic damage**. Bohle *et al* (14) first described the negative correlation between the amount of stromal damage seen in biopsy samples and renal function and prognosis. These observations have subsequently been validated in a diverse range of renal pathologies and also in a number of animal models. Stromal damage can be quantified either using a simple grading system or

more objectively, measured using digital image analysis software. Our group have previously refined this approach and described the Index of Chronic Damage, an established and rigorous morphometric measure that predicts renal outcome (42).

2. **Capillary rarefaction.** Chronic hypoxia plays a role in the evolution of renal fibrosis (43). Progressive CKD is associated with capillary rarefaction and a reduced blood flow within those that remain (32, 44). Studies by our group and others to quantify capillary density have shown a link between a reduction in capillary density and a worse disease outcome (32). This approach is predominantly used as a research tool at present.

1.6 IgA nephropathy as a paradigm of progressive renal fibrosis

This thesis uses the human kidney disease IgA nephropathy as a model of progressive renal injury. Previously thought to be a relatively benign condition, it is now recognised that approximately 30-50% of patients with IgA nephropathy will progress to ESRF requiring RRT after 20 years (45).

First described by Berger in 1968, IgA nephropathy is the most commonly occurring cause of primary glomerulonephritis and is an excellent example of progressive renal disease (46). IgA nephropathy is thought to be caused by the deposition of abnormally glycosylated IgA within the glomerulus leading to mesangial expansion

and loss of glomerular structural integrity (Figure 1.2). Glomerular damage leads to tubulointerstitial inflammation and the loss of functional renal parenchyma.

Figure 1.2

Histological features of IgA nephropathy

(A) A normal glomerulus. **(B)** PAS staining. A glomerulus from a patient with IgA nephropathy showing mesangial expansion. **(C)** Immunofluorescence microscopy. IgA deposition (bright green) can clearly be seen within the diseased glomerulus. [Adapted from (47)]

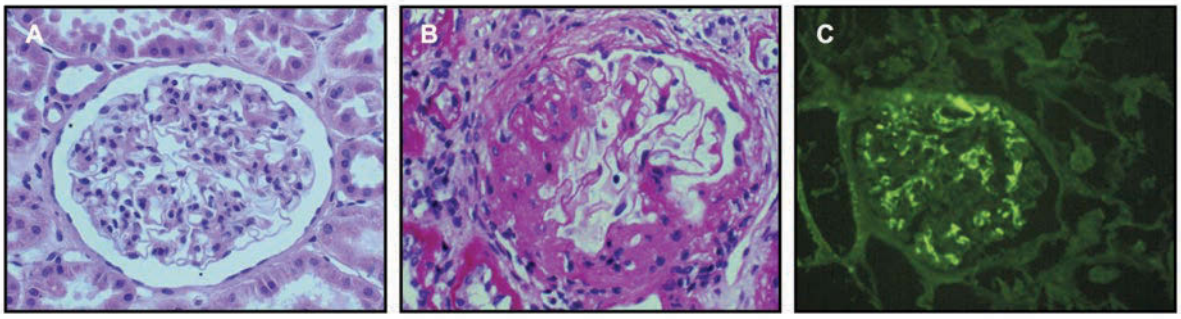

IgA nephropathy is more common in men than women (2:1 ratio) and although the disease can be diagnosed at any age it normally presents between the ages of 20 and 40 (46). There is a strong geographical variation in the prevalence of IgA nephropathy. It is more common in Asia where it is found in approximately 40% of all biopsy specimens collected for the investigation of suspected glomerular disease. Whilst genetic differences may account for this increased prevalence there is also an element of reporting bias (47). There are a number of school screening programs in Asia designed to detect early urine abnormalities suggestive of IgA nephropathy, furthermore the threshold to proceed to renal biopsy is lower in Asia than in the UK.

Regardless of the country of diagnosis, patients are assessed using the clinical and histological predictors of disease progression described above. Thus those patients with poor renal function, elevated blood pressure, persistent proteinuria (ACR >100

mg/mmol) and evidence of tubulointerstitial fibrosis at first renal biopsy are more likely to reach ESRF over time.

1.7 Pathogenesis of progressive renal fibrosis

It is perhaps simplest to consider renal fibrosis as a form of wound healing (48). Renal fibrosis most likely begins as a beneficial response to acute injury. Commonly recognised mechanisms of renal injury are summarised in Table 1.2.

Regardless of the underlying mechanism of injury, the ultimate aim of wound healing is restoration of tissue architecture and function and the renal response to injury resembles that seen elsewhere in the body (49). Following injury, neutrophils infiltrate wounded tissue and epithelial cells proliferate (48). As the healing process evolves, neutrophils are replaced by macrophages and T cells that are supported by resident stromal fibroblasts and dendritic cells (5, 49). Fibroblasts and pericytes proliferate and become myofibroblasts that deposit pathological amounts of matrix and facilitate wound contraction and scar formation (fibrosis) (50, 51). Intriguingly, in the foetus complete tissue regeneration is possible (52). Unfortunately in the post-embryonic state repair involves inflammation (7). In adult tissue, healing is often only partially successful and acute inflammation may evolve into persistent chronic fibrosis associated with the deposition of excessive extracellular matrix (ECM). Consequently the mechanisms of inflammation and fibrosis are interrelated and dysregulation of this process leads to an inappropriate pro-fibrotic response and chronic inflammation (5).

Table 1.2

Mechanisms of renal injury

Cause	Example
Inflammatory process	Infection Primary interstitial nephritis Secondary glomerulonephriitis
Trauma	Vascular Obstruction Radiation
Drugs	Analgesic nephropathy
Metabolic	Diabetes
Hereditary	Polycystic kidney disease Alport's syndrome

[Adapted from (53)]

The discussion that follows describes the main cellular and non-cellular mediators of renal fibrosis. Attention is focused predominantly on the interstitium but it is important to remember that, as discussed above, the glomeruli are also involved in the initiation of renal fibrosis. To simplify discussion, individual mediators are described in isolation and greater emphasis has been placed on the role stromal cells play in this process. Ultimately however, renal fibrosis is a complex interplay between all the factors described.

1.7.1 Cellular mediators

1.7.1.1 Macrophages

The non-inflamed kidney has relatively few tissue macrophages (13). Infiltration of renal tissue by monocyte/macrophages following injury is described in both human disease and animal experimental models (31, 32, 54). In human disease, macrophage infiltration is negatively correlated with renal outcome (31) and fibrosis can be ameliorated in animal models following the systemic depletion of macrophages (55-57). Recruitment of circulating monocytes to the injured kidney is

in response to the upregulation and *de novo* expression of selectins and integrins by endothelial cells of the post-capillary venules, and by chemokine release from the kidney itself. These factors orchestrate rolling, adhesion and transmigration of activated monocytes into the kidney where they are involved in tissue repair; sterilising and debriding injured tissue through the release of cytotoxic substances and phagocytosis (58).

Repetitive injury or chronic inflammation drives aberrant macrophage activation that initiates fibrosis. This occurs through the dysregulated release of reactive oxygen species (ROS) that are directly damaging to tissue and also through the generation of pro-fibrotic cytokines such as TGFβ, FGF and PDGF that promote leukocyte recruitment and ECM deposition by stromal cells (29). Macrophages can also directly remodel renal architecture through the release of metalloproteinases (see below) (59).

In vivo macrophages are a heterogeneous population of cells that can be divided into two polarised activation states (60). The classically activated, also referred to as the M1 macrophage can be induced by exposure to IFNγ, lipopolysaccharide, TNFα or GM-CSF. The M1 macrophages express pro-inflammatory cytokines such as IL-6, IL-1β, TGFβ, PDGF and reactive oxygen species (ROS). Exposure to IL-4 or IL-13 leads to alternatively activated or M2 macrophages, that are thought to promote tissue repair (61). Evidence is mounting that early in the development of injury macrophages adopt an M1 phenotype but at later stages of disease an M2

phenotype predominates. Depletion studies performed in murine models of both liver and kidney fibrosis have demonstrated that macrophage depletion in the context of advanced fibrosis resulted in reduced tissue scarring. In contrast depletion during the recovery phase of injury led to a failure of matrix removal (61, 62).

1.7.1.2 T cells

T cells are rarely found in non-inflamed renal tissue (13) and until relatively recently the idea that T cells play a direct role in the pathogenesis of renal fibrosis has received scant attention. Renal immune-mediated T cell injury is well described within the literature (63). It has long been assumed that T cells generate injury to which fibrosis is the response. An argument supported by early reports suggesting T cells do not directly contribute to the development of renal fibrosis (64). There is now mounting evidence that T cells directly promote renal fibrosis.

Kalluri *et al* used a murine model of Alport's renal disease to demonstrate that T cells are not required for the induction of glomerulonephritis, but they are required for the development of interstitial fibrosis (65). Similarly, Niedermeier *et al* induced renal fibrosis in severe combined immunodeficient (SCID) mice that lack T and B-lymphocytes; demonstrating a substantial reduction in collagen deposition in SCID mice kidneys compared to controls following injury. This phenotype could be replicated in wildtype animals by the administration of an anti-CD4 antibody following disease induction (66).

More recently this approach has been replicated and refined by the adoptive transfer of either $CD8^+$ or $CD4^+$ T cells into $Rag^{-/-}$ mice following injury (67). $CD4^+$ but not $CD8^+$ T cells were found to increase fibrogenesis in this study. The exact mechanism for this effect is unclear, however, three possibilities have been suggested (68):

1. T cells may act directly on resident renal stromal cells to become activated and deposit pathological fibrotic matrix;

2. T cell-macrophage crosstalk might induce an M1 macrophage phenotype that again activates stromal cells; or,

3. Alternatively, T cells may act on tubular epithelial cells to induce the secretion of cytokines and growth factors that subsequently induce indirect stromal cell activation.

1.7.1.3 Dendritic cells

Dendritic cells (DC) are found throughout the renal stroma where they have a role in immune surveillance and antigen presentation (69). Murine proteinuric renal disease models have demonstrated that albumin fragments filtered at the glomerulus can be taken up by proximal tubular cells and presented in draining lymph nodes by renal DCs thus priming $CD8^+$ T cells (70). Furthermore, Heyman *et al* have demonstrated that DCs are intimately involved in the progression of proteinuric renal disease (71, 72); and that DC depletion in a murine model of glomerular injury leads to the rapid resolution of immune cell infiltration and damage. Together these studies provide

further evidence linking the glomerular and tubular compartments in the pathogenesis of renal injury and subsequent fibrosis; and help to explain the clinical observation of the detrimental effect of proteinuria on renal disease progression.

1.7.1.4 Mast cells

An increased number of mast cells is a consistent feature of renal fibrosis, whatever the underlying pathology (73-76); these cells have also been implicated in the pathogenesis of chronic inflammation in non-renal organs (77). Mast cells increase in number in areas of scarring of the renal cortex and have been shown to inversely correlate with renal function (78). Animal studies on the role of mast cells in the development of renal fibrosis have proved inconclusive. Data from models of renal disease, performed in mice deficient in mast cells suggests that fibrosis is worse following injury when compared to control animals (79-81). In contrast other investigators report a protective effect of mast cell deficiency against the development of fibrosis (82). The functional mechanisms by which mast cells mediate fibrosis remain unclear.

1.7.1.5 Renal tubular epithelial cells

Renal tubular epithelial cells (TEC) act as a conduit between the glomerular and interstitial compartments (see section 1.4) and thus play a key role in the pathogenesis of renal fibrosis. TEC can be damaged directly, for example through toxic or ischemic mechanisms (83), and indirectly by glomerular proteinuria or cytokine and ROS release from leucocytes (29, 31). *In vitro* TEC express leucocyte-

directed chemokines and cytokines in response to high concentrations of intermediate weight proteinuria, for example albumin (84). Interventions that decrease proteinuria in human clinical trials (29) are protective and, in animal models of disease, are associated with reduced chemokine expression and inflammation (29). Proteinuria has also been demonstrated to activate complement within the tubular lumen (85). A mechanism that could block some or all of the process outlined above may therefore be protective against fibrosis (86)

TEC injury is reported to lead to cell cycle growth arrest (87), autophagy (88, 89) and apoptosis (90). These processes culminate in tubular atrophy, loss of functional parenchyma and fibrosis. Perhaps more controversially it has been proposed that TEC, through the process of epithelial mesenchymal transformation (EMT), directly contribute to the activated stromal cell populations of the fibrotic kidney (91-93). Evidence for this process in the pathogenesis of renal fibrosis will be discussed in more detail later.

1.7.1.6 **Endothelial cells, the microvasculature and hypoxia.**

Endothelial cell damage and microvascular rarefaction are seen in pathological studies of human renal disease (32, 94) and in numerous animal models (95-97) of renal fibrosis. Cell damage and failure of repair mechanisms compromise renal perfusion and drive tubular atrophy (98). Both acute ischemia and inflammation activate endothelial cells and causes leucostasis, that in turn compromises blood flow (98); injury also induces endothelial cell apoptosis with subsequent failure of capillary

repair (99). Defective angiogenesis seen in animal models of renal fibrosis has been suggested to be due to an imbalance of pro and anti-angiogenic stimuli (100-102). Intuitively the loss of the microvasculature suggests the generation of a hypoxic microenvironment and a 'chronic hypoxia hypothesis' (103) has been suggested as an underlying mechanism of renal fibrosis.

Intra-renal fibrosis itself can exacerbate hypoxia by impairing the efficiency of oxygen diffusion (104). Hypoxia directly recruits inflammatory leucocytes (105), stimulates pro-inflammatory and angiogenic (106) cytokine release from TEC and drives matrix deposition by stromal fibroblasts (107). Destabilisation of the microvasculature in response to injury (51, 95) and endothelial mesenchymal transition (108) has also been considered to potentially play a role in microvascular rarefaction and ECM deposition.

Hypoxia-inducible transcription factors (HIFs) are intricately involved in the kidney's adaptive response to hypoxia (109). HIF is a transcription factor that is degraded under normoxic conditions by von Hippel-Lindau (VHL) disease tumour suppressor protein. In hypoxic tissue HIF escapes degradation and can activate genes with hypoxia response elements in their promoter region (109). HIFs consist of alpha and beta subunits that form heterodimers on activation. Murine models of renal fibrosis have shown that HIFs are upregulated in the kidney in response to chronic injury (110, 111). The ablation of HIF1α in mice has been shown to be protective against

the development of fibrosis (111). In contrast, in the acute setting HIFs have been demonstrated to be protective against ischemic renal injury (112).

1.7.1.7 Stromal fibroblasts

Stromal fibroblasts at renal and non-renal sites are a heterogeneous and functionally diverse cell population (50). Fibroblast heterogeneity was first recognised in the 1960s when Castor *et al* examined the proliferation rates of fibroblasts derived from the dermis, articular cartilage, mesothelial surface and the periostium of bone. Mesothelial surface-derived fibroblasts had a slower proliferation rate and deposited a greater amount of ECM than fibroblasts derived from other sites (113). More recently fibroblasts have been shown to exhibit topographic differentiation, displaying distinct functional identities based on their tissue of origin. Chang *et al* used genome wide mRNA microarray analysis to demonstrate distinct differences in fibroblasts derived from a variety of human tissue sites (114, 115). This positional memory and topographical differentiation persists during *in vit*ro culture. In addition to site-specific differences, fibroblasts are also heterogeneous within individual tissues. In the lung the surface marker Thy-1 has been used to investigate fibroblast subpopulations. Thy-1^+ and Thy-1^- fibroblasts demonstrate morphologically discrete phenotypes (116). Further, Thy-1^+ fibroblasts produced 3-fold more collagen and less fibronectin than Thy-1^- cells (117).

In the kidney resident stromal fibroblast heterogeneity has not been addressed in detail although subpopulations have been reported (108, 118). In normal human

kidney, ‘quiescent’ stromal fibroblasts represent a small population with a low turnover rate (119) that play a homeostatic role maintaining and regulating the deposition and organisation of ECM. Ultrastructurally, renal fibroblasts display a spindle-shaped appearance with elongated, branching processes. Sub-cellularly they have a rough endoplasmic reticulum, a large nuclei and an extensive golgi apparatus (119). Fibroblasts have multiple functions beyond simply maintaining normal tissue architecture. They play an important role in local and systemic adaptive physiology, modulating intrarenal blood flow through their conversion of 5’-AMP to adenosine and also in erythropoiesis through the secretion of erythropoietin(13). Fibroblasts can also secrete prostaglandins and cytokines in a paracrine manner (119). Zeisberg *et al* have also demonstrated that they have endocytic and antigen-presenting capacity (120).

1.7.1.7.1 Activated stromal fibroblasts (myofibroblasts)

The transformation from a quiescent to an activated population of fibroblasts is dependent on a combination of growth factors, cytokines, ECM and environmental stimuli. Aside from the activated form of the fibroblast, known as a myofibroblast, there are no formal nomenclatures or markers to classify fibroblast heterogeneity. The myofibroblast is therefore the prototypical activated stromal fibroblast described within the renal literature.

In contrast to fibroblasts, myofibroblasts are larger, exhibit long processes with bundles of microfilaments which stain positive for alpha smooth muscle actin (αSMA)

(119). αSMA is therefore classically used to define myofibroblasts *in vitro* and *in vivo* (50), although αSMA^{-} fibroblasts are described in the renal literature and are known to contain and express interstitial collagens *in vivo (118)*.

αSMA is a contractile protein that is expressed intracellularly in the cytoplasm of activated fibroblasts and is also found extensively throughout the vasculature (121). Whilst αSMA has been widely used as a myofibroblast marker, the actual functional role of αSMA is less clearly defined. The enhanced expression of αSMA occurs rapidly in response to renal injury. Garin *et al* demonstrated the upregulated expression of αSMA in rat mesangial cells after only 45 minutes of renal ischemia (122). Increased expression of αSMA is also seen in organs other than the kidney in response to injury (49). *In vitro,* αSMA molecules incorporated into actin filaments function to produce the contraction of collagen gels (123) and also limit cell migration and motility by increasing cell adherence to extracellular matrix (124). Intriguingly experimentally-induced tubulointerstitial fibrosis in the αSMA$^{-/-}$ mouse showed that αSMA$^{-/-}$ animals developed more severe fibrosis compared to controls and that fibroblasts isolated from αSMA-null mice produced more type collagen 1 compared to wildtype controls *in vitro* (125). This led the authors to conclude that rather than being pro-fibrotic, αSMA may actually suppress and control myofibroblast activity.

1.7.1.7.2 Origin of activated stromal fibroblasts in the kidney.

The origin of activated stromal renal fibroblasts is both controversial and complex. Recruitment has been proposed to occur either from resident stromal cell populations (peri-tubular fibroblasts and pericytes) or from circulating bone marrow derived precursors (fibrocytes) and through the process of EMT (5). EMT is the process whereby epithelial cells lose their epithelial characteristics and acquire properties typical of mesenchymal cells, thus allowing migration through the extracellular matrix. It is a process normally observed in the developing embryo, and within the matrix of malignant tumours but has also been reported to occur in fibrotic tissue at non-renal sites (e.g lung and liver). More recently endothelial mesenchymal transformation (EndMT) has also been suggested as a source of activated stromal fibroblasts at least in animal models of CKD (108). Iwano *et al* attempted to quantitate the relative importance of the various potential sources of activated fibroblasts. Using bone marrow chimeras and transgenic reporter mice, the authors suggested that resident fibroblasts, EMT and circulating precursors contribute 52%, 38% and 9%, respectively(126). EndMT and pericytes were not looked at in this study.

Multiple stromal markers have been used to try to identify and distinguish between fibroblasts and activated fibroblasts *in vivo* and *in vitro*. Furthermore, these markers whilst imperfect are often also used to try and classify cell origin and fate. The principal fibroblast and activated fibroblast markers described in the literature are summarised in Table 1.3. It should be noted that genetic labelling techniques in mice that permit reliable fate tracing of cell populations *in vivo,* are helping to address many of the problems previously associated with stromal fibroblast markers (127).

The concept that activated stromal fibroblasts are derived from resident renal fibroblasts is intuitive, widely accepted by most authors and long-standing. Other potential sources such as EMT and circulating fibrocytes are contentious and will be discussed here. The evidence that activated stromal cells are derived from resident peri-tubular pericytes will be discussed later (section 1.7.1.10) and framed within our current understanding of the biology of this under recognised cell.

Table 1.3

Renal stromal and activated stromal cell markers

Cell type	Proposed markers	Comment
Resident stromal fibroblasts	CD73, FSP1, CD90, ICAM	Differentiation between medullary and cortical fibroblasts can be made by morphology and position.
Myofibroblasts	αSMA	αSMA is also expressed by the vasculature of the kidney
EMT derived fibroblasts	FSP1	FSP1 is also expressed by some leucocyte populations
Pericytes	αSMA, PDGFRβ, CD73, NG2, Desmin, CD248	Marker expression is highly dependent on developmental stage and activation status.
Fibrocytes	CD34, Collagen I	Represent a small population of cells in most models of renal fibrosis.

[Adapted from (50)]

Fibrocytes, first reported in 1994, are a circulating $CD34^+$ bone marrow-derived, monocyte-like, population of fibroblasts (128). These cells constitute less than 1% of circulating leucocytes and are defined by their co-expression of both leucocyte and of mesenchymal cell markers such as collagen I (129). Fibrocytes are proposed to infiltrate inflamed and fibrotic tissue and become activated stromal cells (130). In kidney fibrosis infiltrating fibrocytes probably represent a small population of cells (126, 127, 130). More recent studies have called the presence of fibrocytes in fibrotic

kidney into question (51, 131). Nevertheless these animal models should be tempered by the observation of fibrocytes in human disease states (132).

For the last 15 years the predominant theory for the origin of activated stromal fibroblast populations, aside from recruitment of resident stromal cells, has been through the process of EMT (50). This concept is well established in the cancer literature. Evidence for EMT occurring in the kidney is based on pioneering work by Strutz and colleagues (133, 134) who first suggested that tubular epithelial cells can de-differentiate to express fibroblast markers in various renal disease states (91, 135-137) raising the possibility that EMT is a potent source for myofibroblasts in CKD.

The fibroblast marker predominately associated with EMT is fibroblast specific protein-1 (FSP-1). Although it should be highlighted that this marker is also expressed on some leucocyte populations (138). Using *in vitro* studies and *in vivo* animal models, TEC are reported to acquire a myofibroblast phenotype and express FSP-1, a process driven by TGFβ (139). In an *ex vivo* study in human IgA nephropathy with preserved kidney function, there was a negative correlation between FSP-1 and renal survival (140). However these observations are confounded by FSP-1 expression on infiltrating leucocytes which by themselves are known determinants of progressive CKD (31). Further, despite the extensive literature on EMT in the kidney as noted by Kriz *et al*, there is no experimental

evidence to demonstrate that *in vivo* tubular derived cells are capable of depositing type I collagen or that they can migrate across the tubular basement membrane (92).

1.7.1.8 Pericytes

Pericytes have been relatively neglected in the renal literature in the last 30 years, with few publications focusing on their structure, function and involvement in renal pathology. More recently, however, there has been an increasing interest in the role that pericytes play in the development of renal disease (51, 95, 127, 141-143). They are emerging not only as a major contributor to the activated, matrix-depositing, stromal cell populations seen in progressive fibrosis, but also, perhaps even more importantly, detachment of renal pericytes from the vasculature may drive the microvasculature rarefaction and subsequent hypoxia associated with CKD (94, 144). Intriguingly, at renal and non-renal sites, the microenvironment in which pericytes reside has been suggested to represent a mesenchymal stem cell niche (145).

First described by Rouget as early as 1873 (146) the pericyte is suggested by some authors to represent the precursor of vascular smooth muscle cells (VSMC) that are seen in larger vessels with which they share some structural and functional similarities (147, 148). However, while VSMC lie largely outside the basement membrane of endothelial cells, pericytes lie in close proximity to the microvasculature (149).

In vivo, pericytes can be recognised by their extensive, branched processes that partially surround the abluminal side of endothelial cells (148, 150). They are

ubiquitously found throughout the microvasculature and are sheathed within a duplication of the underlying vessel basement membrane. Pericyte density is highly variable across vascular beds. Coverage of the abluminal surface of endothelial cells is reported to range between 10-50% (151) and the ratio of pericytes to endothelial cells is 1:1, 1:2.5 and 1:100 for the retina, kidney and skeletal muscle, respectively (143, 151, 152).

Figure 1.3

Pericyte structure

Pericytes (PC) surround the abluminal side of endothelial cells (EC) and are sheathed in capillary basement membrane (CBM). Gaps in the basement membrane permit intercellular crosstalk between pericytes and the underlying endothelial cells through peg and socket processes. [Taken from (141)]

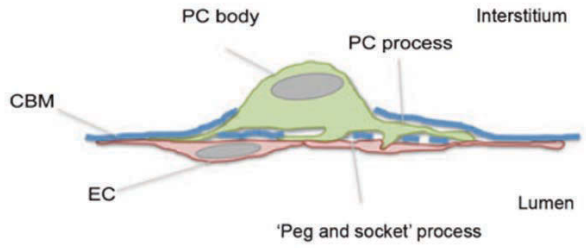

Whilst pericyte processes are always enclosed within the basement membrane, the cell body is often exposed by gaps in the basement membrane thus allowing intercellular crosstalk between pericytes and the underlying endothelial cells (141). Pericyte-endothelial crosstalk is facilitated at these sites through peg-socket contacts (Figure 1.3) (151). These represent membrane invaginations extending either from the pericyte or from the endothelial cell that permit the formation of tight, gap and adherence junctions (151, 153). Through these connections an individual pericyte is capable of linking to multiple endothelial cells, facilitating co-ordination and integration of the underlying endothelium (151).

Renal pericytes were first visualised using transmission electron microscopy (TEM) and described in detail by Courtoy and Boyle in 1983; their initial structural observations suggested a functional role for pericytes in modulating vessel diameter. In the kidney, pericytes are found in the tubulointerstitial space on peri-tubular capillaries and as specialised pericytes within the glomerulus as mesangial cells (141, 143, 154).

1.7.1.8.1 Identifying pericytes *in vivo*

Identifying pericytes *in vivo* is challenging and classical approaches utilising location, morphology and surface markers has presented problems. Pericytes appear morphologically distinct across different organs (150). As noted by Armulik *et al* in the central nervous system, pericytes appear flattened with multiple cytoplasmic processes covering an extensive amount of the endothelial abluminal surface (151). In contrast, pericytes within the glomerulus are compact with minimal abluminal coverage. In view of these problems, TEM has remained one of the best techniques to identify and phenotype pericytes in mature tissues (155). TEM is more difficult during angiogenesis and vascular remodelling as the basement membrane is often not fully developed (156).

While no pan-pericyte markers exist, surface markers for pericytes are recognised although none are entirely specific (Table 1.4). Current markers suffer from limitations as they are dynamically expressed at different developmental stages (51), across species (151), in different organs (150) and in response to the

microenvironment (51, 157). Four of the best described markers used to identify pericytes are: αSMA; desmin; NG2 chondroitin sulphate proteoglycan and PDGFRβ. All of these pericyte markers are temporally and developmentally expressed by pericytes, a phenomenon reported at renal (51, 158) and non-renal sites (151, 159). In the kidney, Lin *et al* have reported that at postnatal day 12, NG2, αSMA and PDGFRβ are expressed by all pericytes, but as the organ matures expression of these markers is lost as pericytes become less active (51).

Consequently, one approach to identifying pericytes *in vivo* is to combine multiple surface markers (160). The development in recent years of transgenic mice (reviewed in detail by Duffield *et al* (127)) has taken this approach a step further. Transgenic animals allow genetic fate tracking and tagging of pericytes thus facilitating not only the *in vivo* localisation of pericytes, but their *ex vivo* isolation (51) and phenotyping. Isolated cells can also be used for *in vitro* co-culture models (161).

Table 1.4

Pericyte markers

Note the overlap between pericyte and fibroblast markers (Table 1.3)

Marker	Comments
CD73	Pericyte and mesenchymal stem cell marker (150). Expression is regulated by tissue hypoxia (162). Expression also seen on erythropoietin producing peritubular fibroblasts of the kidney (150).
CD248 (TEM1, Endosialin)	Recognises pericytes and fibroblasts(163). Temporal expression with high levels in development and low levels in adult tissue (158, 164, 165). Implicated in PDGFRβ mediated pericyte proliferation *in vitro (166, 167)*. Potential therapeutic target.
Alpha smooth muscle actin (αSMA)	Intracellular marker widely described in pericytes(150, 159). Restricted to expression by activated pericytes at sites of vascular remodelling (168). Also expressed by smooth muscle cells and myofibroblasts (50).
Desmin	Intracellular marker expressed on intermediate filament proteins (150). Can be used as an ensheathment marker to estimate vessel stability (169). Expressed on pericytes in direct contact with the underlying endothelium (161, 170). Proposed as an indicator of pericyte ensheathment in underlying basement membrane (168). Expressed by pericytes (mesangial cells) of the glomerulus (171).
NG2 chondroitin sulphate proteoglycan (NG2)	A transmembrane proteoglycan expressed on pericytes but also widely expressed on glial cells of the central nervous system (159). Expressed by nascent pericytes during the early stages of angiogenesis and perists in newly formed blood vessels (168).
Platlet derived growth factor beta receptor (PDGFRβ)	One of the most widely used pericyte markers. Plays a key role in pericyte recruitment, investment and maturation of the microvasculature (150, 161, 170). Cellular expression persists following pericyte-myofibroblast transition (51).

1.7.1.8.2 Pericyte function in vessel development

Pericytes are pivotal to vascular development and remodelling (172, 173). Central to vasculogenesis and angiogenesis is the process of vessel maturation i.e. the transition from a growing vascular bed to a fully formed, stabilised vascular network. A prominent feature of maturation is the investment of pericytes in the vessel wall. Defective maturation is seen in pathological settings including malignancy and fibrosis (168, 174).

Blood vessels are one of the first embryonic organs to develop and they are composed of endothelial cells and mural cells (VSMC or pericytes). During development both of these cell populations are derived from the embryonic mesoderm. The nascent vasculature is formed through the process of vasculogenesis. In the embryo, a rudimentary endothelial tube network is formed from endothelial progenitor cells (172). This network is then branched, pruned and stabilised through the process of angiogenesis and mural pericytes are thereby embedded into the vascular wall (160). Pericytes are important for vessel stability. *Ex vivo* co-culture studies using a 3D gel matrix have demonstrated that the removal of pericytes leads to loss of microvascular integrity (175). *In vivo* pericyte coverage of endothelial cells is essential for maintenance of the blood brain barrier (159). This is an observation mirrored by similar reports across multiple vascular beds emphasising the role pericytes play in stabilising blood vessels (153).

Despite its importance in development, our understanding of the process whereby the vasculature is stabilised is incomplete. Generation of a functioning vascular basement membrane and recruitment and investment of pericytes into the immature vascular network occurs in response to secreted growth factors (160). Numerous growth factors are recognised, but two main signalling systems appear crucial, these being the PDGFRβ/PDGF-BB and the angiopoietin-Tie2 signalling pathways (160). VEGF, a key signalling molecule produced by endothelial cells to stimulate angiogenesis, is involved in both of these pathways.

PDGF-BB is secreted by endothelial cells in response to vascular endothelial growth factor (VEGF) stimulation and is crucial for the recruitment of pericytes to newly formed vessels (176). Studies in mice demonstrate that loss of PDGFRβ, or its ligand PDGF-BB (secreted from endothelial cells), results in defective pericyte recruitment and investment in the microvasculature with subsequent vascular leakage and haemorrhage (176-178). Once pericyte recruitment to the endothelium is achieved, endothelial-pericyte crosstalk and anchoring involves angiopoietin-Tie2 signalling pathways. Angiopoietin (Ang) 1 and 2 both signal through the Tie2 receptor (179) but have different functional roles. Ang 1 is expressed by pericytes and is involved in reducing vessel permeability through strengthening endothelial-pericyte interactions (172). Ang 2 is produced and stored by endothelial cells, antagonises the effects of Ang 1 and is involved in the inflammatory response (150).

1.7.1.8.3 Mesangial pericytes

Pericytes are found within the glomerular and tubulointerstitial compartments of the kidney. There is an extensive literature on the functions and role of glomerular pericytes, more commonly referred to as mesangial cells, in the pathogenesis of renal disease. This is largely due to the relative ease with which these cells can be identified, isolated and cultured *in vitro* from humans and mice using differential sieving techniques. In contrast, tubulointerstitial pericytes are more challenging to isolate. Only relatively recently have transgenic mouse models facilitated their isolation *in vitro*. Here, the two renal pericyte populations will be considered separately.

It was first suggested 20 years ago by Schlondorff that glomerular mesangial cells represented a specialised form of microvascular pericyte (180). Mesangial cells play a central role in stabilising and maintaining the structural architecture of the glomerulus and exhibit many of the features associated with pericytes at non-renal sites described above (150). Mesangial cells differentiate from primitive pericytes during development and have been shown to participate in the subdivision of the capillary network during glomerulogenesis (181). Crosstalk between mesangial cells and the glomerular endothelium is essential to maintain vascular structure, and this again involves PDGF signalling. PDGF-B and PDGFR-β null mice are non-viable and exhibit markedly abnormal glomerular structure with an absence of mesangial cells (182, 183).

In the glomerulus, mesangial cells form a central stalk and constitute approximately 30% of all glomerular cells (180). They express recognised surface markers such as PDGFRβ and CD90. In health, mesangial cells deposit ECM, predominately type IV collagen, laminin and fibronectin, a process that becomes dysregulated in many of the glomerulonephropathies (7, 180). The contractile properties of mesangial cells allow them to fine tune glomerular filtration. They can thus directly sense and respond to changes in capillary stretch which allows modulation of single nephron glomerular filtration rate (184). Mesangial cells are also capable of immune surveillance. Human mesangial cells can acquire a monocyte/macrophage phenotype (185). Also, mesangial cells may represent a glomerular mesenchymal stem cell niche since, like other pericytes, they exhibit pluripotency *in vitro* and can be reprogrammed to form pluripotent stem cells that form teratomas if injected into immuno-deficient mice (186).

1.7.1.8.4 Peri-tubular pericytes

Outside of the glomerular compartment pericytes are found on peri-tubular capillaries of the interstitium (13). Our understanding of the role that pericytes play in the pathogenesis of disease has expanded rapidly in recent years. Reports in the literature dating back 10 years focused on the role pericytes play in regulating medullary blood flow (187). While this remains an active area of research (188), more recently a key role for pericytes in the pathogenesis of CKD has been proposed.

Elegant studies by Lin *et al,* used novel transgenic mouse models that allowed the tracking and phenotyping of renal pericytes in several different murine models of kidney disease (51). Using a mouse that expresses green fluorescent protein (GFP) under regulation of the collagen 1α1 promoter, they demonstrated that pericytes and peri-tubular fibroblasts contributed significantly to interstitial αSMA$^+$ activated stromal fibroblast (myofibroblast) populations in experimental renal fibrosis. Careful tracking and kinetic modelling studies demonstrated that, in response to injury, collagen1α1$^+$ pericytes upregulated classical pericyte markers (PDGFRβ, αSMA), upregulated collagen deposition and detached and migrated away from the underlying endothelium. Later studies by the same group have demonstrated that this process is accompanied by microvascular rarefaction, as loss of pericytes from the vasculature destabilises the vessel and leads to a failure of reparative angiogenesis (95).

One surprising observation from these studies was that despite severe renal injury, epithelial cells did not express collagen transcripts. Therefore they are unlikely to be a source of myofibroblasts, drawing the process of EMT in kidney disease into doubt (51). Additional fate tracking studies were performed by Lin *et al* to support the initial studies. Renal epithelial cells were genetically tagged using Six2-cre and HoxB7-cre drivers. Mesenchymal cells were labelled using the FoxD1-cre driver during embryonic development. Together Six2 and HoxB7 labelled the epithelium and collecting duct epithelium respectively. FoxD1 was expressed by mesenchymal cells and tagged all cells destined to become pericytes. Mice were then backcrossed with appropriate floxed reporter mice strains and the fate of the renal epithelium and pericytes in response to renal injury observed in two different models (51, 143).

FoxD1^{+} cells were found to represent the same population of cells as the collagen1α1 tagged cells reported previously; this population expanded rapidly to form the majority of the αSMA^{+} myofibroblasts seen in response to injury. No tagged epithelial cells were seen to co-express αSMA or the EMT marker FSP-1 within the interstitium in response to injury. *In vitro* Six2 tagged epithelial cells could be induced to express αSMA and FSP-1. They also lost expression of E-cadherin, an epithelial cell marker, in response to stimulation with the pro-fibrotic growth factor TGFβ thus suggesting that EMT may represent an *in vitro* phenomenon (142, 143). These experimental findings were subsequently replicated by two independent groups (88, 89) and have generated much debate within the renal literature.

Targeting endothelial-pericyte crosstalk may prove a valuable tool to treat renal fibrosis. Pericytes are seen to detach from the interstitial capillary within hours of the induction of renal injury (51). As discussed previously pericyte investment in the endothelium is essential for the maintenance of vascular stability. Microvascular rarefaction will itself drive fibrosis by leading to tissue hypoxia (144). Thus pericyte detachment has a double impact for kidney disease. Not only do pericytes become myofibroblasts that deposit matrix leading to fibrosis, but their detachment from the endothelium also exacerbates tissue hypoxia and damage. Stabilising endothelial pericyte crosstalk in CKD may therefore be an effective therapeutic strategy.

1.7.1.9 Stem cells

Haemopoietic (HSC) and mesenchymal (MSC) stem cells have both been implicated in the response to renal injury and repair. Resident pericytes (see above) may represent an MSC niche in solid organs such as the kidney (145). Circulating stem cells are reported to migrate into the kidney in response to damage and are able to transdifferentiate into both glomerular and tubular cell populations (189).

Human studies have reported the presence of Y-chromosome positive TEC in renal female grafts transplanted into male recipients (190, 191). Animal studies have confirmed these observations and suggest recruitment to the kidney of HSCs is under the control of the stromal cell derived factor-1 (SDF-1) /CXCR4 signalling axis (192). Although incompletely understood, blockade of this axis leads to worsening renal fibrosis (193).

MSCs have been shown to attenuate renal fibrosis through immune modulation and these cells can secrete a number of anti-inflammatory factors such as prostaglandin E2 and interlukin10 (IL-10) (194). Infusion of MSCs attenuates renal fibrosis in a rat remnant kidney model of injury (195). Similarly, Ninichuk *et al* demonstrated a reduction in interstitial fibrosis following the infusion of MSCs in a murine model of Alport's disease (196). Perhaps more importantly, this intervention failed to delay the progression of CKD in the studied animals.

1.7.2 Non-cellular mediators

1.7.2.1 Extracellular matrix

The ECM is involved in supporting and fine-tuning the fibrotic response to injury (197). In the kidney as injury evolves, the expanded interstitial space created as a consequence of tubular atrophy is filled with fibrillar matrix. This comprises of predominately collagens type I and III together with fibronectin (198) although type IV collagen, a remnant of basement membrane destruction, is also present.

The ECM is stabilised, through a process of cross-linking by tissue transglutaminases (TTG), making it resistant to degradation by tissue proteases (199). Elevated levels of TTG in human kidney disease have been reported and are found to correlate with the disease severity (200). Mice deficient in TTGs have a reduction in renal fibrosis following injury (201). ECM can directly mediate fibrosis, through the interaction with integrins expressed on fibroblasts (119), whilst fibronectin can act as a scaffold for the deposition of pro-inflammatory cytokines (202). Consequently areas of fibrosis within an inflamed kidney can enter a self-regulating pro-fibrotic cycle. Intriguingly, cleaved ECM fragments have also been suggested to act as chemotractants *in vivo*. Using a murine model of inflammatory lung disease, Weathington *et al* demonstrated that a cleavage product of collagen I can mimic the effect of CXC-chemokine ligand 8 on neutrophils (203).

1.7.2.2 Tissue proteases

Proteases are important modifiers of ECM. They can attenuate renal fibrosis by facilitating matrix degradation, but also can be detrimental through their cleavage of matrix and non-matrix substrates leading to the release of fibrotic growth factors and the induction of EMT (204). Two main families of molecules are described in the literature. The matrix metalloproteinases (MMPs) with their antagonists the tissue inhibitors of matrix metalloproteinases (TIMPs) (205) and the plasminogen-plasmin proteases (206). Dissecting the role proteases play in renal fibrosis is challenging.

The activated protease plasmin is formed by the cleavage of plasminogen by tissue type plasminogen activator (tPA) or urokinase type plasminogen activator (uPA). These activator proteins are antagonised by plasminogen activator inhibitor-1 (PAI-1) (207). Plasmin degrades the matrix proteins fibronectin and laminin and can activate MMPs (207). It has also been suggested to promote the development of activated stromal cells through the destruction of the tubular basement membrane and EMT (208).

Twenty five MMPs are currently recognised (209) and are involved in tissue development and remodelling. Although originally it was thought they only targeted matrix proteins, it has also been shown that they are capable of cleaving cell adhesion molecules such as integrins and growth factors such as TGFβ (210). In contrast, only 4 TIMPS are described; these endogenous tissue enzymes bind and inactivate MMPs. The best characterised MMPs in renal fibrosis are MMP 2 and 9,

proteases capable of degrading collagen IV. Blockade/removal of MMP 2 and 9 has been suggested to be both protective (204, 211) and harmful (212) following renal injury. Similarly mice deficient in TIMP 3 (213) spontaneously develop renal fibrosis but TIMP $1^{-/-}$ mice are not more susceptible to the development of fibrosis than wildtype animals (214).

1.7.2.3 Chemokines

Chemokines are a group of chemotactic cytokines that attract leukocytes in response to inflammation through binding to G protein-coupled receptors (215) and are thought to play a pivotal role in the development of chronic renal injury (216, 217). Chemokines are divided into four families (CCL, CXCL, CX3CL and CL) based on the distribution of cysteine residues within their molecular structure (218). Endothelial cells, podocytes, TEC, fibroblasts and mesangial cells of the kidney are all capable of producing chemokines in response to injury (219), although chemokines are also secreted as part of normal homeostasis.

A switch from the expression of CXCL chemokines such as IL-8, to CCL chemokines such as MCP-1 is thought to accompany the transition from acute to chronic renal inflammation (215, 220). Increased urinary levels of CCL chemokines are associated with progressive CKD and correlate with macrophage infiltration and inversely correlate with renal fibrosis and function in humans (31). Functional blocking studies in animals, targeting CCL chemokines, reduce leucocyte infiltration, proteinuria and tissue damage in response to injury (221, 222).

1.7.2.4 Growth factors

Growth factors, as their name suggests, are capable of stimulating cellular growth, proliferation and differentiation and thus represent a promising treatment target for renal fibrosis (223). Multiple growth factors have been ascribed to play a role in the aetiology of renal scarring. These include: transforming growth factor alpha and beta (TGF-α, TGF-β) (139); bone morphogenic protein 7 (BMP-7) (224); connective tissue growth factor (CTGF) (225); platelet derived growth factor (PDGF) (226); vascular endothelial growth factor (VEGF) (223); fibroblast growth factor 2 (FGF-2) (227) and hepatocyte growth factor (HGF) (228). Here I will focus on three of the best described growth factors implicated in the pathogenesis of renal fibrosis TGFβ, PDGF and VEGF.

1.7.2.4.1 TGFβ

TGFβ is thought to play an essential role in the initiation and progression of fibrosis and was one of the first pro-fibrotic factors described (229). Three isoforms of TGFβ are recognised (β_1, β_2 and β_3), with the majority of the published literature focusing on TGFβ_1 (230). Indeed, polymorphisms in the TGFβ_1 gene have been proposed to predispose to the development of CKD (231). Upregulation of TGFβ is found in animal and human models of CKD (230); and inhibition of TGFβ in animal models of renal fibrosis is protective (232). Consequently TGFβ is an excellent candidate biomarker (233) of kidney fibrosis and a target for treatment. However, the ubiquitous expression of TGFβ and its pivotal immunoregulatory role may preclude long-term blockade in humans.

Latent TGFβ is secreted as a homodimer that binds to ECM and subsequently undergoes significant posttranscriptional regulation (223). Activation occurs through cleavage by tissue proteases or by integrin binding that induces activated TGFβ to bind to cell surface receptors driving phosphorylation of downstream regulators of the Smad pathway (234). Activation of Smads causes their translocation to the nucleus where they function to control gene expression. Smad signalling in the normal kidney is tightly constrained by transcriptional co-repressors, including snoN, Ski and TGIF. Yang *et al* have demonstrated that SnoN and Ski are progressively diminished in fibrotic kidneys raising the possibility that the loss of Smad antagonists serves to amplify the TGF-β response to injury (235).

1.7.2.4.2 VEGF

VEGF is chemotactic for monocytes but primarily functions as an endothelial cell mitogen involved in promoting angiogenesis, vascular stability and permeability (144). The VEGF family includes five members (VEGF-A, -B, -C, -D and placental growth factor (PIGF)) that exist as hetero and homodimers. Each member binds and differentially activates one or more of 4 receptors. To complicate matters further, there are an extensive number of VEGF splice variants.

The VEGF growth factor system is highly complex and our understanding of its involvement in renal disease is limited. VEGF is known to be upregulated in response to hypoxia via the HIF system, a process that occurs rapidly to drive adaptive angiogenesis (144). Human studies have suggested that VEGF is upregulated in

(32), and may protect against renal fibrosis (44). An assertion supported by animal models using VEGF (236) and VEGF receptor antagonists (95). This protective role appears to be mediated through vascular stabilisation and protection against microvascular rarefaction, although a reduction in monocyte recruitment has also been reported (95). In contrast, over expression of VEGF in animal models (237) and treatment with VEGF antagonists (238) in humans can also be detrimental to the kidney.

1.7.2.4.3 PDGF

In contrast to VEGF, our understanding of the PDGF system is further advanced. PDGF is a chemotractant and mitogen for stromal cells, comprising four isoforms (PDGF-A, -B, -C and -D) (239, 240). PDGF-A and –B are secreted as homo or heterodimers and bind to ECM. PDGF-C and –D are secreted only as homodimers. Similarly, PDGF receptors (PDGFR) are dimers composed of α and/or β chains. PDGF-A can bind the α domain only but PDGF-B binds all receptor types. PDGF-C binds PDGFR-$\alpha\alpha$ or -$\alpha\beta$ whilst PDGF–D binds PDGFR$\beta\beta$. Binding to the PDGFR by its cognate ligand leads to phosphorylation of the receptor and activation of tyrosine kinase dependent transcription factors.

In the adult kidney PDGFR –α and β are expressed by mesangial cells of the glomerulus and interstitial pericytes. The importance of the PDGF signalling pathway in renal development and function is evidenced by data from genetically altered mice. Mice deficient in PDGF-A and –B die prenatally. Furthermore, both PDGF-B and

PDGFR–β deficient mice have defective formation of the glomerular mesangium, a phenotype that can be replicated postnatally in young animals using functional blocking antibodies. PDGF, particularly PDGF-B, is also crucial for endothelial cell/pericyte crosstalk and the maturation and stabilisation of blood vessels (176), and is found to be upregulated in a diverse array of animal models and human cohorts of renal disease. PDGFR-β blockade is protective against microvascular rarefaction and fibrosis (95).

1.8 CD248

1.8.1 Identification

CD248 (also known as Endosialin, Tumour endothelial marker-1 (TEM1), CD146L1) belongs to a larger family of proteins that are all implicated in inflammation, tissue remodelling and repair (158). The other family members are discussed individually in the text below. CD248 was first described in the cancer literature almost 20 years ago when it was recognised by a panel of monoclonal antibodies raised against surface antigens on human foetal fibroblasts (241), as being expressed on tumour but not normal tissue.

CD248 was initially named Endosialin reflecting preliminary data suggesting it was expressed exclusively on activated tumour endothelium. Crucially, it was not seen on normal endothelium, thus making it an attractive target for the development of novel anti-angiogenic therapeutics. Further support for the expression of CD248 by activated endothelial cells came a decade after its first identification. St Croix *et al*

used serial expression of gene analysis (SAGE) to identify CD248 as the most highly upregulated gene transcript on the tumour endothelium of colon carcinoma, when compared to adjacent normal endothelium (242). This report was followed by a number of publications describing its expression on endothelial cells in different tumour types (163, 243-247).

Despite these early reports it is now recognised that CD248 is expressed by stromal pericytes and fibroblasts and not by endothelial cells. More recently in humans, CD248 has been shown to be expressed by a population of $CD8^+$ T cells and also a population of vascular leukocytes has been reported (248, 249). The confusion surrounding the cellular expression of CD248 arises due to technical problems in early studies. St Croix *et al* isolated endothelial cells from human malignancies using beads designed to bind to CD146 (242). Although endothelial cells express CD146, it is also expressed by pericytes, epithelial cells, smooth muscle cells and myofibroblasts (250). Early localisation of CD248, in tissue sections from human malignancies used *in situ* hybridisation (17) and immunohistochemistry (242) but did not employ dual labelling techniques. This made the discrimination between pericytes and the underlying endothelium impossible (163).

In addition to the technical limitations described above, it should also be noted that CD248 cannot be detected, either at the mRNA or protein level, on endothelial cells *in vitro* and attempts to induce expression using pro-angiogenic factors have proved unsuccessful (163). In contrast, stromal fibroblast lines *in vitro* express high levels of

CD248. Doubling labelling confocal microscopy has also confirmed expression of CD248 by pericytes and fibroblasts but not by endothelial cells *in vivo* (157).

1.8.2 Structure of CD248

CD248 is a type 1 transmembrane glycoprotein that is highly conserved between mice and humans (251, 252). In humans, CD248 is coded for by an intronless gene located on chromosome 11. The gene has an open reading frame of 2274bp and encodes a protein 757 amino acids long with a predicted molecular mass of 80.9 KDa. In mice CD248 is coded for on chromosome 19 with an open reading frame of 2295bp encoding 765 amino acids with a predicted molecular mass of 92 (251).

Structurally CD248 (Figure 1.4) is formed from an N-terminal C-type lectin like domain, a complement control (sushi) domain, 3 epidermal growth factor (EGF)-like repeats, a mucin like region, a short transmembrane segment and a short cytoplasmic tail. The core protein is highly sialyted with O-linked oligosaccharides (241). Opavsky *et al* have identified 3 potential phosphorylation sites in the cytoplasmic tail that could participate in signal transduction (251).

Figure 1.4

CD248 family members

CD248, CD141, CD93 and Clec14A belong to a family of proteins that are all implicated in inflammation, tissue remodelling and repair. They exhibit shared homology in their extracellular globular domains, but with each molecule having a different number of EGF modules. The Ser/Thr/Pro-rich mucin-like region also varies greatly between the molecules [Adapted from (253)].

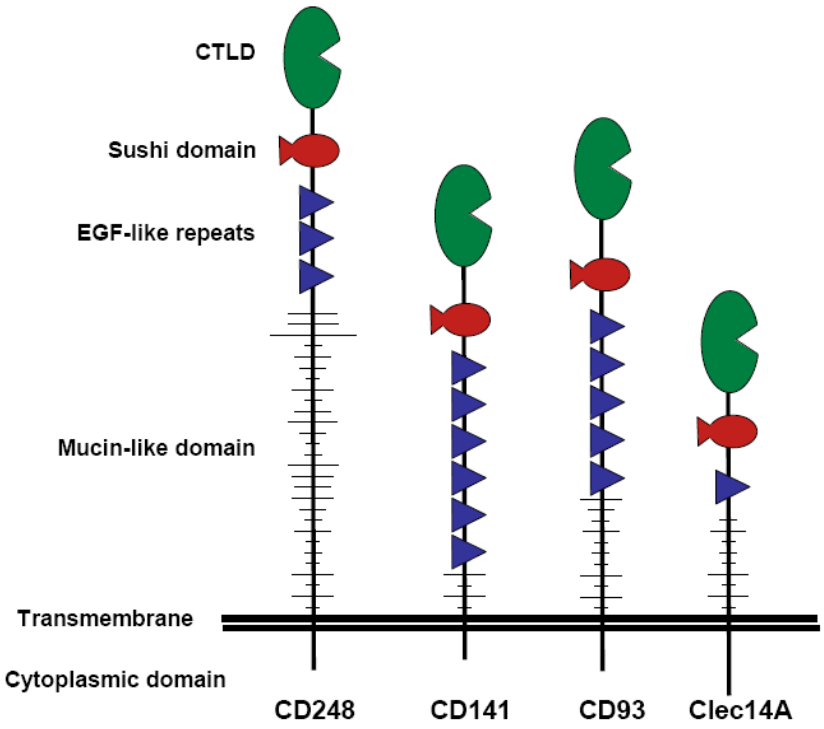

1.8.3 CD248 family members

Proteins that contain a C-type lectin-like domain can be divided into 14 family groups based on sequence and analysis of domain organisation (254). In this classification the CD248 family of proteins represents group 14. In addition to CD248 group 14 includes the proteins thrombomodulin (CD141), CD93 (complement 1q receptor protein (C1qRp)), and C-type lectin domain family member 14A (Clec14A). The globular domains of these 4 proteins is highly conserved in mice and humans, although the overall amino acid sequence varies widely between individual family

members (253). All members appear to have a functional role in cell adhesion and the regulation of inflammation and cancer.

CD141 is a well characterised natural anticoagulant (255) expressed throughout the vasculature on the endothelium. CD141$^{-/-}$ mice develop spontaneous, fatal thrombotic events in both the arterial and venous system (256). Beyond its role as a natural anticoagulant, CD141 also mediates neutrophil adhesion to the endothelium in response to exogenously administered endotoxin (257). Further through its ability to sequester thrombin, CD141 can modulate inflammation (258). A gene duplication of CD141 has been proposed to give rise to CD93. Both genes are expressed on chromosome 20 in humans and exhibit a high degree of sequence homology (259, 260).

CD93 is expressed by myeloid and endothelial cells, particularly during embryogenesis and has also been reported to be expressed by mesenchymal stem cells (261-263). It is recognised to participate in a number of innate immune defence mechanisms through its interaction with C1q, a subcomponent of complement factor C1, including phagocytosis, cytokine modulation and generation of superoxide release by neutrophils (255).

CLEC14A is an endothelial cell marker implicated in tumour angiogenesis (264). It is also thought to mediate cell-cell adhesion through its C-type lectin domain (265). Mura *et al* have demonstrated that CLEC14A is functionally important in vascular

development in zebrafish and, by using *in vitro* assays, showed that it facilitates endothelial cell migration and tube formation. CLEC14A expression is also linked to low shear stress suggesting expression occurs in response to the disorganisation of the vascular network that is often described within tumour stroma (264).

1.8.4 Renal expression of CD248

At basal levels in the adult human and mouse kidney, CD248 is expressed on mesangial cells in the glomerulus. In human renal cell carcinoma (RCC) expression is significantly increased and large rafts of $CD248^{+}$ fibroblasts can be seen within the interstitium (266). Apart from these observations, little else is known about the expression and function of CD248 in renal disease.

1.8.5 Regulation of stromal CD248 expression *in vitro*

Opavsky *et al* have demonstrated that *in vitro,* CD248 expression is cell density dependent and suggested that gene expression occurs in response to peri-cellular hypoxia (251). This suggestion is supported by studies performed by Ohradnova *et al* who identified a HIF2α response element in the promoter region of CD248 (267). Furthermore, HIF2α appears to be able to both directly activate CD248 through binding to the promoter region, and indirectly activate it through interactions with the hypoxia dependent transcription factors SP1 and ETs-1.

1.8.6 Ligands and downstream signalling pathways for CD248

Our understanding of the ligands for CD248 and downstream signalling pathways is incomplete. *In vitro* studies have shown that the endothelial basement membrane proteins fibronectin, collagen type I and collagen type IV can act as specific ligands for CD248 (268). Cells transfected with CD248 exhibit enhanced adhesion to fibronectin and enhanced migration through matrigel. This effect is blocked with humanised antibodies directed against CD248. In addition, Becker *et al* have shown that a C-terminal fragment of the CD248 extracellular domain binds the galectin binding protein Mac-2BP/90K (269). As well as binding to galectin 3, Mac-2 BP/90K also binds to ECM components including collagens V and VI through the same C-terminal fragment. *In vivo* analysis of Mac-2 BP/90K and CD248 expression in malignant tumours and *in vitro* studies suggest that CD248 and Mac-2 BP/90K may mediate cellular positioning signals that act to separate the epithelial and mesenchymal compartments of malignant tumours.

The downstream signalling pathways of CD248 are linked to PDGF signalling (166, 167). Tomkowicz *et al* have demonstrated that CD248 regulates pericyte proliferation *in vitro* through effects on PDGF receptor signalling. Knock down of CD248 using siRNA, reduced PDGF-BB mediated proliferation. This effect was found to be mediated through phosphorylation of the MAP kinase ERK-1/2 and the subsequent downstream expression of the transcription factor c-fos. In these studies no difference in PDGFR-β surface expression following CD248 knockdown was detected.

1.8.7 CD248 transgenic mice

Transgenic mice in which CD248 is deleted have been generated in order to understand its function and expression *in vivo*. Huang *et al* created a CD248 knock in animal in which the normal CD248 gene was disrupted and replaced with a lacZ reporter to detect CD248 in the developing and adult mouse (270). CD248 was first detectable in the heart, the umbilical vessels and the vasculature at E9.5; and from E10.5 to E14.5 CD248 was seen in the whisker follicles, the eye and the lung. In the kidney, CD248 expression was observed in the glomerulus and primitive interstitium from E16.5. Post-natally CD248 expression decreased in most solid organs. High levels of expression persisted in the renal glomerulus and in the uterus, where expression pattern varied according to the oestrous cycle. These murine observations of the basal expression of CD248 parallel earlier studies using archived normal human tissue samples (242, 245).

Two different approaches to generating $CD248^{-/-}$ mice have been reported by independent investigators. Nanda *et al* developed a transgenic animal where CD248 was constitutively removed by targeted homologous recombination (271). These animals develop normally and have normal postnatal growth. An alternative approach to the generation of CD248 transgenic mice was reported by Maia *et al (272, 273)*. In addition to generating animals where the CD248 gene is floxed to allow backcrossing to cre reporter strains, they also generated mice with CD248 lacking the short cytoplasmic domain ($CD248^{CyD/CyD}$). Again these animals develop normally. The results of experimental models using these animals are discussed below.

1.8.8 CD248 expression *in vivo*

In vivo murine models have demonstrated that CD248 is anatomically and temporally regulated with high levels of expression found in the embryo and newborn tissue, and low levels in normal adult tissues (158). In humans and mice, CD248 expression is upregulated on fibroblasts and pericytes found in inflammatory and cancer stroma suggesting a role in tissue remodelling and repair (157, 274).

Carcinomas from a diverse range of malignancies have been reported to express CD248 on the tumour vasculature including breast, colon, stomach, pancreas, liver and lung (241). A number of authors have studied the link between CD248 expression in malignant tumours and clinicopathological outcome measures in humans (246, 275-277). Models in $CD248^{-/-}$ mice have shown that if tumours are implanted in the abdominal cavity, there is impaired tumour growth, invasion and metastasis, highlighting a critical role for CD248 in determining tumour behaviour (271). Furthermore, there was a significant increase in the number of smaller, immature vessels (<50 μm diameter) in tumours from $CD248^{-/-}$ mice compared to those from wildtype animals. Studies using $CD248^{CyD/CyD}$ mice have highlighted the importance of the cytoplasmic domain of CD248 in mediating tumour growth (273). In contrast, no defects were seen when wound healing assays were performed in the skin of $CD248^{-/-}$mice (271).

CD248 is also implicated in lymphoid tissue remodelling in response to inflammation and in the pathogenesis of inflammatory arthritis. Lax *et al* used a salmonella-

induced model of splenic enlargement to explore the expression of CD248 during the initiation and resolution of inflammation (165). CD248 defined a discreet subpopulation of stromal cells within the tissue. CD248 was maximally expressed at the peak of splenic enlargement and expression was downregulated as injury resolved. Similarly, CD248 expression is required for efficient lymph node expansion in response to immunisation (164), via effects on cell proliferation and migration, but not differentiation *in vivo* and *in vitro*.

In inflammatory arthritis CD248 is expressed in synovial fibroblasts isolated from patients with rheumatoid arthritis (163, 272). Maia *et al* demonstrated using a murine model of arthritis, that CD248 contributes to synovial hyperplasia, fibrosis and leucocyte accumulation in inflammatory arthritis and, as such, CD248 may represent a target for the treatment of arthritis.

1.8.9 Origin of CD248$^+$ cells in inflammatory stroma

The origin of CD248$^+$ cells in inflammatory stroma remains poorly defined. Intuitively they may arise from local resident stromal cells. However CD248 has been found on a subset of vascular leucocytes that are able to integrate into, and form blood vessels *in vivo (278)*. Similarly, Bagley *et al* have reported an endothelial progenitor cell population that expresses CD248 (279); and it is also highly expressed by MSCs isolated from bone marrow (266, 280). Our group has also reported that CD248 is expressed on a small population of naive CD8$^+$ human T cells and regulates proliferation (281). These observations, however, may not be so surprising when

framed in the context of the tissue pericytes potentially representing a MSC niche (145).

1.8.10 CD248 as a therapeutic target

CD248 is an attractive therapeutic target. Expression is low in healthy tissue but upregulated in diseased tissue at times of remodelling. It is expressed at the cell surface and can therefore be targeted by circulating neutralizing or activating antibodies. Rettig *et al* has previously demonstrated that monoclonal antibodies to CD248 are bound and internalised by surface receptors (241). Similarly, Rouleau *et al* have conjugated saporin to anti-CD248 antibodies and inhibited cell growth in vitro (282). Indeed, a monoclonal anti-human CD248 antibody (MORAb-004) (268) is currently undergoing phase 1 clinical trials for the treatment of solid tumours (ClinicalTrials.gov identifier: NCT008470544).

1.9 Summary

Drawing all of the ideas described above together, it is apparent that CD248 is involved in stromal and vascular remodelling, key processes implicated in the pathogenesis of renal fibrosis and CKD. CD248 is expressed on resident renal pericytes; a cell population that is emerging as a key mediator of microvascular rarefaction and as a source of myofibroblast progenitors. Our understanding of the distribution and function of CD248 in the human kidney in health and disease is incomplete. Therefore the aim of this thesis was to examine the role of CD248 in the pathogenesis of renal fibrosis.

1.10 Thesis hypothesis

CD248 expressed on renal stromal cells is involved in the pathogenesis of renal fibrosis

Aims

1. To characterise the expression of CD248 in human kidney disease. Can CD248 be used to predict renal outcome?

2. To examine the cellular origin and function of CD248 in murine models of renal fibrosis? Does the constitutive removal of CD248 exacerbate/ameliorate the development of renal injury?

CHAPTER 2

MATERIALS AND METHODS

CHAPTER 2

MATERIALS AND METHODS

2.1 Methods for Chapter 3: Human studies

Unless otherwise stated all reagents used in this thesis are purchased form Sigma Aldrich, Poole, UK.

2.1.1 Antibodies

The primary, secondary and isotype control antibodies used for the human studies are detailed in Tables 2.1, 2.2 and 2.3.

Table 2.1 Isotype controls

Isotype	Supplier	Working dilution
Mouse IgG_1	Dako	Appropriate to primary antibody
Mouse IgG_{2a}	Dako	Appropriate to primary antibody
Polyclonal rabbit	R&D Systems	Appropriate to primary antibody

Table 2.2 Primary antibodies

Specificity	Isotype	Clone	Supplier	Working dilution
CD31	mouse IgG_1	JC70A	Dako	1:20
CD45	polyclonal rabbit	polyclonal	Abcam	1:150
CD248	mouse IgG_1	B1/35	In house	IHC 1:600 WB 1:6000
αSMA	mouse IgG_{2a}	1A4	Sigma	1:50
βactin	polyclonal rabbit	polyclonal	Sigma	1:5000
Cytokeratin	mouse IgG_1	MNF116	Dako	1:50
Desmin	mouse IgG_1	D33	Dako	1:50
Vimentin	mouse IgG_1	V9	Dako	1:50

Table 2.3 Secondary antibodies

Specificity	Conjugate	Host	Supplier	Working dilution
Anti-mouse IgG_1	Alexa488	goat	Invitrogen	1:1000
Anti-mouse IgG_{2a}	Alexa555	goat	Invitrogen	1:1000
Anti-rabbit IgG	HRP	goat	Amersham	1:10000
Anti-mouse IgG	HRP	goat	Amersham	1:10000

2.1.2 Human cell lines

Following NRES ethical approval (REC approval number 08/H1203/8) and under the regulations described within the Human Tissue Act 2004, human renal fibroblasts were isolated from the normal pole of nephrectomy samples removed for the treatment of malignant disease as described below. Conditionally Immortalised human glomerular endothelial cells (GEC) and podocytes were a kind gift from Dr Simon Satchell (University of Bristol, UK). Human Umbilical Vein Endothelial Cells (HUVEC) were a gift from Mrs Sahithi Panchagnula and were isolated from human umbilical cords (REC approval number 05/Q2708/30) obtained from the Birmingham Women's Hospital, UK.

2.1.3 Isolation of human renal fibroblasts

Human renal fibroblasts were isolated from fresh nephrectomy tissue using the method of Grimwood (283). Six-well plates were coated with 2ml of 1% gelatin solution and incubated for 30 minutes at 37^{o}C. Residual gelatin was aspirated and the plates gently washed twice with phosphate-buffered saline (PBS). Nephrectomy tissue was collected from the Pathology Department of the Queen Elizabeth hospital (QEH) and transported to the laboratory in ice cold Dulbecco's Modified Eagle's Medium (DMEM). Tissue was washed in ice cold PBS to remove any residual blood and the renal cortex was dissected away from the medulla under sterile conditions. The cortex was then minced using two scalpel blades. The minced tissue was transferred into the gelatin coated 6-well plate. Approximately 0.5-1 mm^3 of tissue was added to each well. The tissue was adhered to the plate by making 'cross-wise'

scratches into the surface of the plate with a scalpel blade. Enough complete fibroblast medium was then added to cover the tissue. Samples were incubated overnight at 37^{o}C with 95% oxygen and 5% CO_2. The next day cultures were supplemented with an additional 2ml of complete fibroblast medium. Explants were incubated for 72 hours to allow for the initial outgrowth of cells from the tissue. A full medium change was then performed. Medium was changed twice weekly until cultures reached confluence. Once confluence was reached cultures were passaged into a T25 flask.

2.1.4 Cell culture

Cells were grown at 37 ^{o}C in an atmosphere of 5% carbon dioxide. The media recipes used to culture individual cell lines are detailed in Table 2.4. Cells used for the *in vitro* studies described were all between passages 2 to 8 with the exception of the immortalized cell lines that were used until passage 40.

2.1.5 Passaging

Cells were passaged when confluence was reached. Cells were passaged by washing in 2.5ml of 0.02% EDTA (Ethylenediaminetetraacetic Acid Disodium Salt), followed by the addition of 2.5ml of 1x Trypsin/EDTA for 1-2 minutes at 37 ^{o}C. Firmly tapping the flask dislodged the cells from the surface. The trypsin was neutralised with 5mls of complete medium and cells were centrifuged at 300 g for 6 minutes at room temperature. After discarding the supernatant the pellet was re-suspended in 1 ml fresh medium and cells counted in a haemocytometer. Cells were reseeded in

T75 culture flasks at a dilution of 1:3, or into chamber slides at 10,000 cells per well. The cells were incubated at 37 ^{o}C until confluence was achieved.

Table 2.4 Media recipes for human cell line

Cell type	Ingredient	Volume	Final concentration	Source
Renal fibroblasts	Dulbecco's modified eagles medium (DMEM)	395mls	-	Sigma
	Fetal calf serum (FCS)	100mls	20%	Lonza
	Gluatmine,penicillin, streptomycin (GPS) solution	5mls	1.75mM 87U/ml 87μg/ml	Sigma
HUVEC	Medium 199	100ml	-	Gibco
	Hydrocortisone	10μl	1μg/ml	Sigma
	Penicillin and streptomycin	1ml	1mM	Sigma
	Endothelial growth factor (EGF)	10μl	1ng/ml	Sigma
	L-Glutamine	1ml	20mM	Sigma
	Amphotericin	1ml	2.5μg/ml	Sigma
	FCS	20ml	20%	Sigma
GEC	Endothelial growth medium	500ml	Endothelial growth medium kit (EBM-2)	Lonza
	Human fibroblast growth factor β (hFGF-β)	2ml		
	Gentamicin sulphate, Amphotericin-B	500μl		
	FCS	25ml		
	Insulin like growth factor-1	500μl		
	Hydrocortisone	200μl		
	Vascular endothelial growth factor (VEGF)	500μl		
	EGF	500μl		
Podocytes	Roswell park memorial institute (RPMI) 1640 medium	100ml	-	Sigma
	FCS	10ml	10%	Sigma
	Penicillin and streptomycin	1ml	1mM	Sigma
	L-Glutamine	1ml	20mM	Sigma
	ITS solution	1ml	10μg/ml Insulin 5.5μg/ml Transferrin 5ng/ml Sodium selenite	Sigma

2.1.6 Freezing of cell cultures for long term storage

Trypsin and EDTA were used to remove the cells from the flasks as described above. The cells were pelleted at 300 g for 6 minutes at room temperature to form a pellet that was then re-suspended in FCS with 10% Dimethyl sulfoxide (DMSO).

2.1.7 Characterisation of human renal fibroblasts

Cells were characterised using phase contrast microscopy to assess morphology and confocal microscopy to look for the expression of recognised cell markers. To assess morphology cells were seeded into 6 well plates (Corning) at 10,000 cells per well and were allowed to grow to confluence at 37^{o}C. Medium was removed, and each well washed 3 times with PBS to remove any detached cells or debris. Cells were then covered with medium. Phase contrast images were captured using an IX71 inverted microscope (Olympus).

For confocal microscopy cells were seeded in 8 well glass chamber slides (BD Falcon) at 10,000 cells per well and were allowed to grow to confluence at 37^{o}C. Medium was removed, and each well washed three times using 200µl PBS. The plastic well chambers were separated from the glass slide leaving adherent cell cultures. Fixation was achieved by adding 100µl of ice-cold methanol to each culture on the slide for 10 minutes at -20^{o}C. The slides were then washed by immersion in PBS for 10 minutes with gentle agitation. The primary antibody was then added in 50µl of PBS + 2% BSA and 1% FCS, and incubated overnight at 4^{o}C. Slides were again washed in PBS and the secondary antibody was then added in PBS,

containing 2% BSA and 1% FCS, for 1 hour at room temperature before being washed in PBS and mounted in SlowFade (Invitrogen). Slides were visualised using a Zeiss confocal LSM 510 microscope (Zeiss, Germany) and processed using Zeiss LSM Image Examiner software (Zeiss).

2.1.8 Reverse transcription polymerase chain reaction

Cells were grown to confluence in 6 well plates. A Qiagen RNeasy Mini Kit (Qiagen, Valencia, CA) was used to isolate RNA according to the manufacturer's protocol. cDNA was generated using a TaqMan® Reverse Transcription (Applied Biosysystems). PCR was performed using the primers shown in Table 2.5-2.8 (Alta Bioscience). A total of 10μl of sample and 2μl of 6x loading buffer were run at 100 volts on a 2% agarose gel containing ethidium bromide.

Table 2.5 Reverse transcription mix

Ingredient	Volume	Concentration
10x RT buffer	1μl	1x
25mM Magnesium chloride	2.2 μl	5.5mM
dNTPs (10mM each)	2 μl	500μM
Random hexamers	0.5 μl	2.5μM
RNAase inhibitor	0.2 μl	0.4U/μl
RNA	1μl	1μg
Multiscribe reverse transcriptase	0.625μl	3.125U/μl
RNAase free water	2.475μl	-
Total volume	10μl	

Table 2.6 Reverse transcription program cycle

Stage	Temperature	Time
1	25 ^{o}C	10 minutes
2	37 ^{o}C	60 minutes
3	48^{o}C	30 minutes
4	95^{o}C	5 minutes
	Hold at 10^{o}C	

Table 2.7 CD248 and TBP PCR primers

Target	Sequence
CD248 forward	TTTGGCTTCGAGGGCGCCTG
CD248reverse	TCACACTGCTGCTCGCACGG
TBP forward	AACTTCGCTTCCGCTGGCCC
TBP Reverse	GCTGTGGTGCCTGGCCTGAG

Table 2.8 PCR mix and program cycle

Ingredient	Volume	Concentration
10x buffer	5μl	1x
dNTP	5μl	2mM
cDNA	1μl	1μg
Taq	1.5 μl	7.5U
Forward primer	1μl	3.125mM
Reverse primer	1μl	3.125mM
RNAase free water	36.5μl	-
Total volume	50μl	-

Stage	Temperature	Time
Initial denaturation	95 ^{o}C	3 minutes
Denaturation	95 ^{o}C	30 seconds
Annealing	61^{o}C	30 seconds
Extension	72^{o}C	1 minute
Final extension	72^{o}C	10 minutes
	Hold at 10^{o}C	

50 cycles

2.1.9 Western blotting

Recipes for the solutions and gels prepared for Western blotting are detailed in Tables 2.9 and 2.10.

Table 2.9 Solutions for Western blotting

Solution	Ingredient	Quantity	Source
10% Ammonium persulphate (APS)	Ammonium persulphate	100mg	Sigma
	Distilled water	1ml	Sigma
10x Tris buffered saline (pH to 7.6 with pure HCL)	Tris HCL	24.2g	Sigma
	Sodum chloride	80g	Sigma
	Distilled water	Make up to 1litre	Sigma
Tris buffered saline-tween 20	10x Tris buffered saline	100ml	Sigma
	Tween 20	1ml	Sigma
	Distilled water	Make up to 1litre	Sigma
Transfer buffer	Glycine	2.93g	VWR
	Tris-base	8.51g	Sigma
	Sodium dodecyl sulfate	0.375g	Sigma
	Methanol	200ml	VWR
	Distilled water	Make up to 1litre	Sigma
Running buffer	Glycine	14.2g	VWR
	Tris-base	3g	Sigma
	Sodium dodecyl sulfate	100mg	Sigma
	Distilled water	Make up to 1litre	Sigma
6x loading buffer	1 M Tris-HCL	3.5ml	Sigma
	Sodium dodecyl sulfate	1.28g	Sigma
	75% glycerol	4.8ml	Sigma
	β-mercaptoethanol	0.5ml	Sigma
	Bromophenol blue	100mg	Sigma
	Distilled water	Make up to 10ml	Sigma
1.5 M Tris HCL (pH to 8.8 with pure NaOH)	Tris HCL	236.64g	Sigma
	Distilled water	Make up to 1litre	Sigma
0.5 M Tris HCL (pH to 6.8 with pure NaOH)	Tris HCL	78.78g	Sigma
	Distilled water	Make up to 1litre	Sigma
Coomassie stain	Methanol	400ml	VWR
	Distilled water	500ml	Sigma
	Acetic acid	100ml	Sigma
	Brilliant blue dye	1 g	Sigma
Destain	Distilled water	500ml	Sigma
	Methanol	400ml	Sigma
	Acetic acid	100ml	Sigma

Table 2.10 Non-denaturing gels

Ingredient	Resolving (10%)	Stacking (10%)
Protogel Acrylamide/Bis-acrylamide (30:1) (Geneflow, UK)	3.33ml	1.3ml
TrisHCl pH8.8	2.5 ml	-
Tris HCL pH6.8	-	2.5 ml
10% APS	100μl	100μl
Tetramethylethylenediamine	10μl	10μl
Distilled water	4 ml	6.2ml
Final volume	10 ml	10 ml

Cells were lysed in CellLyticMT sample buffer. Protein content was quantified using the method of Bradford (284) using a commercial kit (BioRad). Equivalent amounts of protein were run on a 10% w/v non-denaturing SDS-PAGE gel. Gels were wet transferred onto polyvinylidenedifluoride (PVDF) membrane for 90 minutes at 80 volts, blocked with 5% BSA in tris-buffered saline containing Tween 20 (TBS-T) and incubated with the primary antibodies at 4^{o}C overnight followed by horseradish peroxidase-conjugated secondary for 1 hour at room temperature (Amersham, Buckinghamshire, UK). Immunodetection was carried out using the ECL Kit (Amersham, Buckinghamshire, UK) according to the manufacturers protocol followed by exposure to X-ray film for 15 minutes.

2.1.10 Patient samples

Following local ethical approval (NRES 07/Q2602/42) I identified patients who underwent a percutaneous renal biopsy at the University Hospital Birmingham NHS Foundation Trust for the investigation of renal disease between June 1998 and November 2009. A prevalent cohort of 93 patients with a histological diagnosis of IgA nephropathy, who also had archived formal saline fixed paraffin tissue, was used for the study. Clinical and demographic data was collected from patient records. Normal

tissue sections were derived from nephrectomy samples taken during the course of routine clinical care for malignant disease and were also purchased commercially (Abcam).

2.1.11 Immunohistochemistry

Immunohistochemistry was performed on 4μm tissue sections cut onto glass slides from paraffin blocks. Sections were dewaxed in xylene and re-hydrated through a series of graded alcohols to water. Antigen retrieval was performed using Dako Target Antigen Retrieval solution in a waterbath at 95^{o}C for 30 minutes. Sections were stained according to the Dako Envision-HRP kit protocol. Primary antibody was applied overnight at 4^{o}C. An isotype control was substituted for primary antibody on serial sections. Sections were either counterstained with Mayer's haematoxylin or left unstained for quantitative analysis. To allow confocal microscopy the same technique was followed but fluorescently labelled secondary antibodies were substituted for the Envision kit. Similarly, DAPI (Invitrogen) was substituted for Mayer's haematoxylin. Slides were visualised using a Zeiss confocal LSM 510 microscope.

2.1.12 Digital image analysis

An interactive image analysis system was used for blinded assessment of interstitial CD248^{+} fibroblast numbers. Our group has previously found this to be a reliable method for the analysis of renal tissue sections (31, 32). The sections were blinded to the operator and stained for CD248. They were visualised at a magnification of x200. Images were captured using a Nikon Eclipse E400 microscope with a digital

imaging system controlled by NIS Elements software version 3.0 (Nikon). Images were stored as TIFF files and imported into Aequitas IA image analysis software (DynamicData Links) where the digitalised image was converted to a two-colour scale image. Using the threshold function the image was processed so that positive staining was represented by yellow pixels measured as a percentage of the area of total image analysed. Sections with excessive background staining that made it impossible to digitally differentiate specific staining were excluded from analysis. For each patient the mean measurement of interstitial CD248 staining of 5 randomly selected non-confluent microscopic fields was determined. Blood vessel and glomerular staining was identified by the operator and excluded from the analysis using the computer software.

2.1.13 Quantification of chronic damage

The extent of chronic tissue damage within each biopsy specimen was assessed using the index of chronic damage (ICD), an established and rigorous predictor of renal outcome previously developed by our group (42). For each biopsy, one section was stained by periodic acid-methenamine silver and was examined by a consultant histopathologist (Professor AJ Howie, UCL, London, UK).

2.1.14 Statistical analysis

Linear regression analyses were performed to determine correlations between normally distributed data variables. Variables determined to not follow a Gaussian distribution by normality testing for skewness were normalised by transformation prior

to analysis. Correlations are presented by expressing the Beta correlation coefficient along with the P-value. Linear regression multivariate analysis of these correlations with a dependent variable was also performed. Renal outcome was assessed by Kaplan-Meier survival analysis with log rank testing and multivariate Cox regression analysis after categorisation of tubulointerstitial CD248, urinary ACR and the index of chronic damage into tertiles. All statistical tests were performed using SPSS v17 (IBM) and graphs were prepared using Prism 4 (GraphPad, USA). The level of significance was set at $p<0.05$.

2.2 Methods for Chapter 4 and 5: Murine studies

2.2.1 Antibodies used for murine studies

The primary, secondary and isotype control antibodies used for the murine studies described are detailed in Tables 2.11, 2.12 and 2.13.

Table 2.11 Isotype controls

Isotype	Format	Source
Rat IgG_{2a}	ebioscience	Appropriate to primary antibody
Rat IgG_{2b}	ebioscience	Appropriate to primary antibody
Mouse IgG_{2a}	Dako	Appropriate to primary antibody
Polyclonal rabbit	R&D Systems	Appropriate to primary antibody

Table 2.12 Anti-mouse primary antibodies

Specificity	Isotype	clone	Supplier	Working dilution
CD248	polyclonal rabbit	polyclonal	In house	WB 1:3000 IHC 1:100
Bovine serum albumin	polyclonal rabbit	polyclonal	Invitrogen	1:1000
αSMA	mouse IgG_{2a}	1A4	Sigma	1:50
CD31	hamster IgG	2H8	Serotec	1:100
E-cadherin	rat IgG_1	-	Abcam	1:100
CD3	polyclonal rabbit	polyclonal	Abcam	1:100
F4/80	rat IgG_{2b}	A3-1	Serotec	1:100
Gp38 (podoplanin)	Syrian hamster IgG	ebio8.1.1	ebioscience	1:100
Synaptopodin	mouse IgG_1	G1D4	Progen	neat
GAPDH	polyclonal rabbit	polyclonal	Abcam	1:2500
BrdU	mouse IgG_1	B44	BD Biosciences	1:100
CD45	rat IgG_{2b}	30-F11	ebioscience	1:100
PDGFRβ	rat IgG_{2a}	APB5	ebioscience	1:100

Table 2.13 Anti-mouse secondary antibodies

Specificity	Conjugate	Host	Supplier	Working dilution
Anti-mouse IgG_1	Alexa 488	goat	Invitrogen	1:100
Anti-mouse IgG_{2a}	Alexa555	goat	Invitrogen	1:100
Anti-hamster IgG	Cy3	goat	Jackson	1:100
Anti-rat IgG	Cy5	goat	Jackson	1:100
Anti-rat IgG	Alexa 488	goat	Invitrogen	1:200

2.2.2 Mice

129SvEv mice were purchased from a commercial breeder and used to establish a colony (Taconic, Denmark). Mice were maintained in 12 hour light/12 hour dark cycle with free access to food and water. All procedures were performed in accordance with UK Home Office guidelines. Generation of CD248$^{-/-}$ mice by targeted homologous recombination, was performed by Professor David Huso's group (John Hopkins University, USA)(271). These animals were backcrossed onto a 129SvEV background by Professor Clare Isacke (Breakthrough Breast Cancer, London, UK). This strain of mice was chosen due to its availability and susceptibility to develop renal disease following injury. Adult (>8 weeks old) male mice were used for all experiments. As control, age and sex matched animals were used. Unless otherwise stated all *in vivo* studies had six mice in each experimental group.

2.2.3 Genotyping of CD248$^{-/-}$ mice

Genomic DNA was isolated from ear clippings of newborn mice. DNA was extracted using a DNAeasy Tissue Kit (Qiagen) as per the manufacturer's instructions. Mice were genotyped using primers (table 2.14) designed to distinguish WT and CD248$^{-/-}$ genotype as previously described (271). The mix and programme used for PCR is detailed in Table 2.15. Samples were run on either a 0.5%, or a 1% agarose gel containing ethidium bromide at 130 volts and visualised under UV light. The presence of the wild type CD248 gene was denoted by a 1507bp fragment and the recombinant, disrupted CD248 gene by a 3000bp fragment; heterozygous animals displayed both bands (3000bp and 1507bp) (Figure 2.1).

Figure 2.1

Genotyping of wildtype (WT) and CD248$^{-/-}$ mice (KO).

The presence of the wild type CD248 gene was denoted by a 1507bp fragment (a) and the recombinant, CD248 disrupted gene by a 3000bp fragment (b).

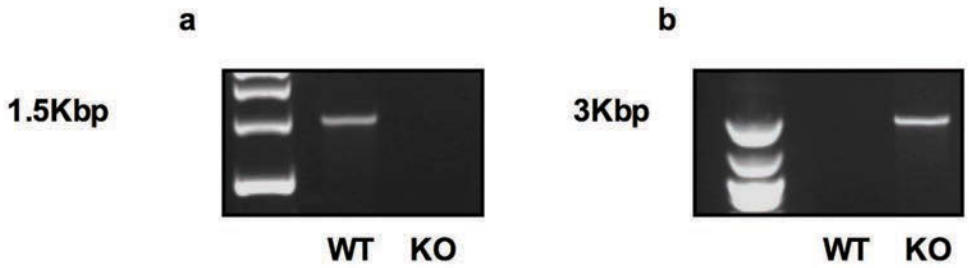

Table 2.14 **CD248 and TBP PCR primers**

Target	Sequence
CD248$^{-/-}$ forward	5'- CTTGTGTAGCGCCAAGTGCC-3'
CD248$^{-/-}$ reverse	5'-GCTGGGAAGGATCTGGCAGG-3'
Wildtype forward	5'- CCTGGTTTCCAGCGAGTTCG-3'
Wildtype reverse	5'- GCCTGCAAGACCTGACTCTG -3'

Table 2.15 **PCR mix and program cycle**

Ingredient	Volume
Reddy Mix PCR Master Mix (1.1X) (Thermo scientific)	25µl
Forward Primer (10pmoles/µl)	2µl
Reverse Primer (10pmoles/µl)	2µl
RNAase free water	16µl
DNA	5µl
Total for 1 reaction	50µl

Wildtype program 30 cycles

Stage	Temperature	Time	
Initial denaturation	95 ^{o}C	2 minutes	
Denaturation	95 ^{o}C	30 seconds	} 30 cycles
Annealing	61.3^{o}C	30 seconds	
Extension	72^{o}C	160 seconds	
Final extension	72^{o}C	5 minutes	
	Hold at 4^{o}C		

CD248$^{-/-}$ program- 30 cycles

Stage	Temperature	Time	
Initial denaturation	95 ^{o}C	2 minutes	
Denaturation	95 ^{o}C	30 seconds	} 30 cycles
Annealing	62.4^{o}C	30 seconds	
Extension	72^{o}C	300 seconds	
Final extension	72^{o}C	10 minutes	
	Hold at 4^{o}C		

2.2.4 Tissue collection

Animals were first weighed and then culled by cervical dislocation and rapidly perfused post-mortem with PBS. Both the kidneys were then removed and weighed. Samples were either fixed in 10% formal saline for histology or snap frozen in liquid nitrogen.

2.2.5 Renal function

Baseline urinary protein loss was determined in wildtype and CD248$^{-/-}$ mice by placing them in metabolic cages for 24 hours with free access to food and water (n=10). Urinary albumin and creatinine was measured using an AlbuwellM (Exocell) and creatinine companion kit (Exocell) respectively as per the manufacturer's instructions. The ACR was then calculated. Blood was obtained by cardiac puncture, allowed to clot for 1 hour at 4^{o}C then centrifuged at 10 000 rpm for 10 minutes, plasma was removed, transferred to a sterile 1.5 ml eppendorf and snap frozen in liquid nitrogen. Samples were then and sent to MRC Harwell (Oxford, UK) on dry ice for biochemical analysis.

2.2.6 Histology

The Queen Elizabeth Hospital Birmingham Pathology Department prepared paraffin tissue blocks from tissue fixed in 10% formal saline. Tissue sections (4μm) were cut onto glass slides. The pathology department then stained the sections, using haematoxylin and eosin, periodic acid silver or Masson's trichrome. Slides were

visualised on a Nikon Eclipse E400 microscope with a digital imaging system controlled by NIS Elements Version 3.0 (Nikon). Slides prepared from the same paraffin blocks were also used for immunoenzyme histochemistry as described above in section 2.1.11.

2.2.7 Confocal microscopy

Frozen sections (4μm) were prepared using a cryostat from kidney tissue snap frozen in liquid nitrogen. Sections were fixed by immersion in acetone for 20 minutes at 4^{o}C. Following fixation sections were allowed to air dry at room temperature for 1 hour and then stored at -20^{o}C or were used immediately. Tissue sections were stained as described in section 2.1.11 (human immunocytochemistry)

2.2.8 *In vitro* functional analysis of cells from wildtype and CD248$^{-/-}$ mice

2.2.8.1 Embryonic fibroblasts

Mouse embryonic fibroblasts (MEF) were isolated from E14 and E15 embryos from wildtype and CD248$^{-/-}$ mice (a gift from Dr Debbie Hardie). Internal organs including the liver, heart, lungs, digestive tract, kidneys, thymus and lymph nodes were removed from decapitated bodies. The body shell was mashed in 1 ml of PBS, vortexed and 1ml of 1:1 10x Trypsin (5%) /EDTA (2%) (Sigma) in PBS and incubated at 37^{o}C for 30 minutes. Digestion was stopped by the addition of 3.5ml RPMI containing 10% FCS. The cell suspension was centrifuged at 300 g for 5 minutes, re-

suspended in 10mls of complete MEF media (Table 2.16) and placed into T25 flasks and cultured at 37^{o}C in 5% CO_2.

2.2.8.2 Isolation of murine renal cell populations

Renal cell populations were isolated from murine kidney using the Dynabead method of Takemoto *et al* (285) with adaptations. These 4.5 μm magnetic beads physically lodge in the glomerular blood vessels, the kidney can then be digested and the tubular and glomerular fractions separated using a magnet.

Animals were culled by cervical dislocation and a midline laparotomy was performed to visualise the abdominal aorta. The vessel was ligated above and below the renal vessels using surgical microclips (Harvard Apparatus, Kent, UK) (Figure 2.2).

Figure 2.2

Renal perfusion with magnetic beads

Renal cell populations were isolated from murine kidney. The vessel was ligated above and below the renal vessels. Magnetic beads inactivated in BSA were infused via a 30 gauge aortic cannula.

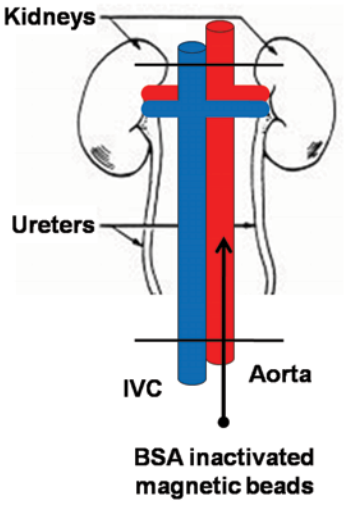

A 30-gauge cannula (Harvard apparatus, Kent, UK), was inserted and $4x10^5$ of 4.5 μm beads (Invitrogen M450, Dynal Biotech, UK) that had previously been blocked in 10% BSA overnight, were infused using a syringe pump at a rate of 1ml/minute. The kidneys were then harvested, minced using two scalpels in a laminar flow cell culture hood and digested with 1 mg/ml collagenase A and 100 U/ml deoxyribonuclease I (Roche) diluted in Hanks buffered saline solution (HBSS) and incubated for 30 minutes at 37°C. The digest was then passed through a 100μm sieve twice and washed with 10mls of HBSS. The cells were pelleted at 200g for 5 minutes at 4°C. The pellet was re-suspended in 10mls HBSS. The glomeruli were then separated from the tubules using a 15 ml falcon magnetic separator (Invitrogen). The glomerular and tubular fractions were plated in media selective for either glomerular mesangial pericytes, tubulointerstitial fibroblasts or proximal tubular epithelial (see Table 2.16).

2.2.8.3 Murine primary cell culture

Cells were cultured, passaged, stored and characterised as described in section 2.1.4 - 2.1.6. The media recipes used to culture primary murine cell lines are detailed in table 2.16.

2.2.8.4 Wound healing assay

Cells were seeded at 3 $x10^5$ cells per well into 6 well plates and cultured to confluence. Using a sterile 200 ml pipette tip a straight scratch was made in the

confluent cell monolayer. Phase contrast images were captured from the plate using an Olympus IX71 inverted microscope at 0, 6, 12 and 24 hours following monolayer injury. The microscope stage was marked using tape so that the plate could be returned to the same position every time an image was acquired. Image analysis was performed using NIH ImageJ. Images were imported into ImageJ, the leading edge of the both sides of the wound was marked and measured and expressed as a percentage of the wound area at time 0.

2.2.8.5 Proliferation

Cell proliferation was assessed using an MTT (3- [4,5-dimethlythiazol-2-yl]-2,5 diphenyltetrazo-lium bromide) based assay. Following 6 days incubation under treatment or control conditions the cell media was harvested and the cells incubated with a solution of MTT (20 μl of 5 mg/ml MTT in 100 μl un-supplemented media) and incubated at 37 ^{o}C for 4 hours. Viable cells reduce the MTT compound to a blue formazan product. There is a linear relationship between the number of cells and the amount of formazan product produced. MTT solution was poured off at the end of the incubation and after drying the cells were incubated with DMSO at 37 ^{o}C to dissolve the formazan crystals. The amount of product produced was then measured by a spectrophometer at 540nm.

Table 2.16

Media recipes for murine primary cell lines

Cell type	Ingredient	Volume	Final concentration	Source
Mesangial cells	Roswell park memorial institute (RPMI) 1640 medium	385ml	-	Gibco
	FCS	100ml	20%	Sigma
	Gluatmine,penicillin, streptomycin (GPS) solution	5ml	1.75mM 87U/ml 87μg/ml	Sigma
	HEPES	5ml	15mM	Sigma
	Sodium Pyruvate	5ml	1mM	Sigma
Renal fibroblasts	Dulbecco's modified eagles medium/F12 (DMEM/F12)	445ml	-	Gibco
	FCS	50ml	10%	Sigma
	Gluatmine,penicillin, streptomycin (GPS) solution	5mls	1.75mM 87U/ml 87μg/ml	Sigma
Proximal tubular epithelial cells (PTEC)	DMEM/F12	395ml	-	Gibco
	FCS	2.5ml	0.5%	Sigma
	Gluatmine,penicillin, streptomycin (GPS) solution	5ml	1.75mM 87U/ml 87μg/ml	Sigma
	ITS solution	5ml	10μg/ml Insulin 5.5μg/ml Transferrin 5ng/ml Sodium selenite	Sigma
	Endothelial growth factor (EGF)	50μl	1ng/ml	Sigma
	Tri-idothyramie	1μl	5pg/ml	Sigma
	Dexamethasone	1μl	5μg/ml	Sigma
	Amphotericin	1ml	2.5μg/ml	Sigma
Mouse Embryonic Fibroblast (MEF)	Dulbecco's modified eagles medium/F12 (DMEM/F12)	395 ml	-	Gibco
	FCS	100ml	20%	Sigma
	Gluatmine,penicillin, streptomycin (GPS) solution	5mls	1.75mM 87U/ml 87μg/ml	Sigma

2.2.8.6 Collagen deposition

A Picosirus red dye-binding assay originally described by Heng *et al* (286) was used for measuring collagen accumulation *in vitro*. Following a 6-day treatment period media was removed and the cell layers were washed in PBS. The cell layers were then fixed in Bouin's solution for 1 hour at room temperature. The solution was then removed and plates washed in running tap water and air dried overnight. Sirius red dye solution (1 mg/ml in picric acid) was added to each well for 1 hour and placed under mild shaking. The dye solution was then removed and each well washed with 0.01 N of hydrochloric acid to remove unbound dye. The bound dye in each well was eluted with 1 ml of 0.01N sodium hydroxide under mild shaking for 30 minutes. Optical density was then measured at 550nm using 0.1 N as a blank. Wells without cells treated identically were used as a background control.

2.2.8.7 Crystal violet

Crystal violet dye binding assay was used to determine the relative DNA content of each well. Cells were fixed in either 2% paraformalydehyde or Bouins solution (Sigma Aldrich, Poole, UK). Cell were rinsed with phosphate buffered saline and 0.1% crystal violet dye solution was added to each well and placed under mild shaking for 30 minutes at room temperature. The unbound dye was removed by rinsing under running water. The plates were air-dried and bound dye eluted with 1% triton X-100. The elution was collected and absorbance at 550nm was determined using triton X-100 as a blank. Data were recorded as total absorbance units per well

and culture wells without cells were used as background control. This assay was used to normalise the collagen deposition assay relative to total cell number.

2.2.8.8 Stimulation with growth factors

Cells were seeded at 50,000 cells per well in a 96-well plate in either differentiation media or normal growth media for 6 days. The media was changed every 2 days. Culture media was supplemented with either PDGF-BB at 100ng/ml or TGF-β_1 at 10 ng/ml and proliferation was compared to control conditions (un-supplemented media). Initial growth factor concentrations were decided on from the literature and through pilot studies using embryonic fibroblasts.

2.2.9 Small animal models of renal fibrosis

Two small animal models of renal disease previously described within the literature were piloted in Birmingham. A successful application was made to the United Kingdom Home Office for the award of a project licence and a personal licence under the Animals Scientific Procedure Act 1986 (Holder Stuart Smith PPL 40/3352, PIL 40/9528). All experiments were performed at the Biomedical Services Unit (BMSU) at the University of Birmingham, UK.

2.2.9.1 Protein overload model

A bovine serum albumin nephrotoxicty model developed by Eddy *et al* (287) was used to induce renal fibrosis (Figure 2.3). Animals received injections of low

endotoxin BSA (Sigma Aldrich, Poole, UK, A-9430) five times a week for a total of 6 weeks. The BSA was dissolved in saline (0.33 mg/mL) and injected into the peritoneal cavity. The final dose of 10 mg BSA/g body weight was reached by incremental increases in the dose over the first week, beginning with 2mg/g body weight. All control animals received intra-peritoneal injections of an equal volume of saline on an identical schedule. Prior to sacrifice and tissue collection animals were placed in metabolic cages for 24 hours as described in section 2.2.5 to allow assessment of urinary protein loss.

2.2.9.2 Unilateral Ureteric Obstruction

Renal fibrosis was modelled using the established model of unilateral ureteric obstruction (UUO). Kidneys were harvested at days 3, 7 and 14 after UUO (Figure 2.4). Using inhalational anaesthesia (4% Isofluorane, 2% oxygen) mice underwent a midline laparotomy; the left ureter was identified and ligated with an atraumatic micro-haemoclip (Weck) (Figure 2.5). Sham operated control mice underwent an identical procedure except the left ureter was mobilised but not ligated. Animals received a single subcutaneous dose of opiate based analgesia (Temgesic) at a dose of 0.05 mg/kg at the time of ligation. Following laparotomy animals were recovered and observed in a warming box for 24 hours.

Figure 2.3

Outline of the protein overload model of renal fibrosis.

Renal injury was induced using daily injections into the peritoneal cavity of low endotoxin bovine serum albumin for a total of 6 weeks.

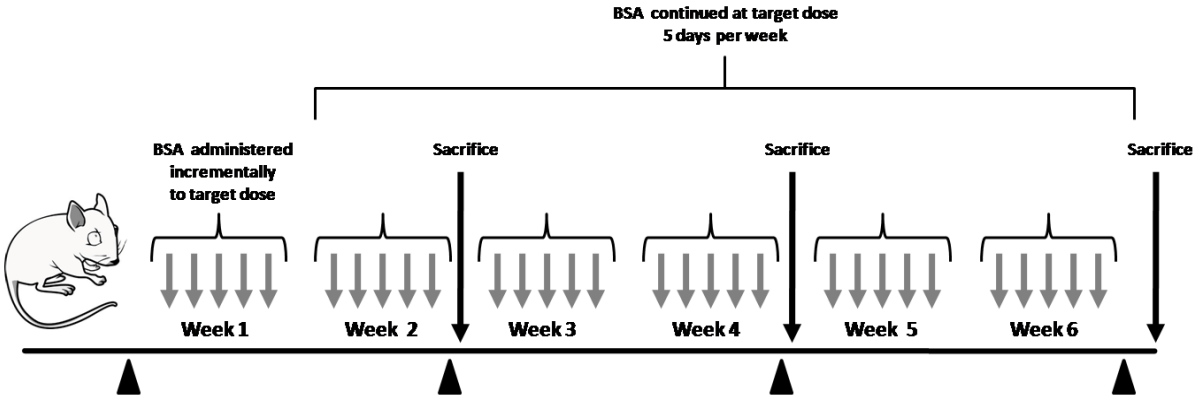

Figure 2.4

Unilateral ureteric obstruction model

Renal fibrosis was induced using the established model of unilateral ureteric obstruction (UUO). Kidneys were harvested at days 3, 7 and 14 after induction of injury

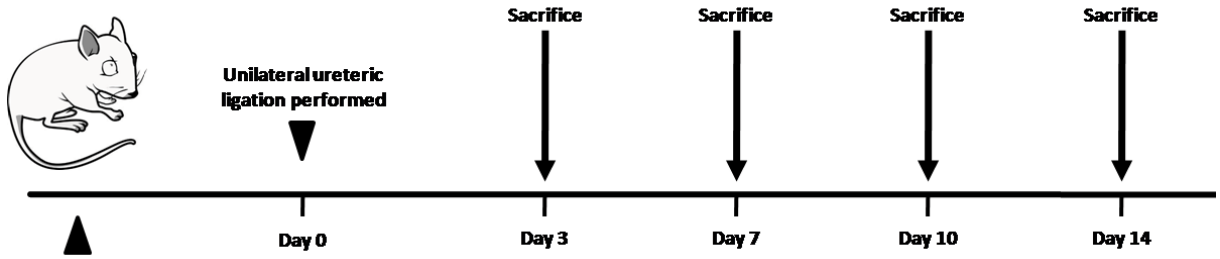

Figure 2.5

Surgical technique used to perform the UUO model.

(A &B) Under inhalational anaesthesia mice underwent a midline laparotomy. (C) The abdominal contents was reflected and covered with gauze soaked in saline. (D&E) the left ureter was identified and ligated with an atraumatic micro-haemoclip. (F) The wound was repaired using sutures to the peritoneal cavity and skin clips. Clips were removed 7 days following the procedure.

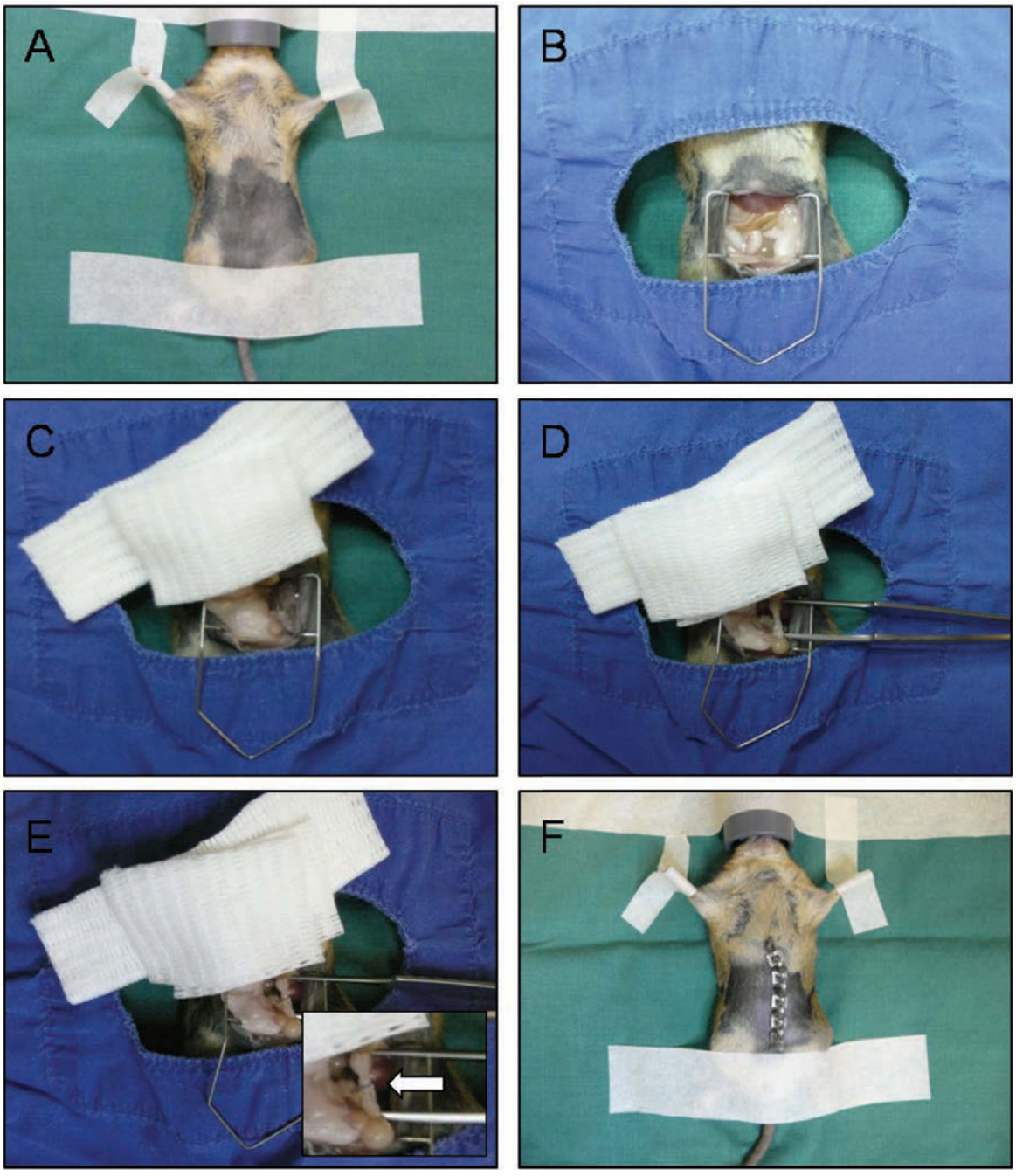

2.2.10 Analysis of renal fibrosis in small animal models

2.2.10.1 Tissue collection and analysis of renal function

Tissue collection and analysis of renal function was performed as described in section 2.2.4-2.2.6.

2.2.10.2 Sirius red staining

Renal fibrosis was visualised and quantified with use of picosirius red staining. Twelve non-overlapping field at x400 magnification from each section were captured using a Nikon microscope and digital camera (Nikon, UK) with identical illumination and exposure. Digital image analysis was performed using Adobe Photoshop in a blinded manner. The colour range tool was used to threshold the images for positive staining. Threshold image settings were stored as a template and all images were analysed in batches with equivalent settings. The thresholded pixels were expressed as a percentage of the total pixels. This was taken to represent the percentage area staining positively for collagen.

2.2.10.3 Immunohistochemistry

Immunohistochemistry was performed on murine kidney sections cut from paraffin-blocked tissue and frozen tissue sections as described in section 2.1.11.

2.2.10.4 Western blotting

Western blotting to confirm protein expression in murine tissue was performed as described in section 2.1.9 with the substitution of appropriate primary and secondary antibodies.

2.2.10.5 Real time polymerase chain reaction

RNA was extracted from whole kidney homogenates and transcribed into cDNA as described in section 2.1.8. Quantitative polymerase chain reaction was performed on 384 well plates using TaqMan Gene Expression assays; CD248 (Mm00547485), F4/80 (Mm00802529), CD3 (Mm00438095), α-SMA (Mm00725412), FSP-1 (Mm00803372), Collagen 1A (Mm00801666), E-cadherin (Mm01247357), TGF β1 (Mm00441726) and GAPDH (4352339E) was used as a housekeeping gene. Assays were run on a 7900HT Real Time PCR System (Applied Biosystems).

Table 2.17 Quantitative PCR mix and program cycle

Ingredient	volume	concentration
cDNA	2μl	20ng/μl
Primer	1μl	x20
Master mix	10μl	x2
dH_20	7μl	
Total volume	20μl	

Stage	temperature	time
1	50°C	2 minutes
2	95°C	10 minutes
3	95°C	15 seconds
4	95°C	1 minute
	Hold at 10°C	

40 cycles

The cycle number (C_t) for the target gene was subtracted from the C_t for the control gene and the relative quantity was calculated as $2^{-\Delta CT}$. This was then normalised to a control sample and results expressed as mRNA fold change relative to control.

2.2.10.6 Stromal cell subpopulations

Fibroblast subpopulations were assessed using confocal microscopy as previously described by Zeisberg *et al* (108). A Zeiss LSM 510 Meta scanning confocal microscope was used to capture ten visual fields per kidney at x630 magnification. These images were analysed for co-localization of stromal cell markers using cell counting.

2.2.10.7 Myofibroblast cell counts

Myofibroblasts were detected in tissue sections of the kidney from wildtype and $CD248^{-/-}$ mice following 14 days following UUO. Sections were co-labelled with DAPI and myofibroblasts were detected using an antibody directed towards α-smooth muscle actin. Quantification of the number of myofibroblasts (α-SMA positive cells) was performed by detection of CY-3 immunofluorescence (secondary antibody, red stained cells) using confocal microscopy. The percentage of α-SMA positive cells (positive CY-3 immunofluorescence) per high-powered field was quantified in 10 cortical interstitial fields randomly selected at original magnification ×400. $\alpha\text{-SMA}^+$ cells were identified by greater than 75% of the cell area immediately surrounding nuclei (detected by DAPI) staining positive with Cy3 fluorescence indicative of the antigen expression. Blood vessels were excluded from the analysis. Results were

expressed as Mean ±SEM of 10 fields of view per mouse tissue section with an n=6 mice per group.

2.2.10.8 Vascular studies

For microvascular studies mouse tissue sections were stained with anti-CD31 antibody as described above. Specific cells were counted in 10 cortical interstitial fields randomly selected at ×400 magnification per mouse tissue section. Vessel fluorescence was detected using CY-3 fluorescence and analysed in images at ×400 magnification captured from CD31-stained sections of 10 different fields from six different animals. Quantification of the number of fluorescence pixels was calculated using Adobe Photoshop version 7. All images and analysis was performed using constant fluorescence intensity and standardised confocal settings. A Zeiss confocal LSM 510 microscope (Zeiss, Germany) was used to visualize staining with images captured and processed using the Zeiss LSM Image Examiner software (Zeiss). Representative images were chosen from each experiment for figure editing.

The percentage area per field covered by vessels (positive CY-3 immunofluorescence) was then expressed as a percentage of the total pixel count. For vascular length studies whole sections were imaged using the Leica LSI TCS Zoom confocal. The vessel length was calculated for all vessels within a randomly selected field of view (4 fields of view per tissue section in 4 animals per treatment group) with the exclusion of vessels crossing the boarder of the selected area.

Vessel length was expressed in mm and calculated using the ruler tool in the LAS AF version 2.3.5 software.

2.2.10.9 *In vivo* Bromodeoxyuridine (BrdU) studies

Mice were administered, via an intraperitonal injection, with 200μl of bromodeoxyuridine (BD Biosciences) diluted to a concentration of 10mg/ml in PBS. Animals were left for 48 hours before tissue was collected to allow the incorporation of BrdU into proliferating stroma.

2.2.10.10 Bone marrow chimera

Foetal liver cells were isolated from C57BL/6J mice expressing enhanced yellow fluorescent protein (eYFP) in all tissues under the control of the Rosa26 promoter and ubiquitin (gift from Professor Graham Anderson). E14 and E15 embryos were removed and transferred to a class II biological hood for dissection. The liver was identified, dissected and homogenised into a single cell suspension in RPMI using a 1 ml pipette. The homogenate was then filtered through a 30μm sieve into a 15 ml falcon tube. Cell yield was assessed using a haemocytometer. Cells were stored in the dark on ice until needed. Thirty minutes prior to injection cells were centrifuged at 400g for 5 minutes at 4 ^{o}C then re-suspended in 10mls of PBS and passed through a 40μm filter.

Adult male C57BL/6J mice aged 8-14 weeks were purchased from Harlan laboratories. At least 1 week before irradiation and cell transfer, mice were given Baytril (Enrofloxacin). Mice were given lethal total body irradiation of 900 rads in two divided doses of 450 rads separated by 3 hours. One hour later they were reconstituted with 5 $x10^6$ fetal liver cells injected intravenously. Animals were left to reconstitute for 8-12 weeks. Only healthy mice with no signs of graft versus host disease were used in experiments.

2.2.11 Statistical analysis

Results are presented as means +/- SEM. The statistical significance of differences between means was assessed using one-way or two-way analysis of variance (ANOVA) with appropriate post-test analysis or two-tailed Student's t-test. Values of $P<0.05$ were considered significant. Analysis and graphs were prepared using Prism 4 (GraphPad, USA).

CHAPTER 3

EXPRESSION OF CD248 IN

HUMAN RENAL DISEASE

CHAPTER 3

EXPRESSION OF CD248 IN HUMAN RENAL DISEASE

3.1 Introduction

CD248 is expressed on resident stromal cells of the kidney. Observations from human studies, using small numbers of samples, suggest that at basal levels in the adult kidney, CD248 is expressed in the glomerulus on specialised pericytes more commonly referred to as mesangial cells (266). Analysis of human malignant tissue has shown that in renal cell carcinoma (RCC) expression is significantly increased and large rafts of CD248 positive stromal fibroblasts can be seen within the interstitium (266). More recently the group of Huang *et al* have generated a knock in mouse where CD248 expression can be tracked using a LacZ reporter gene (270). These studies again confirm CD248 expression by mesangial pericytes of the glomerulus.

Despite these reports a detailed analysis of CD248 expression in human kidney disease has not been performed. I therefore hypothesised that CD248 expression is increased in human kidney disease and that expression may provide a tool to predict disease outcome. Initially I reaffirmed and expanded on earlier observations from other groups (157, 163) concerning the expression of CD248 in normal renal tissue, before characterising CD248 expression in a large cohort of patients with progressive CKD. *In situ* CD248 expression was analysed against recognised determinants of renal disease progression and outcome, to assess the relevance of this molecule in

human kidney disease, both as a predictor of disease progression and as a candidate therapeutic target.

3.2 Results

3.2.1 Characterisation of CD248 expression in cultured human renal cells.

Renal fibroblasts were isolated from the non-affected pole of human kidney samples removed for the treatment of malignant disease to allow the examination of CD248 expression *in vitro* (Figure 3.1). CD248 was expressed by renal fibroblasts (n=3) but not by glomerular endothelial cells (GEC), podocytes (POD) or human umbilical vein endothelial cells (HUVEC). Cellular protein and RNA expression was confirmed by Western blotting and reverse transcription polymerase chain reaction respectively (Figure 3.2).

3.2.2 Characterisation of CD248 expression within normal kidney.

To examine CD248 expression in human renal stromal cells *in vivo* I performed immunohistochemistry on a control group of patients with archived tissue taken from the non-affected pole of nephrectomies performed for the treatment of malignant disease (n=22. 9 females, 11 males. Median age 65, range 39-85). All control patients had normal renal function (eGFR>90). These studies confirmed CD248 expression within the glomerulus, localised to mesangial cells (Figure 3.3). Tubulointerstitial staining was scant and when present it was localised to the interstitial space.

Figure 3.1

Isolation of renal fibroblasts from human nephrectomy tissue.

Phase contrast and confocal microscopy images are shown. During the early stages of primary culture (Day 7, passage 2), fibroblast cultures were contaminated by cobblestone shaped proximal tubular epithelial cells (arrow). Passaging lead to the over growth by fibroblasts and by day 4 passage 4 all of the cultured cells displayed a mesenchymal pattern. These cells stained uniformly positive for the fibroblast marker vimentin but negative for CD31 (endothelial marker), desmin (mesangial cell marker) and cytokeratin (epithelial cell marker).

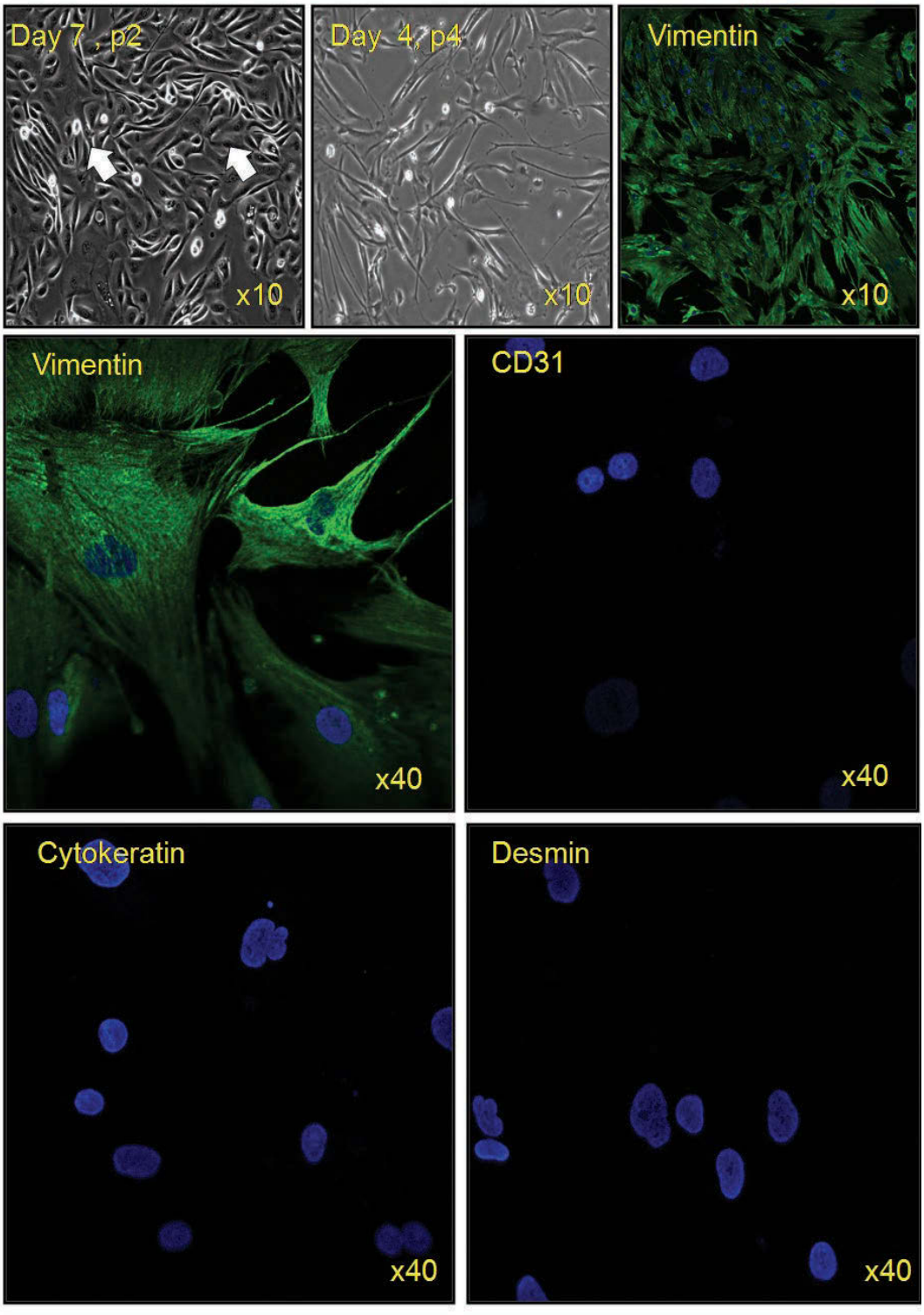

Figure 3.2

CD248 expression by human renal fibroblasts *in vitro*

Top: Confocal microscopy studies demonstrated CD248 (green) expression by renal fibroblasts (RF) but not by human umbilical vein endothelial cells (HUVEC), glomerular endothelial cells (GEC) or podocytes (POD), data not shown (n=3). Middle and bottom: RT-PCR and Western blotting confirmed the immunostaining pattern observed. Beta actin (β-Actin) and TATA binding protein (TBP) were used as positive controls.

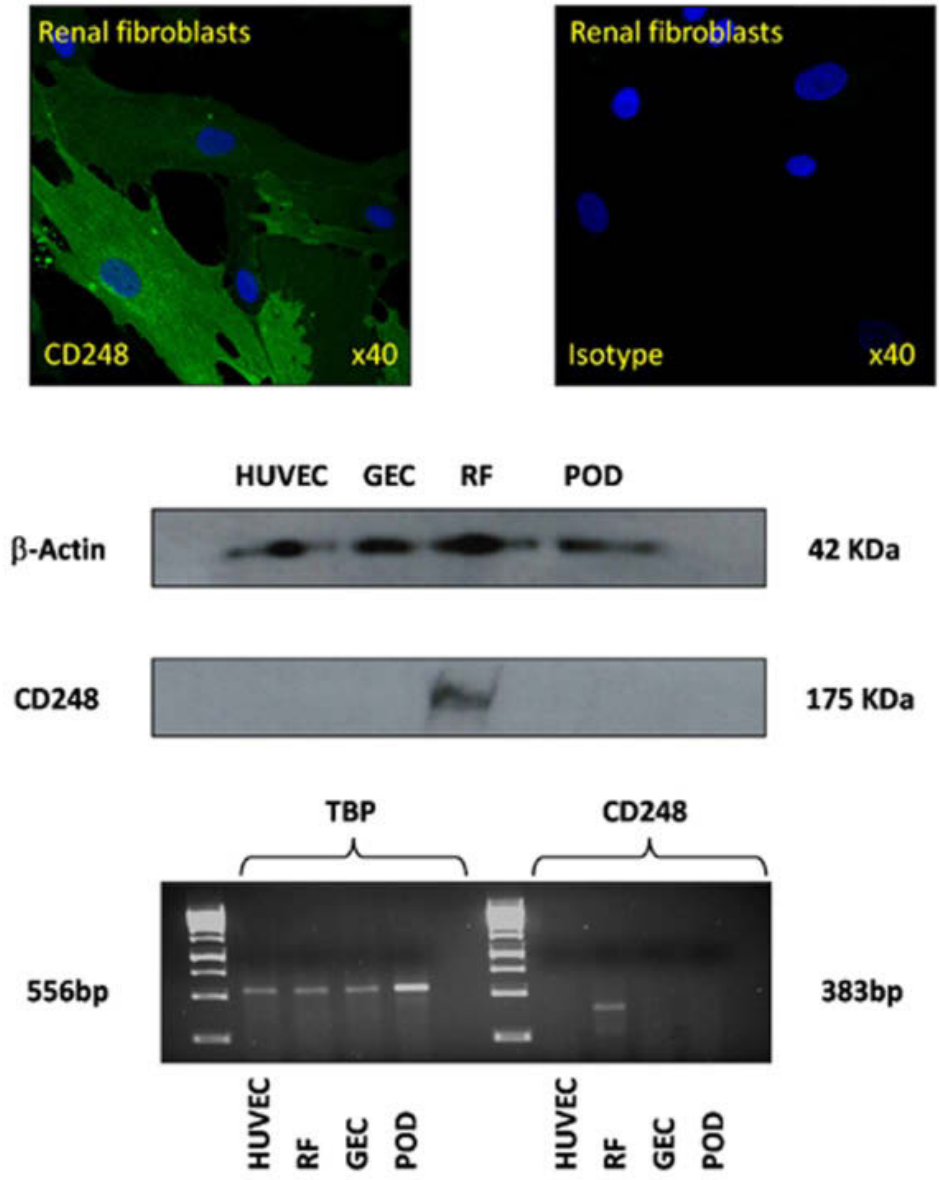

3.2.3 CD248 expression and determinants of renal progression

To investigate the potential role CD248 may play in the tissue remodelling that accompanies progressive CKD, I performed a detailed histological analysis of a cohort of patients with IgA nephropathy. IgA nephropathy was chosen as progression in these patients is known to be tightly linked to albuminuria and interstitial fibrosis at diagnosis (discussed in detail in Chapter 1)(46).

One hundred patients with an adequate renal biopsy to make a diagnosis of IgA nephropathy were identified. Ninety-three had archived tissue and clinical data suitable for analysis (60 males and 33 females). Table 3.1 summarises the clinical, pathological and experimental characteristics analysed.

Table 3.1

Study population: Clinical, pathological and experimental characteristics (n=93). (See Chapter 1, section 1.5.3.4 for a description of the index of chronic damage).

	Median	Range
Age (years)	42	18-82
eGFR (ml/min/1.73m^2)	56	6-99
ACR (mg/mmol)	60	0.8-1097
Index of chronic damage (%)	17	0-94
Tubulointerstitial CD248 (%)	6.8	1.42-31.57

Histological analysis of the biopsy samples demonstrated diffuse tubulointerstitial staining for CD248 (Figure 3.3). CD248 expression was also found to be increased in the mesangial cells of the glomerulus in inflamed kidney tissue (Figure 3.3f). Quantification of the interstitial staining using an interactive image analysis system showed expression to be greater in patients with more advanced disease. Previous

studies by our group (31, 32) have demonstrated a relationship between albuminuria, renal function, index of chronic damage and progressive CKD. I therefore analysed the relationship between these parameters and CD248 expression *in situ* in the cohort of 93 patients with IgA nephropathy.

By univariate analysis; the urinary ACR correlated with tubulointerstitial expression of CD248 (correlation 0.500; P<0.0000) (Table 3.2; Figure 3.4). Estimated glomerular filtration rate (eGFR) inversely correlated with urinary ACR but not as strongly as tubulointerstitial CD248 expression (correlation -0.360; P=0.0004) (Table 3.2; Figure 3.4)). Interstitial CD248 expression correlated with renal fibrosis as assessed by the index of chronic damage (correlation 0.539; P<0.0000), and eGFR (correlation -0.679; P<0.0000) (Table 3.2; Figure 3.4)). These univariate correlations were maintained in a multivariate linear regression analysis of the variables. Tubulointerstitial CD248 expression, urinary ACR, index of chronic damage and eGFR were all interdependent variables (Table 3.3). Notably tubulointerstitial CD248 expression independently associated with urinary ACR (0.299; p=0.002). Again, as our group has previously published (31, 32) using other disease cohorts, classical determinants of CKD progression (for example, urinary ACR and eGFR) were interdependent.

Figure 3.3

Immunohistochemistry for CD248.

Normal human kidney (n=22). (a) x100 CD248 (Brown) localises to the vascular pole (arrow) with weak expression seen in the mesangial cells of the glomerulus. There is scant expression in the tubulointerstitium on peri-tubular fibroblasts (*). (b) x400 glomerular expression of CD248. (c) In progressive CKD (n=93) there is diffuse expression of CD248 throughout the tubulointerstitium. Images shown are taken from a renal biopsy specimen from a patient with CKD stage IV. Shown at higher power in panel d and e (arrow to CD248 staining). (f) magnification x630. Glomerular expression of CD248 was also increased in the mesangial cells of inflamed kidney.(g) magnification x100. Confocal microscopy to co-localise CD248 (green) and aSMA (red). Distinct subpopulations (**) can be seen and are described in more detail in figure 5. (h) CD248 (green) was not expressed by CD45 positive cells (red)(arrow).

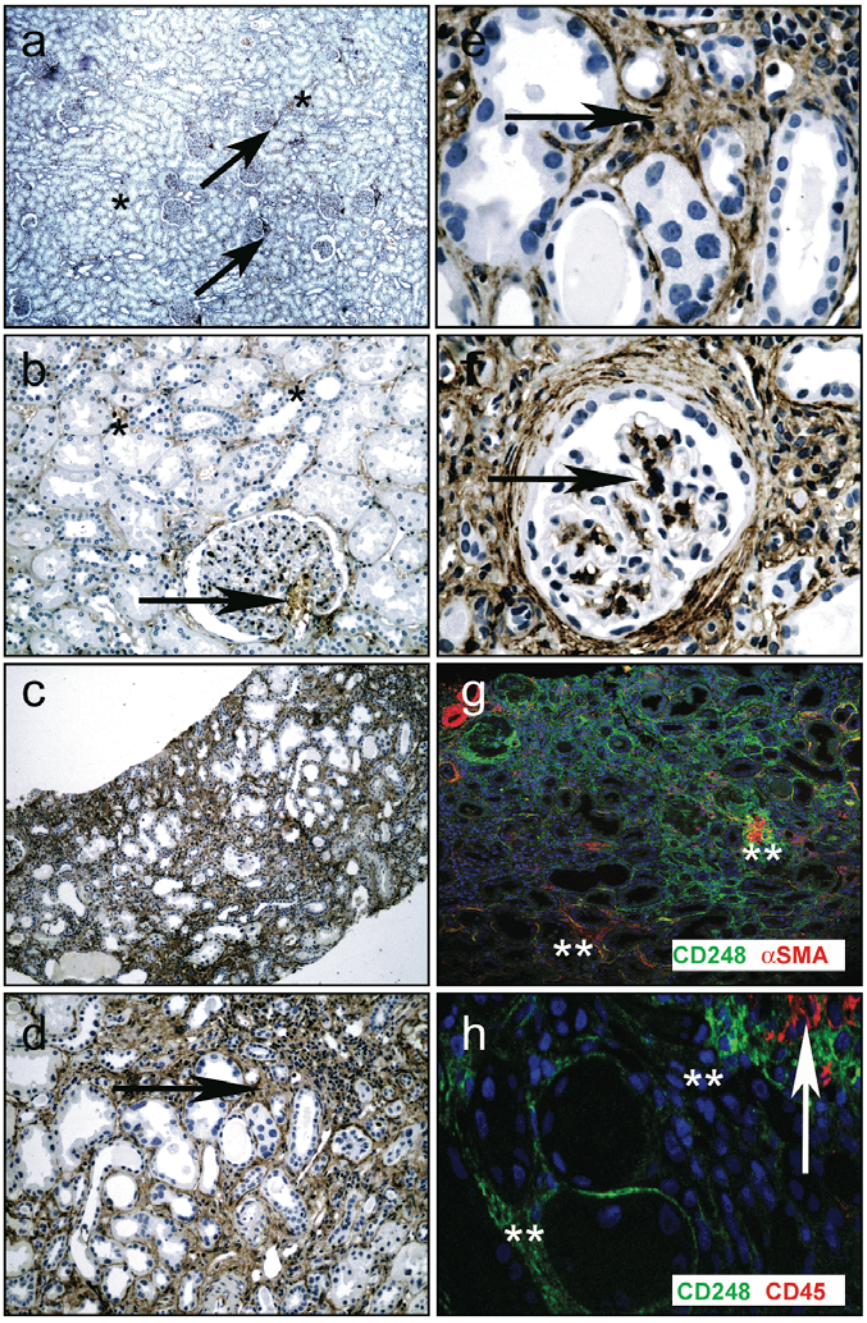

Table 3.2

Univariate correlations

Univariate analysis of correlations between urinary ACR, tubulointerstitial CD248, index of chronic damage and eGFR (n=93)

	Urinary ACR Correlation; P-value	Tubulointerstitial CD248 Correlation; P-value	Index of chronic damage Correlation; P-value
Urinary ACR	NA		
Tubulointerstitial CD248	0.500; 0.0000*	NA	
Index of chronic damage	0.512;0.0000*	0.539;0.0000*	NA
eGFR	-0.360;0.0004*	-0.515; 0.0000*	-0.679;0.0000*

Table 3.3

Multivariate linear regression analysis

Multivariate linear regression analysis between urinary ACR, tubulointerstitial CD248, index of chronic damage and eGFR (n=93).

	Dependent variable			
	Urinary ACR Beta; P-value	**Tubulointerstitial CD248 Beta; P-value**	**Index of chronic damage Beta; P-value**	**eGFR Beta; P-value**
Urinary ACR	NA	0.299;0.002*	0.253;0.003*	0.517;0.577
Tubulointerstitial CD248	0.329;0.002*	NA	0.150;0.097	-.225;0.019*
Index of chronic damage	0.380;0.003*	0.204;0.097	NA	-0.584;0.000*
eGFR	0.067;0.577	-0.268;0.019*	-0.510; 0.000*	NA

ACR=albumin-creatinine ratio NA=not applicable eGFR=estimated glomerular filtration rate

Figure 3.4

Correlation of CD248 expression against determinants of renal progression

Plots of correlation (correlation; P-value). (top) between ACR and tubulointerstitial CD248 staining (0.500; p<0.0000), between (middle), between Index of chronic damage and tubulointerstitial CD248 (0.539;p<0.0000) (bottom) eGFR and tubulointerstitial CD248 (-0.679; p<0.0000)

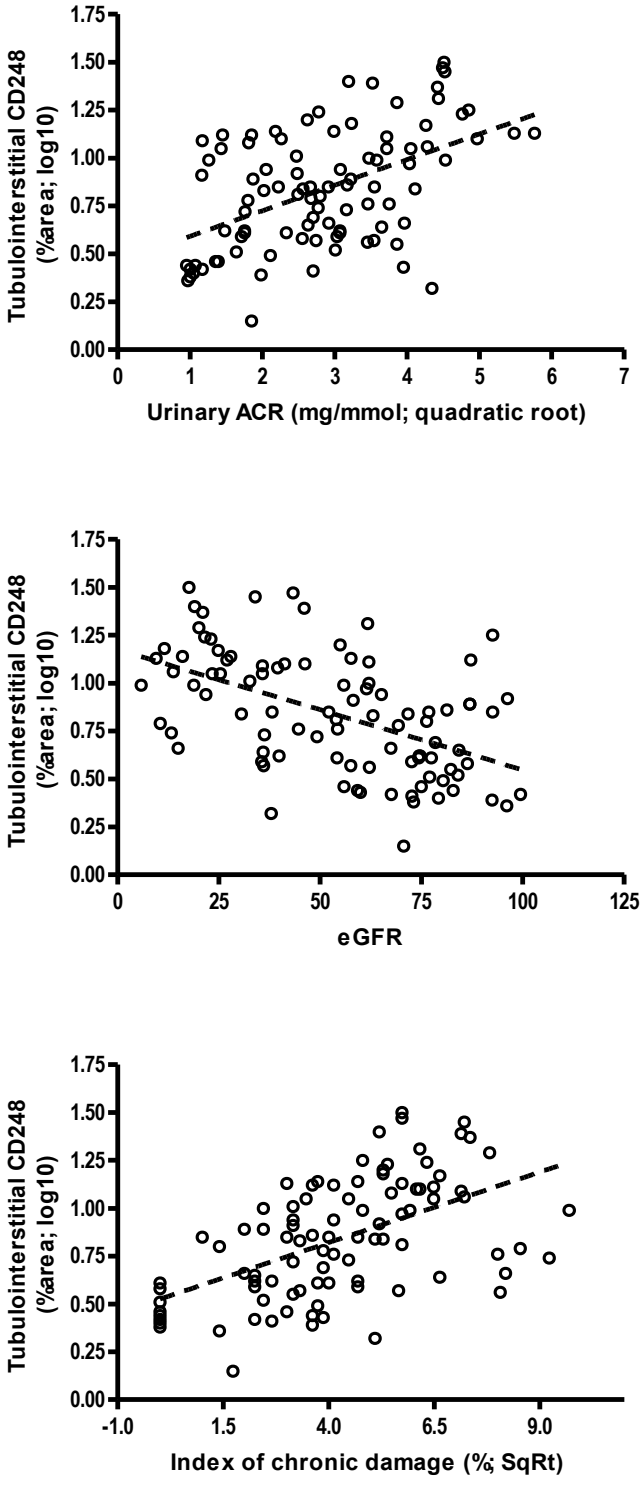

3.2.4 CD248 defines subpopulations of stromal cells

Depletion of αSMA has previously proven detrimental to the progression of renal disease (125). I therefore wished to identify if CD248 was expressed by αSMA+ myofibroblasts to help determine if CD248 may represent a viable target for the treatment of CKD. Confocal microscopy was used to localise αSMA and CD248 in advanced IgA nephropathy (n=3). Again, CD248 was found to be localised to the tubulointerstitium. Immunofluorescence demonstrated 3 subsets of $CD248^{+}$stromal cells: $CD248^{+}\alpha SMA^{-}$, $CD248^{+}\alpha SMA^{+}$ and $CD248^{-}\alpha SMA^{+}$ (Figure 3.5). CD248 did not co-localise with the leukocyte marker CD45 (Figure 3.3).

Figure 3.5

Confocal microscopy of human IgA nephropathy renal biopsy samples

Confocal microscopy of human renal biopsy samples from patients with CKD 3 and 4 (n=3) were stained to co-localise αSMA (red) and CD248 (green). Nuclei are shown in blue. $CD248^{+}\alpha SMA^{-}$, $CD248^{+}\alpha SMA^{+}$ and $CD248^{-}\alpha SMA^{+}$ subpopulations can be seen in all biopsy samples and specific cell populations are highlighted in each panel. Panel (a) $CD248^{+}\alpha SMA^{-}$ (arrows). Panel (b) $CD248^{-}\alpha SMA^{+}$ (arrows).Panel (c) $CD248^{+}\alpha SMA^{+}$ (arrows).

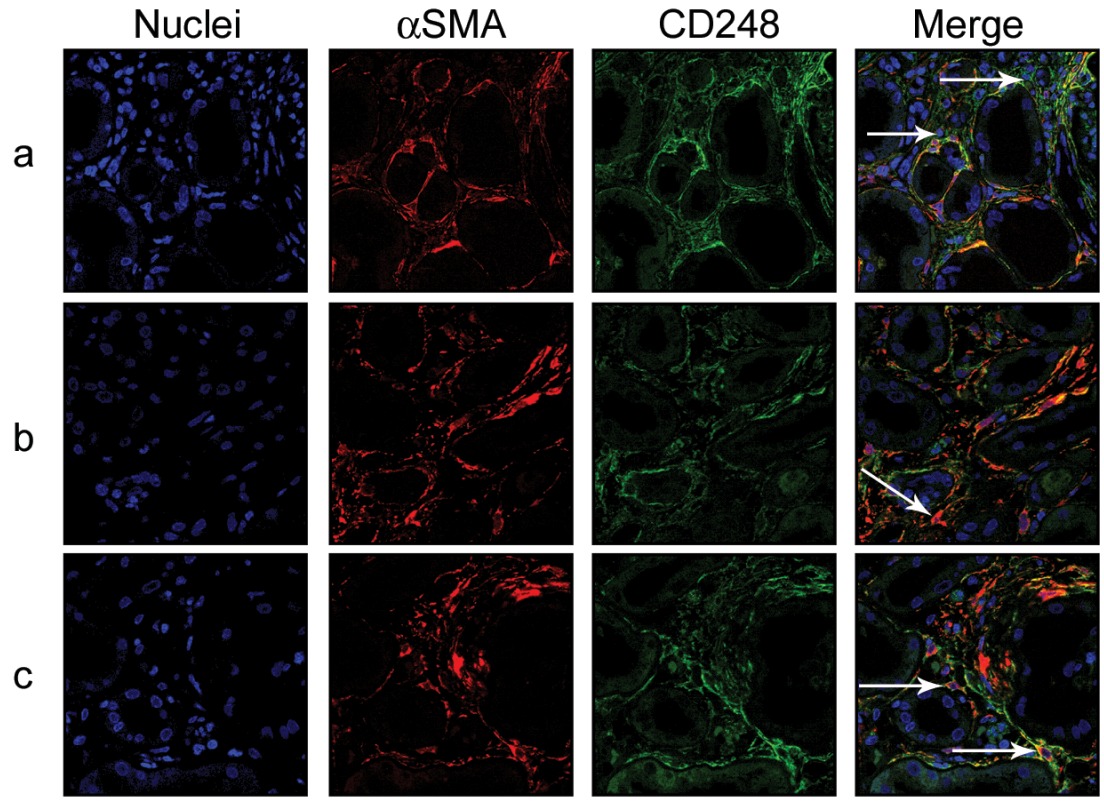

3.2.5 Renal survival

To assess if CD248 expression is an independent predictor of renal survival I reviewed the renal outcomes of my patient cohort. Data on renal outcome was available for all ninety-three patients studied. Patients were followed for up to 1095 days following renal biopsy. Nineteen patients reached a renal end-point (7 patients doubled their serum creatinine; 12 patients reached ESRF) after a mean period of 285 days (range 1-975 days; one patient commenced dialysis at day 1). Kaplan Meier survival analysis demonstrated that patients with extensive tubulointerstitial staining for CD248, particularly tubulointerstitial CD248>9.8%, was predictive of poorer renal outcome (Log rank testing for equality of survivor function statistic χ_2=18.28, P=0.0001). Similar predictive outcomes were seen for albuminuria (χ_2=25.72, P=0.0001) and index of chronic damage (χ_2=31.74, P=0.0001) (Figure 3.6). Therefore univariate and multivariate analysis of these variables was performed. This demonstrated CD248 to be an independent predictor of renal survival in our cohort (Table 3.4).

Table 3.4

Univariate and multivariate analysis of renal survival

	Urinary ACR Exp(B); P-value; 95% CI	**Tubulointerstitial CD248 Exp(B); P-value; 95% CI**	**Index of chronic damage Exp(B); P-value; 95% CI**	**Age Exp(B); P-value; 95% CI**	**Sex Exp(B); P-value; 95% CI**	**eGFR Exp(B); P-value; 95% CI**
Univariate	2.120; <0.0001 1.428-3.146	44.997; <0.0001 7.649-264.712	1.666; <0.0001 1.324-2.096	1.008; 0.561 0.982-1.034	1.113; 0.821 0.438-2.82	0.935; <0.0001 0.908-0.963
Multivariate	NS	12.09; 0.008; 1.89-77.39	NS	0.968; 0.008 0.942-0.995	NS	0.934; <0.0001 0.905-0.964

NS=Not significant

Figure 3.6

Kaplan-Meier survival analysis

(Top) Effect of urinary ACR on renal outcome.(χ_2=25.72, P=0.0001). (Middle) Effect of the index of chronic damage on renal outcome.(χ_2=31.74, P=0.0001). (Bottom) Effect of tubulointerstitial expression of CD248 on renal outcome.(χ_2= 18.28, P=0.0001)

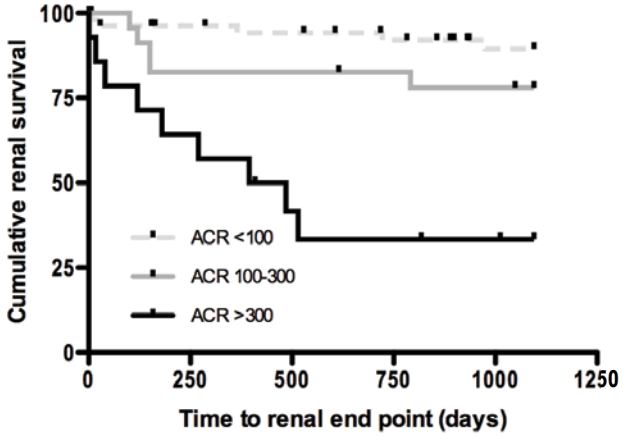

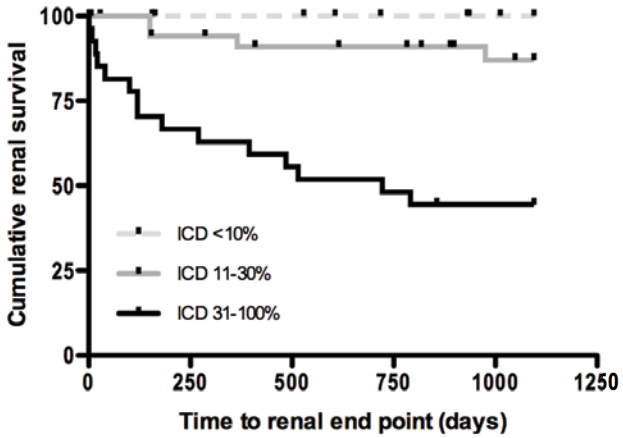

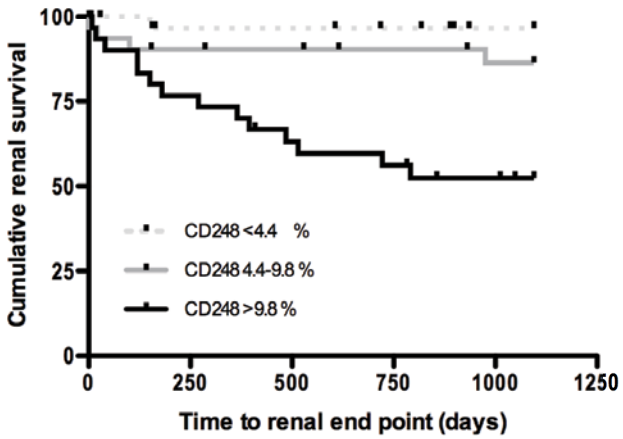

3.3 Discussion

This chapter characterises the expression of the stromal cell marker CD248 in normal kidney and in the kidney tissue of a cohort of patients with progressive renal disease. IgA nephropathy was chosen as a model of progressive human CKD because classical determinants of renal progression are recognised to be important in determining long-term renal survival in these patients (31, 140). CD248 has previously been demonstrated to be expressed on fibroblasts and pericytes found within inflammatory stroma (266).

The in-house anti-CD248 antibodies used here have been extensively characterised in the literature both *in vitro (163, 164)* and *in vivo (157, 165)* to recognise fibroblasts and pericytes and the studies presented here are further confirmation of this specificity. Importantly they do not recognise endothelial cells or leucocytes(165). Although in humans a population $CD8^+CD45^+$ T cells and also a population of vascular leukocytes have been reported (248, 249), importantly no $CD248^+CD45^+$ cells were seen in my studies.

In vitro and *in vivo* studies have shown that in healthy non-inflamed kidney that CD248 is expressed by resident pericytes and on stromal fibroblasts. In injured human fibrotic kidney tissue, CD248 is increased and expressed on a subpopulation of myofibroblasts ($CD248^+\alpha SMA^+$) in addition to a population of $CD248^+\alpha SMA^-$ stromal fibroblasts. $CD248^-\alpha SMA^+$ myofibroblasts were also seen. I was unable to phenotype these cells further using the tissue samples that were available. This is

the first description of a novel myofibroblast population that is $CD248^{+}\alpha SMA^{+}$ and also of a population of $CD248^{+}\alpha SMA^{-}$ fibroblasts.

The origin and heterogeneity of renal stromal myofibroblasts is diverse and recruitment may occur either from the resident cell populations, from circulating bone marrow derived precursors or through the process of EMT(5). Zeisberg *et al* have demonstrated, using lineage tracing techniques in mice, that EndMT may also contribute to the fibroblast populations observed in renal disease. They demonstrated that 30-50% of fibroblasts seen in an animal model of renal fibrosis co-expressed the endothelial cell marker CD31 and both fibroblast and myofibroblast surface markers (108). Here I have identified a novel subset of $CD248^{+}\alpha SMA^{+}$ myofibroblasts and also a population of $CD248^{+}\alpha SMA^{-}$ fibroblasts thus emphasising the heterogeneity of the fibroblast and myofibroblast populations found in CKD. Furthermore, αSMA^{-} fibroblasts are described in the renal literature and are known to contain and express interstitial collagens *in vivo* (118). Fibroblasts isolated from αSMA null mice produce more type collagen 1 compared to wildtype controls(125).

Studies by Lin *et al* have highlighted the importance of the renal pericyte and of injury to the vasculature in driving fibrosis (51). Their observations in murine models of renal injury are supported further by the identification of CD248 expression by resident renal pericytes in close approximation to the vasculature; and the accompanying upregulation of CD248 in human disease. However, the studies

described here fall short of demonstrating categorically that in progressive human renal disease, $CD248^+$ cells, or a sub-population thereof, are derived from pericytes.

The extent of tubulointerstitial fibrosis seen at kidney biopsy has been repeatedly demonstrated to be a rigorous predictor of renal progression (14, 31) and my data is the latest confirmation of this long known association. The current studies do not, however demonstrate that a causal role is played by CD248 in progressive renal scarring, but the close association with albuminuria and renal scarring which are known determinants of renal disease progression and also the association between CD248 and renal survival outcomes is intriguing. Importantly this relationship was maintained in a multivariate analysis.

In conclusion, in this chapter I have demonstrated that the stromal fibroblast and pericyte marker CD248 is upregulated in chronic kidney disease and that this is linked to known determinants of renal progression. The expression of CD248 on stromal fibroblasts and pericytes is already robustly established in the literature. However, here I report the additional observation that CD248 defines a subpopulation of myofibroblasts and also a subpopulation of $CD248^+\alpha SMA^-$ fibroblasts that are linked to albuminuria and tubulointerstitial damage, suggesting that CD248 may be implicated in the tissue remodelling seen in CKD. Immunostaining for CD248 positive cells may not only provide a valuable histological guide to predict renal progression but also raises the possibility that CD248 positive stromal cells may be a potential target for the modulation of renal disease using

novel anti-angiogenic drugs such as the anti-human CD248 monoclonal antibody MORAb-004.

CHAPTER 4

MURINE RENAL EXPRESSION AND

IN VITRO FUNCTION OF CD248

CHAPTER 4

MURINE RENAL EXPRESSION AND *IN VITRO* FUNCTION OF CD248

4.1 Introduction

In Chapter three I described how renal biopsy samples were used to characterise the stromal cell expression of CD248 in healthy and diseased human tissue. *In situ* expression of CD248 increased in biopsy specimens taken from patients with progressive renal disease. CD248 expression was found to be linked to known determinants of renal disease progression. Furthermore, histological assessment of renal biopsy samples for CD248 expression was a predictor of renal disease outcome. These studies did not, however, demonstrate a definitive causal role for CD248 in the development of renal fibrosis. To investigate the potential for this I have used transgenic mice in which CD248 has been constitutively removed ($CD248^{-/-}$ mice) to look for functional defects in cells and tissue that might evidence a role for CD248 in the development of renal fibrosis.

In this chapter the expression of CD248 in resting murine kidney will be described and the *in vivo* structure and function of healthy kidney tissue taken from $CD248^{-/-}$ animals assessed. *In vitro* studies using cells isolated from wildtype and $CD248^{-/-}$ animals have been performed to try and identify functional defects in stromal cells isolated from $CD248^{-/-}$ animals. I found that murine CD248 expression patterns appear similar to those observed in the human kidney and that $CD248^{-/-}$ mice have normal renal structure and function. Stromal pericytes and fibroblasts, but not epithelial cells, isolated from $CD248^{-/-}$ mice exhibit functional defects *in vitro* that

suggest these animals may be protected against the development of fibrosis following renal injury.

4.2 Results

4.2.1 Expression of CD248 in normal murine kidney

Expression of CD248 during renal development was examined in wildtype mice. Tissue was removed from mice at embryonic day 16 (E16), postnatal day 2 (p2) and at 2, 4, 6, 8 and 10 weeks of age. Immunohistochemistry was used to localise CD248 expression in paraffin-embedded tissue sections (Figure 4.1). At E16 it was not possible to remove the kidneys due to their size; therefore whole embryos were fixed, sectioned and stained. CD248 expression was high in the embryonic kidney (E16) where it was diffusely expressed in the developing tubulointerstitial space and glomerulus, expression remained high postnatally at postpartum day 2 (p2). Expression decreased during the course of postnatal development and by adulthood (week 6) expression was observed in mesangial cells of the glomerulus and on a scattered population of peri-tubular cells. No difference in expression could be identified between weeks 6 and 10. Co-localisation studies to confirm mesangial pericyte expression of CD248 were performed on frozen adult murine kidney tissue (Figure 4.2). CD248 was expressed by mesangial pericytes (PDGFRβ^+) of the glomerulus, but not by glomerular endothelial cells (CD31$^+$) or podocytes (Synaptopodin$^+$). In the tubulointerstitium CD248 was seen on a population of peri-tubular cells that morphologically appeared to represent pericytes. These CD248$^+$

stromal cells had long processes that wrapped around peri-tubular blood vessels but were themselves CD31$^-$ (Figure 4.2, m-o).

Figure 4.1

Temporal and developmental expression of CD248

Paraffin sections of murine tissue from 129SvEv animals. In common with most pericyte markers CD248 (brown), is temporally regulated during development. (n=3)

(A) Embryonic day 16 (E16) x40 magnification. CD248 is expressed throughout the developing tubulointerstitium and within early mesangial pericytes of developing glomeruli.

(B, C&D) High power magnification of panel A. (E) At postpartum day 2 CD248 expression is downregulated in the kidney, x40 magnification.

(F&G) Adult murine tissue, x100 & 200 magnification. CD248 expression is low and limited to mesangial pericytes of the glomerulus and peri-tubular cells (panel G, **)

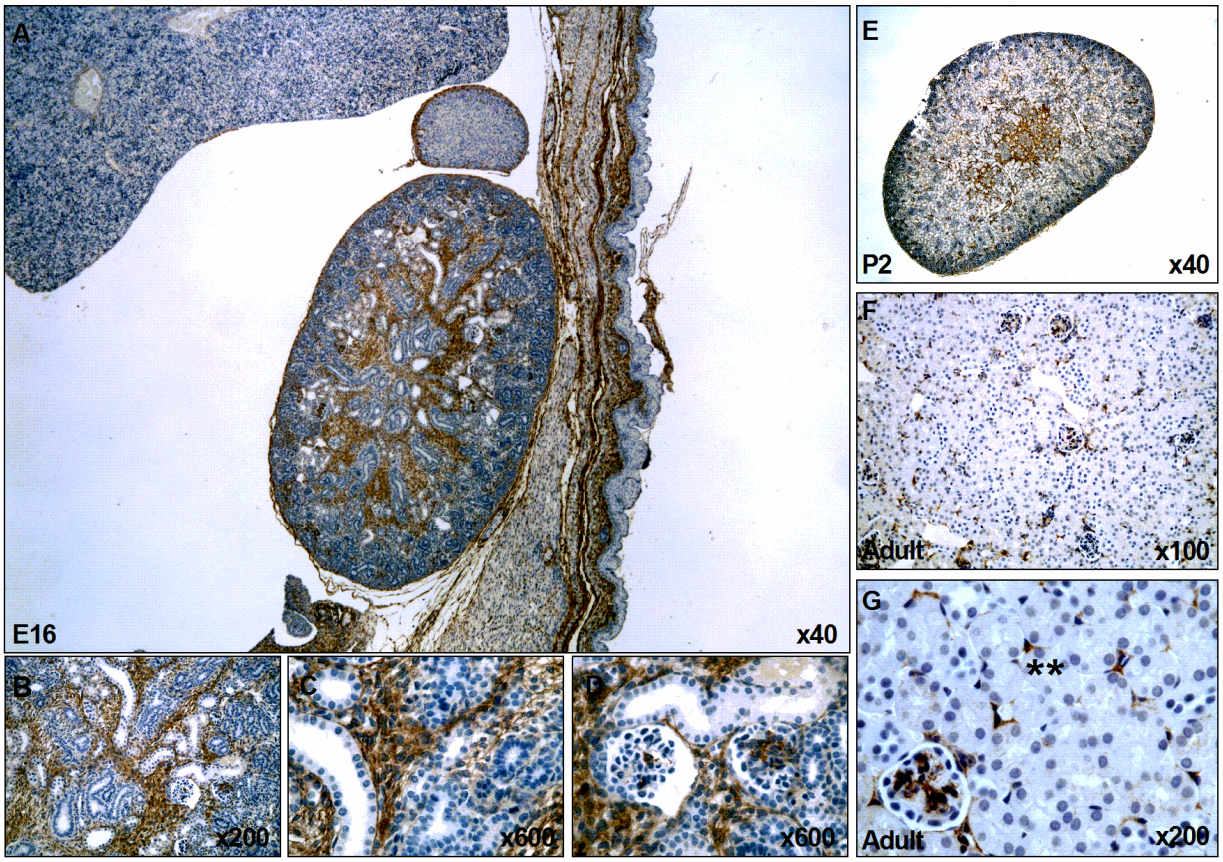

Figure 4.2

In normal, non-inflamed kidney CD248 is expressed by resident renal pericytes.

Analysis of adult murine tissue using confocal microscopy (n=3).

(a,c,&d) CD248 (blue) localises to mesangial pericytes of the glomerulus identified by PDGFRβ (panel **a** green and panel **d** at the arrow showing as cyan)

(**b&f**). CD248 (blue) does not co-localise with CD31 positive endothelial cells (red)

(**g&e**) CD248 (blue) does not co-localise with podocytes identified with synaptopodin (blue)

(**d&h**) show composite images.

(**i, j&k)** Tubulointerstitial expression of CD248. CD248 (blue) is expressed by pericytes wrapped around peri-tubular blood vessels. E-cadherin (green) identifies tubular epithelial cells.

(l,m,n&o) Merged image shown in **l** and zoomed images in **m,n & o.** CD31(red) (arrow panel **n**) positive endothelial cells within the tubulointerstitium are supported by CD248 positive pericytes (blue) (arrow panel **m**).

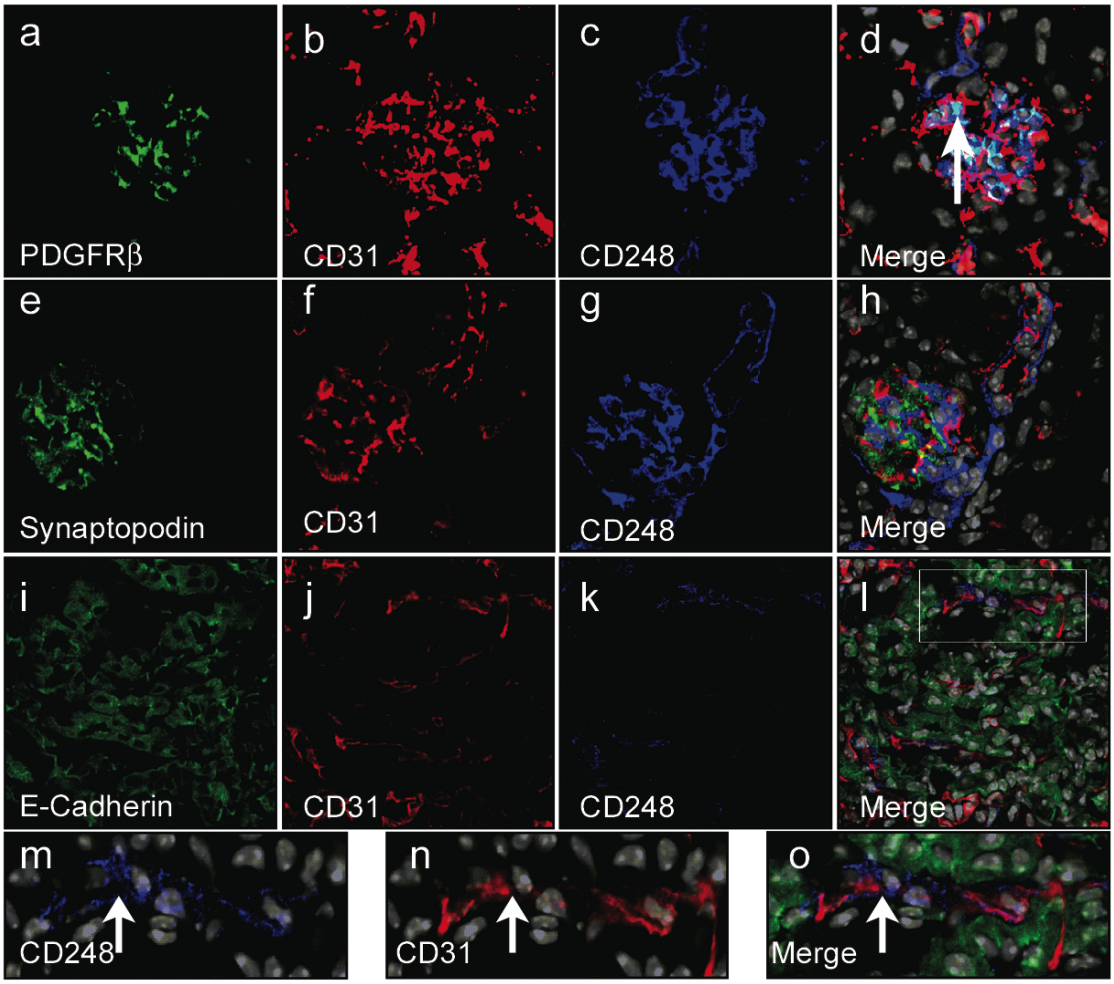

4.2.2 Renal phenotype of CD248$^{-/-}$ mice

The baseline renal phenotype of CD248$^{-/-}$ mice was characterised compared to wildtype control animals. Histological examination of the tubulointerstitial and glomerular compartments revealed no difference between wildtype and CD248$^{-/-}$ animals (n=10) (Figure 4.3 A and B). Furthermore, there was no significant difference in body weight, urinary protein loss or renal function between the two groups (student t-test P>0.05, ns, n=10) (Figure 4.3 C-F).

Figure 4.3

Wildtype and CD248$^{-/-}$ mice have identical renal function and architecture.

(A) Haematoxylin and eosin and (B) periodic acid silver staining of kidney tissue from adult mice. Wildtype and CD248$^{-/-}$ mice had normal glomerular and tubulointerstitial structure. No significant difference (student t-test P>0.05, ns, n=10) in body weight(C), Urinary albumin creatinine ratio (D), serum creatinine (E) or blood urea nitrogen levels (F) were observed in wildtype and CD248$^{-/-}$ mice (n=10).

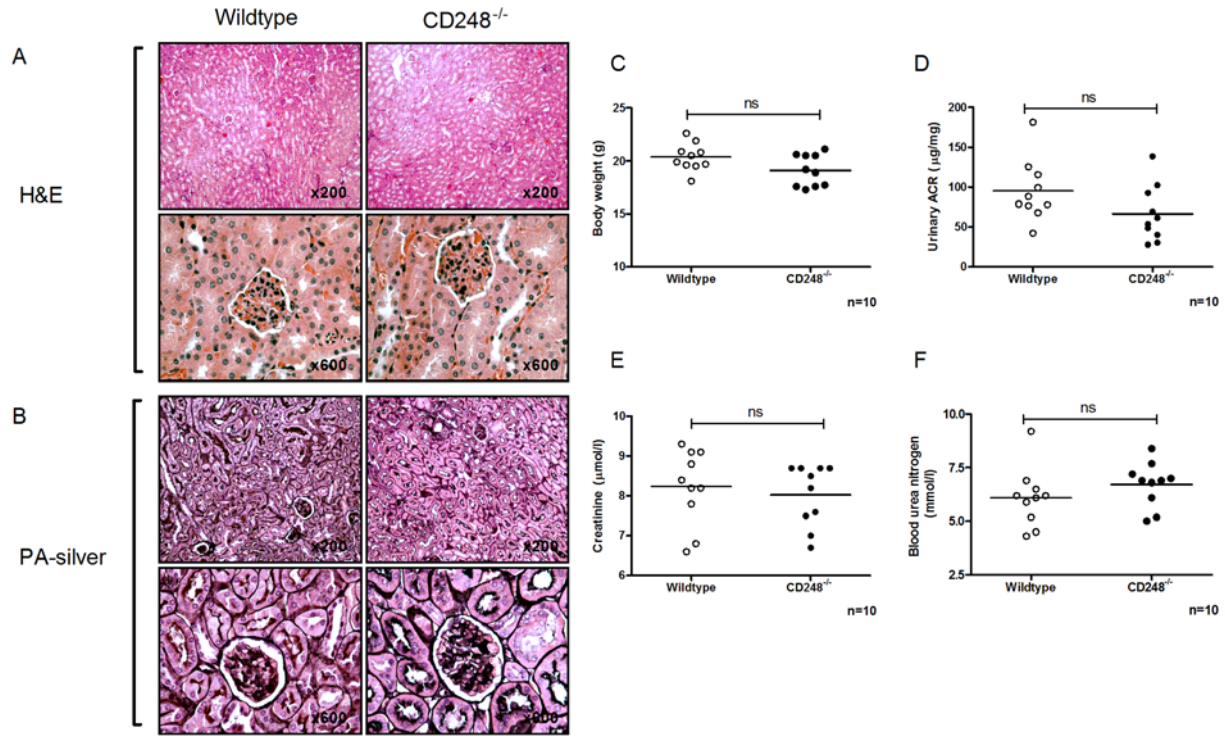

4.2.3 *In vitro* functional studies

To assess a potential functional role for CD248 expression on stromal cells, *in vitro* assays to measure cell proliferation and collagen deposition were performed. CD248 expression is high during murine development and therefore plate-based assays were first optimised on embryonic fibroblasts isolated from wildtype and CD248$^{-/-}$ animals.

Cells were treated with growth factors to assess their responses. PDGF-BB was chosen as it has previously been implicated in CD248 signalling pathways (166). TGFβ_1 was chosen as expression is upregulated in fibrotic tissue and this growth factor is well recognised to participate in stromal cell activation in response to injury. Murine embryonic fibroblasts (MEFs) were seeded into 96 well plates to assess proliferation and collagen deposition. A time course and growth factor dosing study was first performed on cells isolated from wildtype animals (Figure 4.4).

Maximal cellular proliferation and collagen deposition was observed by day 6 following seeding (Figure 4.4). This time point was therefore used for all subsequent studies. In response to PDGF-BB, wildtype MEF proliferated and deposited collagen. A concentration of 100 ng/ml of PDGF-BB induced a significant response compared to control; this concentration of growth factor was therefore used in all subsequent experiments, and is a comparable concentration to that used by other studies found within the literature. Similarly, in response to stimulation with TGFβ_1, the proliferation of wildtype MEF was reduced and collagen deposition increased (Figure 4.4). A

concentration of 10 ng/ml was found to induce a significant response compared to control and this dose was therefore used in subsequent experiments.

Having established the optimal time point and growth factor concentration to stimulate wildtype MEFs, $CD248^{-/-}$ MEFs were then assessed. Preliminary studies demonstrated a significant reduction in the proliferative capacity and the amount of collagen deposited by $CD248^{-/-}$ MEFs compared to wildtype MEFs (Figure 4.5). Thus to accurately assess collagen deposition following stimulation with PDGF-BB and TGF-β_1, cell number was quantified using a crystal violet assay and collagen deposition corrected for total cell number.

In response to stimulation with PDGF-BB (Figure 4.5) wildtype MEFs demonstrated a significant increase in proliferation relative to control. In contrast $CD248^{-/-}$ MEFs failed to proliferate. In response to TGF-β_1 wildtype and $CD248^{-/-}$ MEFs both demonstrated a reduced proliferative response. In contrast, in response to TGFβ_1 $CD248^{-/-}$ MEFs failed to deposit collagen but wildtype MEFs deposited large amounts of matrix. This trend in collagen deposition was also seen in response to stimulation with PDGF-BB but to a lesser extent.

Figure 4.4

Wildtype MEFs time course and growth factor dose titration

(A) Proliferation studies. (B) Collagen deposition studies.

Maximal cellular proliferation and collagen deposition was observed by day 6 following seeding.

In response to PDGF-BB, wildtype MEFs proliferated and deposited collagen. A concentration of 100 ng/ml of PDGF-BB induced a significant response compared to control. In response to stimulation with TGFβ_1, the proliferation of wildtype MEF was reduced and collagen deposition increased. A concentration of 10 ng/ml was found to induce a significant response compared to control. Growth factor titration studies (middle and far right panels) show data collected at day 6 of treatment. (One-Way ANOVA with Bonferroni post-test, n=3 *p=<0.05, **p<0.001, ***p=<0.0001).

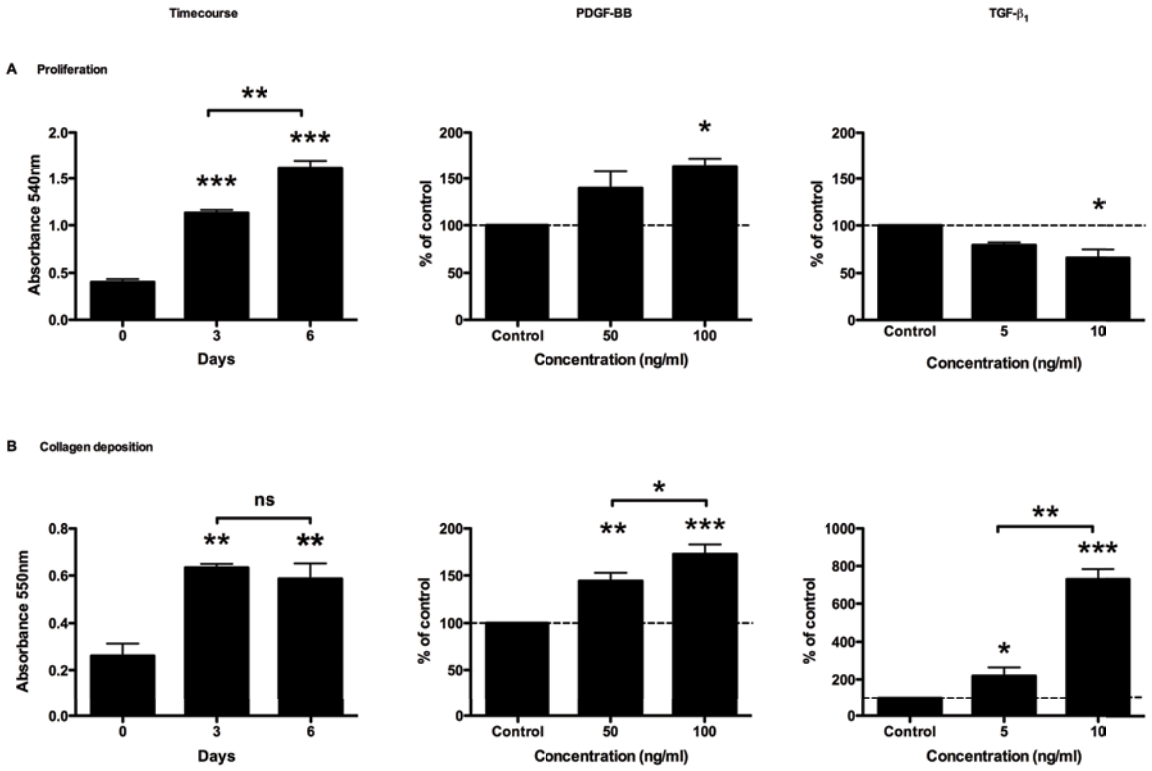

Figure 4.5

Proliferation and collagen deposition of MEFs isolated from wildtype and CD248$^{-/-}$ mice

(A) Proliferation studies. (B) Collagen deposition studies.

A significant reduction in the proliferative capacity and the amount of collagen deposited by CD248$^{-/-}$ MEFs compared to wildtype MEFs was observed at baseline in unstimulated cells.

In response to stimulation with PDGF-BB wildtype MEFs demonstrated a significant increase in proliferation relative to control. CD248$^{-/-}$ MEFs failed to proliferate following stimulation. In response to TGFβ_1 CD248$^{-/-}$ failed to deposit collagen but wildtype MEFs deposited large amounts of matrix. This trend in collagen deposition was also seen in response to stimulation with PDGF-BB but to a lesser extent.

In response to TGF-β_1 wildtype and CD248$^{-/-}$ MEFs both demonstrated a reduced proliferative response and a significant difference was seen between the two different cell groups (Two way ANOVA, n=3, *p=<0.05, **p<0.001, ***p=<0.0001

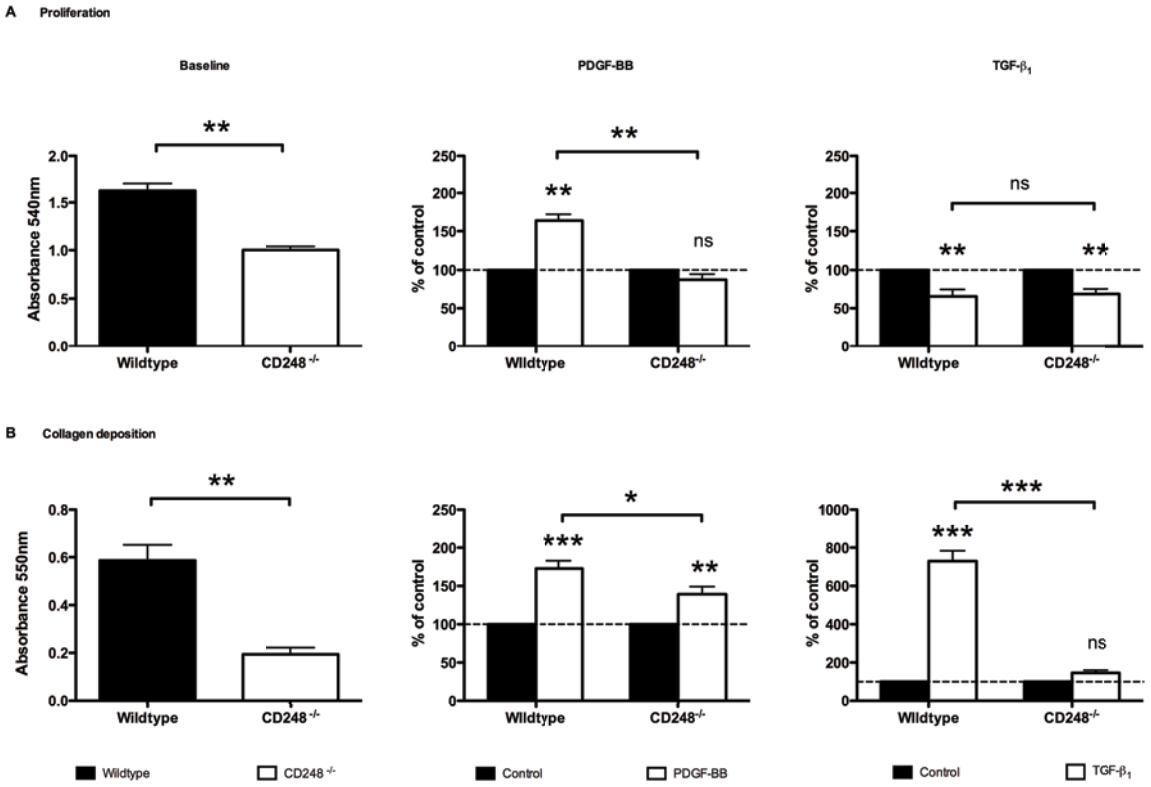

4.2.4 Isolation of renal cell populations from wildtype and CD248$^{-/-}$ mice

To assess the function of CD248 in renal stromal cell populations, mesangial pericytes and tubulointerstitial fibroblasts were isolated from wildtype and knockout animals. Proximal tubular epithelial cells were isolated as a control. Isolation was achieved by infusing magnetic beads into the renal vasculature (Figure 4.6). Beads were localised in the glomeruli, but not the tubulointerstitium, in tissue sections taken from the perfused kidney (Figure 4.6 A). Digestion of the kidney using collagenase and magnetic separation, split the kidney into glomerular and tubular fractions (Figure 4.6 B&C). Glomeruli were not seen in the tubular fraction. To assess yields following digestion, glomeruli were counted using a haemocytometer. No difference in the number of glomeruli isolated from wildtype and CD248$^{-/-}$ mice was seen (Figure 4.6 D). To characterise the phenotype of the isolated cells, morphology and surface marker expression was assessed. Phase contrast microscopy of mesangial pericytes and interstitial fibroblasts demonstrated a mesenchymal cell pattern, in contrast to epithelial cells, which displayed a 'cobble-stone' morphology (Figure 4.8). No difference in the morphology of cells isolated from wildtype and knockout animals was observed. Assessment of cell surface markers using confocal microscopy demonstrated that all cells were negative for CD45 (leucocyte marker), CD31 (endothelial marker) and synaptopodin (podocyte marker). Mesangial pericytes and tubulointerstitial fibroblasts were positive for markers of mesenchyme (CD90, vimentin, fibronectin) but negative for the epithelial cell marker (Cytokeratin). Mesangial pericytes expressed desmin but tubulointerstitial fibroblasts did not. Proximal tubular epithelial cells expressed cytokeratin (Figure 4.9).

Figure 4.6

Isolation of renal cell populations

Isolation was achieved by infusing magnetic beads into the renal vasculature.

(A) Beads were seen in haematoxylin and eosin stained tissue sections. x630 magnification.

(**B&C**) Digestion of the kidney and magnetic separation split the kidney into glomerular (B) and (C) tubular fractions

(**D**) To assess yields following digestion glomeruli were counted using a haemocytometer No difference in the number of glomeruli isolated from wildtype and CD248$^{-/-}$ mice was seen (student t-test, $p>0.05$, $n=6$).

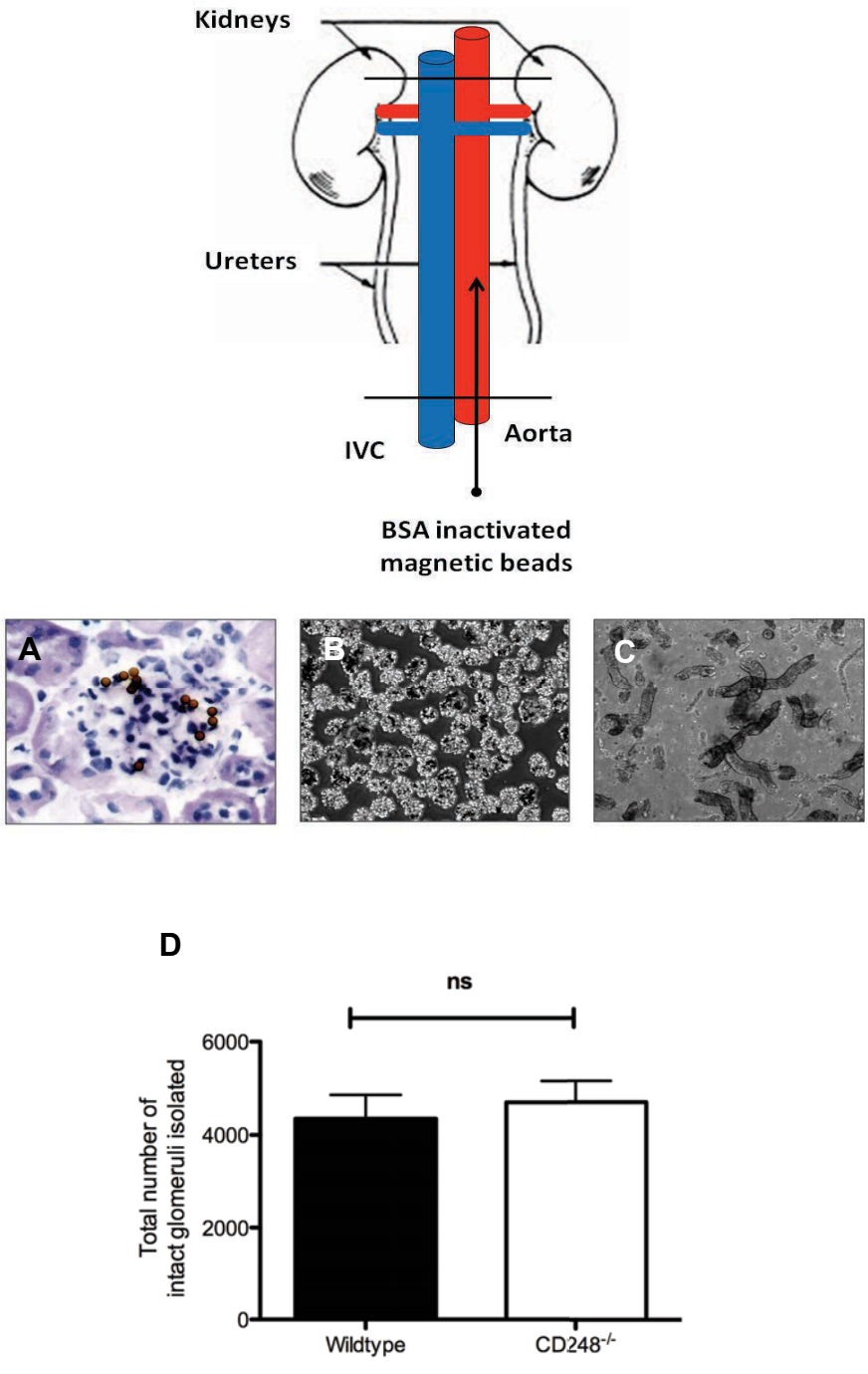

Figure 4.7

Morphology of isolated primary cell cultures

Phase contrast microscopy of primary renal cells. x100 magnification. Mesangial pericytes and interstitial fibroblasts displayed a mesenchymal cell pattern. In contrast, epithelial cells displayed classical 'cobblestone' morphology

(A) Interstitial fibroblasts. (B) Mesangial pericytes. (C) proximal tubular epithelial cells.

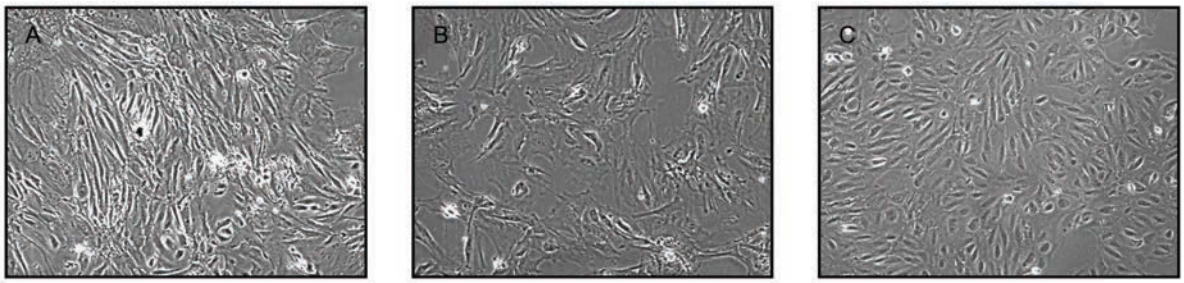

Figure 4.8

Confocal microscopy to characterise renal cell populations

(A) Mesangial cells

(B) Tubulointerstitial fibroblasts

(C) Proximal tubular epithelial cells

All cells were negative for CD45 (leucocyte marker), CD31 (endothelial marker) and synaptopodin (podocyte marker). Mesangial pericytes and tubulointerstitial fibroblasts were positive for markers of mesenchyme (CD90, vimentin, fibronectin) but negative for the epithelial cell marker (Cytokeratin). Mesangial pericytes expressed desmin but tubulointerstitial fibroblasts did not. Proximal tubular epithelial cells expressed cytokeratin. Magnification x400.

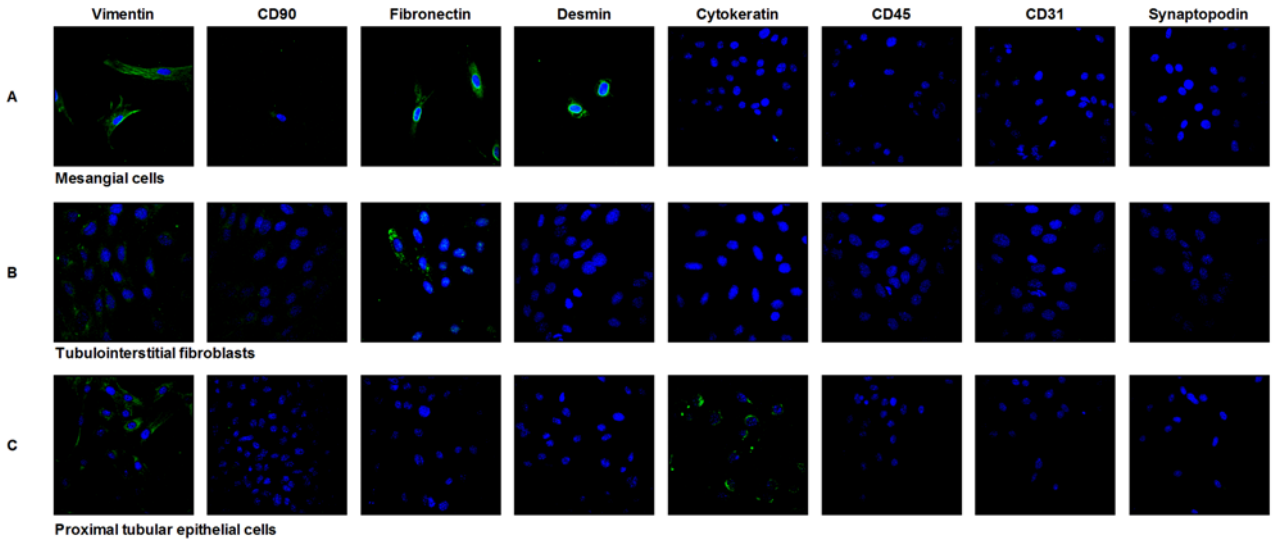

4.2.5 *In vitro* functional studies using specific renal cell populations

To assess the function of CD248 in renal stromal cell populations the assays performed in section 4.2.3 on MEFs were repeated using mesangial pericytes, tubulointerstitial fibroblasts and proximal tubular epithelial cells isolated from wildtype and CD248$^{-/-}$ animals.

Mesangial pericytes and tubulointerstitial fibroblasts from CD248$^{-/-}$ animals, but not proximal tubular epithelial cells demonstrated a baseline proliferative defect after 6 days of culture (figure 4.9). *In vitro* CD248$^{-/-}$ stromal cells, but not epithelial cells demonstrated a deficiency in PDGF-BB mediated proliferation. In response to the mitogenic effects of PDGF-BB all cell populations proliferated, however, this response was significantly blunted in CD248$^{-/-}$ stromal cell populations but not in epithelial cells. Mesangial pericytes isolated from CD248$^{-/-}$ demonstrated a significant proliferative response to TGF-β1, in contrast this effect was not observed in tubulointerstitial fibroblasts or proximal tubular epithelial cells.

To confirm the baseline defect in proliferation seen in the 96 well plate assays an *in vitro* wound healing assay was performed (figure 4.10). Again in response to injury CD248$^{-/-}$ stromal cells proliferated significantly slower than cells isolated from wildtype animals. No difference between wildtype and CD248$^{-/-}$ PTECs was seen in response to injury.

Figure 4.9

Proliferation studies using renal cell populations

***In vitro* CD248$^{-/-}$ mesangial pericytes and interstitial fibroblasts but not proximal tubular epithelial cells exhibit a deficiency in PDGF-BB mediated proliferation.** (Two way ANOVA, n=3, *p=<0.05, **p<0.001, ***p=<0.0001).

(A-C) Mesangial cells and interstitial fibroblasts but not proximal tubular epithelial cells demonstrated a baseline proliferative defect (t test, n=3, *p<0.05, **p<0.01).

(D-I) Day 6 proliferation data following growth factor treatment (PDGF-BB 100ng/ml TGFβ1 10ng/ml) Mean^{+}/-SEM expressed as percentage of control (vehicle alone).

(D-F) In response to the mitogenic effects of PDGF-BB all cell populations proliferated, however, this response was significantly blunted in CD248$^{-/-}$ stromal cell populations but not in epithelial cells.

(G-I) Mesangial cells isolated from CD248$^{-/-}$ demonstrated a significant proliferative response to TGF-β1 but this effect was not observed in fibroblasts or epithelial cells.

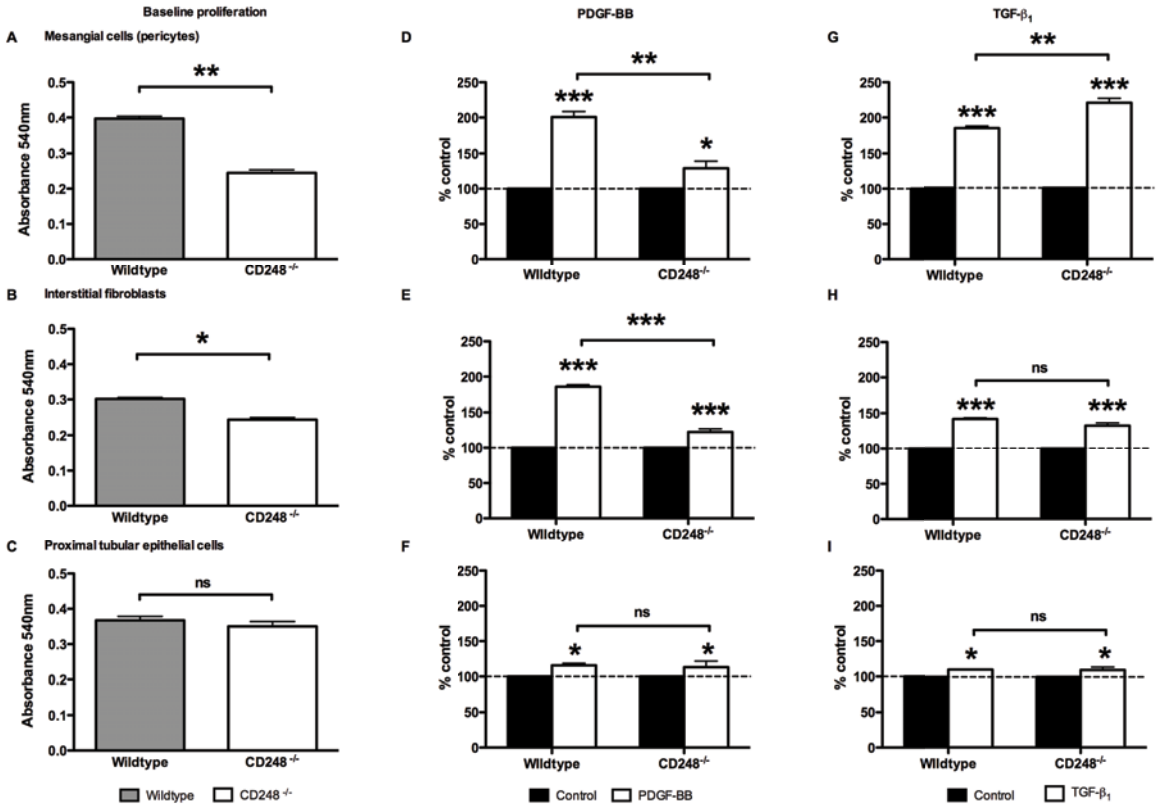

Figure 4.10

Wound healing assay

Cells were seeded into 6 well plates and cultured to confluence. Using a sterile 200 ml pipette tip a straight scratch was made in the confluent cell monolayer. Phase contrast images were captured from the plate at 0, 6, 12 and 24 hours following monolayer injury.

Image analysis was performed by marking the leading edge on the both sides of the wound using NIH imageJ; the distance was measured and expressed as a percentage of the wound area at time 0. In response to injury CD248$^{-/-}$ stromal cells proliferated slower than cells isolated from wildtype animals. No difference between wildtype and CD248$^{-/-}$ PTECs was seen in response to injury. (Two-way ANOVA with Bonferroni post-test relative to control, n=3 *p=<0.05).

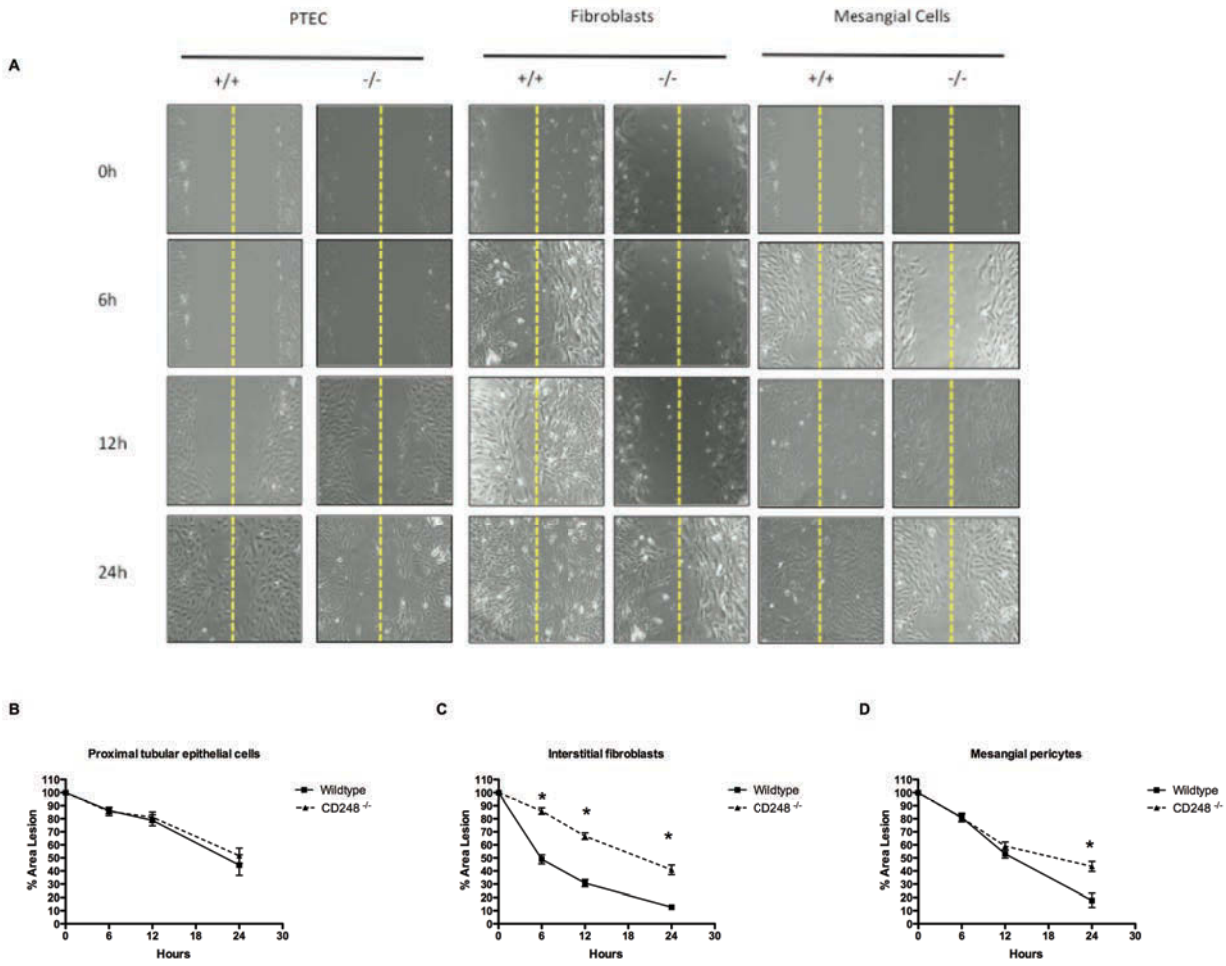

The capacity for matrix deposition by CD248$^{-/-}$ renal cell populations was also assessed (figure 4.11). As previously seen in CD248$^{-/-}$ MEFs, mesangial pericytes and tubulointerstitial fibroblasts isolated from CD248$^{-/-}$ mice had a baseline defect in collagen deposition *in vitro*. No defect in collagen deposition by epithelial cells isolated from wildtype or CD248$^{-/-}$ animals was observed.

In response to stimulation by the growth factors PDGF-BB and TGFβ1, interstitial fibroblasts and PTEC deposited matrix. Interstitial fibroblasts deposited greater amounts of matrix than PTEC. Wildtype and CD248$^{-/-}$ isolated cells responded similarly. In contrast, mesangial pericytes isolated from CD248$^{-/-}$ animals responded differently to stimulation than wildtype cells. Wildtype mesangial pericytes increased matrix deposition in response to stimulation with PDGF and TGFβ1, however, CD248$^{-/-}$ mesangial pericytes significantly decreased collagen deposition in response to stimulation (figure 4.11)

Figure 4.11

Collagen deposition studies using renal cell populations

Mesangial pericytes (A) and tubulointerstitial fibroblasts (B) isolated from CD248$^{-/-}$ mice had a baseline defect in collagen deposition *in vitro*. No defect in collagen deposition by epithelial cells (C) isolated from wildtype or CD248$^{-/-}$ animals was observed.

In response to growth factor stimulation interstitial fibroblasts and PTEC deposited matrix. Wildtype and CD248$^{-/-}$ isolated cells responded similarly. In contrast CD248$^{-/-}$ mesangial pericytes significantly decreased collagen deposition in response to stimulation (Two-way ANOVA, n=3, *p=<0.05, **p<0.001, ***p=<0.0001)

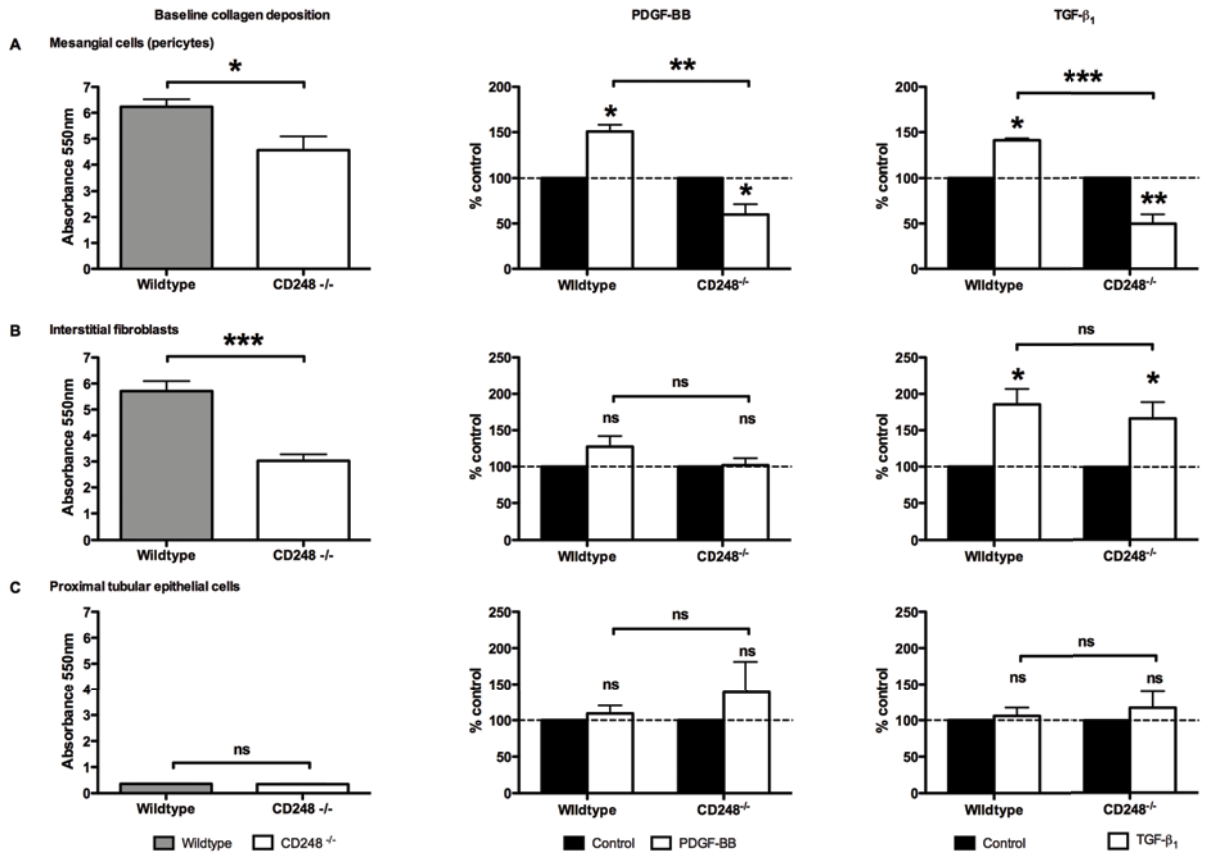

4.3 Discussion

The expression of CD248 in murine kidney is poorly described and the renal architecture and function of $CD248^{-/-}$ mice has not previously been assessed in detail. In the studies described above the pattern of murine CD248 expression seen in wildtype mice mirrored the expression patterns identified in chapter 3 using human kidney tissue.

As previously described at non-renal sites, expression was high during development and became downregulated in adult tissue. $CD248^{+}$ cells were observed to represent mesangial pericytes of the glomerulus and also a population of peri-tubular stromal cells that were seen to associate with the interstitial vasculature. Histopathological examination demonstrated that $CD248^{-/-}$ mice had normal renal architecture with no gross glomerular or tubular abnormalities. An observation supported by no discernable biochemical difference between wildtype and $CD248^{-/-}$ renal function or urinary protein loss, which suggests glomerular and tubular structures are intact.

These studies support and extend earlier morphological descriptions of murine CD248 expression *in vivo*. Macfadyen *et al* have previously identified weak expression in the murine glomerulus but failed to identify the interstitial population of $CD248^{+}$ stromal cells seen in these present studies (158). This may be due to differences in CD248 expression between mouse strains. The studies reported by Macfadyen *et al* used the C57/BL6 background, not 129SvEV mice and strain differences are recognised (288), however, an identical population of cells was also

seen in the human tissue samples analysed. It is therefore more likely that the earlier studies failed to identify the interstitial population due to technical issues. The interstitial space is difficult to analyse using simple immersion fixation as the space and capillaries collapse and the tubules swell when histologically fixed without first perfusing the animals to support the renal architecture, thus small populations of cells can easily be missed (13). Similarly high amounts of endogenous alkaline phosphatase in proximal tubular epithelial cells of the kidney can make it difficult to reduce non-specific immunostaining and a small population of cells in the interstitium could easily be missed.

In the studies reported here a $CD248^+$ interstitial population of cells was identified in human and murine tissue using immunoenzyme histochemistry and confocal microscopy, further all murine samples were perfused prior to fixation to preserve interstitial architecture. In contrast to the studies reported here, Huang *et al* (270) have recently reported CD248 to be expressed by podocytes and endothelial cells in the glomerulus in addition to mesangial cells. These studies used a CD248-LacZ knock-in mouse and an antibody against vimentin as a marker of podocytes. Vimentin is expressed on mesangial pericytes and this may confound these observations. Huang *et al* also used CD31 immunostaining to identify $CD248^+$ endothelial cells; only 50% of endothelial cells were identified to express CD248. Low powered confocal microscopy images were used to quantify expression and this raises the possibility that the $CD31^+$ staining is an artefact due to bleed through from adjacent $LacZ^+$ mesangial pericytes. CD31 was not seen to co-localise with CD248 in the studies reported in this chapter and by others previously (158, 163, 253).

Histomorphological evaluation of haematoxylin and eosin stained and periodic acid silver stained tissue sections demonstrated no difference between wildtype and CD248$^{-/-}$ kidney structure. This is perhaps surprising given the profound renal and vascular abnormalities seen in PDGF-BB and PDGFRβ knock out mice. Both PDGF-B and PDGFR–β deficient mice have defective formation of the glomerular mesangium, a phenotype that can be replicated postnatally in young animals using functional blocking antibodies (177, 178, 223). The functional role and importance of CD248 in renal development *in vivo* is therefore unclear, but the *in vitro* studies performed here do suggest that the constitutive removal of CD248 leads to a functional defect in renal stromal cells.

Stromal cells (tubulointerstitial fibroblasts and mesangial pericytes) isolated from CD248$^{-/-}$ mouse kidneys had a significantly reduced baseline proliferative, wound healing and matrix depositing capacity compared to cells isolated from wildtype animals. A similar trend in proliferation was also seen using CD248$^{-/-}$ MEFS, and this recapitulates earlier studies reported by our group using a 5-hydroxytryptamine-3H uptake assay to measure proliferation (164).

In response to the mitogenic effects of PDGF-BB all cell populations proliferated, however, this response was significantly blunted in CD248$^{-/-}$ stromal cell populations but not in epithelial cells. Mesangial cells isolated from CD248$^{-/-}$ demonstrated a significant proliferative response to TGF-β1 but this effect was not observed in fibroblasts or epithelial cells. Similarly wildtype mesangial pericytes increased matrix

deposition in response to stimulation with PDGF and TGFβ_1, however, CD248$^{-/-}$ mesangial pericytes significantly downregulated collagen deposition in response to stimulation. This confirms earlier knock-in *in vitro* studies of CD248 function and suggests that CD248 signals in coordination with the PDGF receptor (166). In addition a role for TGF-β_1 signalling and CD248 in mesangial pericytes but not fibroblasts is also suggested. However, the studies presented here require further confirmation and evaluation that was not possible during the time frame of this thesis. It is possible the functional defects observed are due to contamination of primary cultures by other renal cell types, although morphological and immunohistochemical assessment was used to characterise the cells used. The purity of these cultures could also be assessed using flow cytometry. Similarly blocking antibody studies against PDGF-BB and TGF-β_1 could be incorporated into the studies described here and protein analysis of downstream signalling molecules in the PDGF and TGFβ signalling pathways performed.

In conclusion, in the resting kidney CD248 is found in the tubulointerstitium on vascular pericytes and fibroblasts, and in the glomerulus on mesangial pericytes. Resting CD248$^{-/-}$ animals have normal renal structure and function. The functional defect observed in stromal cells following the constitutive removal of CD248 are suggestive that CD248$^{-/-}$ mice may be protected against the development of renal fibrosis following injury. Stromal cell proliferation and matrix deposition are key stages in disease progression. Furthermore pericyte proliferation and detachment from the vasculature is a source of myofibroblasts and vessel destabilisation and the removal of CD248 may ameliorate or reduce this process.

CHAPTER 5

RENAL FIBROSIS IN CD248$^{-/-}$ MICE

CHAPTER 5

RENAL FIBROSIS IN CD248$^{-/-}$ MICE

5.1 Introduction

The description of the *in vitro* studies detailed in Chapter 4 suggest that renal stromal cell populations isolated from CD248$^{-/-}$ mice have an impaired functional response to pro-fibrotic growth factors. The human studies described in Chapter 3 have demonstrated that CD248 expression is increased in renal disease and expression is linked to the outcome of renal disease.

It was not possible to identify any renal abnormalities in healthy adult CD248$^{-/-}$ mice and therefore, in this chapter the function of CD248 *in vivo* in response to renal injury will be examined. Prior to the work described in this thesis our research group did not have an established model of murine renal fibrosis available to it. I will first describe two pilot studies of murine models of renal injury that were established in Birmingham. Following the development work undertaken in the pilot studies one of these models was then selected for use to induce renal injury in CD248$^{-/-}$ mice; and the disease phenotype in these animals was compared to that seen in wildtype animals of the same strain. The degree of fibrosis and microvascular damage following injury was characterised and stromal and leucocyte populations assessed. The origin of CD248^{+} cells in this study was tracked using techniques that employed bone marrow chimeras.

It was established from this work that in response to renal injury CD248 expression is increased in the murine kidney and that $CD248^{+}$ stromal cells are derived from resident renal cell populations. As previously described in human disease, CD248 can be used to define subsets of stromal cells that are found in the injured kidney. $CD248^{-/-}$ mice were found to have fewer interstitial myofibroblasts following injury than wildtype animals, but no difference in leucocyte infiltration was observed. Crucially therefore, in response to renal injury $CD248^{-/-}$ mice are protected from the development of renal fibrosis and microvascular rarefaction.

5.2 Small animal models of kidney disease

Two established small animal models of renal injury were selected for use from the renal literature to be used in pilot studies to assess feasibility and outcome. The two models selected were the unilateral ureteric obstruction (UUO) model and the bovine serum albumin protein overload (BSAO) model.

The UUO model was first developed in the early 1970s in rabbits where ligation of the ureter was shown to induce proliferation of αSMA positive myofibroblasts and increased interstitial deposition of collagen I, III and IV (289). The surgical technique has evolved and UUO is now most frequently performed in mice where it is safe, reproducible and well characterised. Within 24 hours complete UUO in mice initiates a rapid decline in renal blood flow and glomerular filtration rate. Following the procedure hydronephrosis develops and the interstitium is infiltrated by leukocytes. These infiltrating cells are predominately macrophages which secrete growth factors

and cytokines which act to induce an imbalance between tubular apoptosis and proliferation (290). Tubular epithelial cell death occurs with eventual progression to deposition of ECM and fibrosis and ultimately, after 7-14 days, loss of functioning renal parenchyma. The animals do not become uraemic as the contralateral kidney can maintain overall renal function.

One limitation of the UUO model is that renal function and proteinuria cannot be measured, therefore, the second model piloted was the BSAO model first described by Eddy *et al* in the late 1980s using rats (291), this method was also later used to induce disease in mice (287). The serial intra-peritoneal administration of bovine serum albumin (BSA), over a period of weeks, leads to progressive irreversible fibrosis with marked leucocyte infiltration and stromal cell activation. Importantly the BSAO is able to model the signs of chronic disease, and the treated animals develop proteinuria, renal impairment and fibrosis.

5.3 Results

5.3.1 Small animal models of renal fibrosis-pilot studies

Two small pilot studies (n=3 per group) were performed to assess the UUO and BSAO models of renal fibrosis. For the UUO model a sham operated control group were used, in the BSAO model a control group received vehicle only intra-peritoneal injections on an identical schedule. Tissue histology and renal weight was assessed in all animals at the end of the pilot. In the BSAO model tissue was also immunostained to localise injected BSA in the kidney and urinary proteinuria was assessed. All animals tolerated the pilot studies with no adverse events.

Serial injection of BSA failed to induce renal injury with no evidence of renal inflammation or fibrosis, small amounts of BSA were seen to localise to the glomerulus and proximal tubule in the treatment group but no significant increase in urinary protein loss could be detected (Figure 5.1). In contrast following UUO marked interstitial inflammation, tubular atrophy and renal fibrosis developed in the injured kidney. Renal mass, relative to body weight was also significantly reduced after 14 days of injury (Figure 5.2). Sham operated animals were unaffected. After consideration and evaluation of the outcomes of the pilot studies, a decision was therefore made to use the UUO model for further experiments investigating the development of renal fibrosis in $CD248^{-/-}$ mice.

Figure 5.1

Results of the BSAO pilot study

(A) Kidney weight corrected for body weight.

(B) Urinary protein loss and immunoenzyme histochemistry to localise BSA (brown) within the kidney.

(C) Tissue histology

(A &C) Serial injection of BSA failed to induce renal injury with no evidence of renal inflammation or fibrosis. (B) Small amounts of BSA were seen to localise to the glomerulus and proximal tubule in the treatment group but no significant increase in urinary protein loss could be detected. (Students t-test, $p>0.05$, $n=3$).

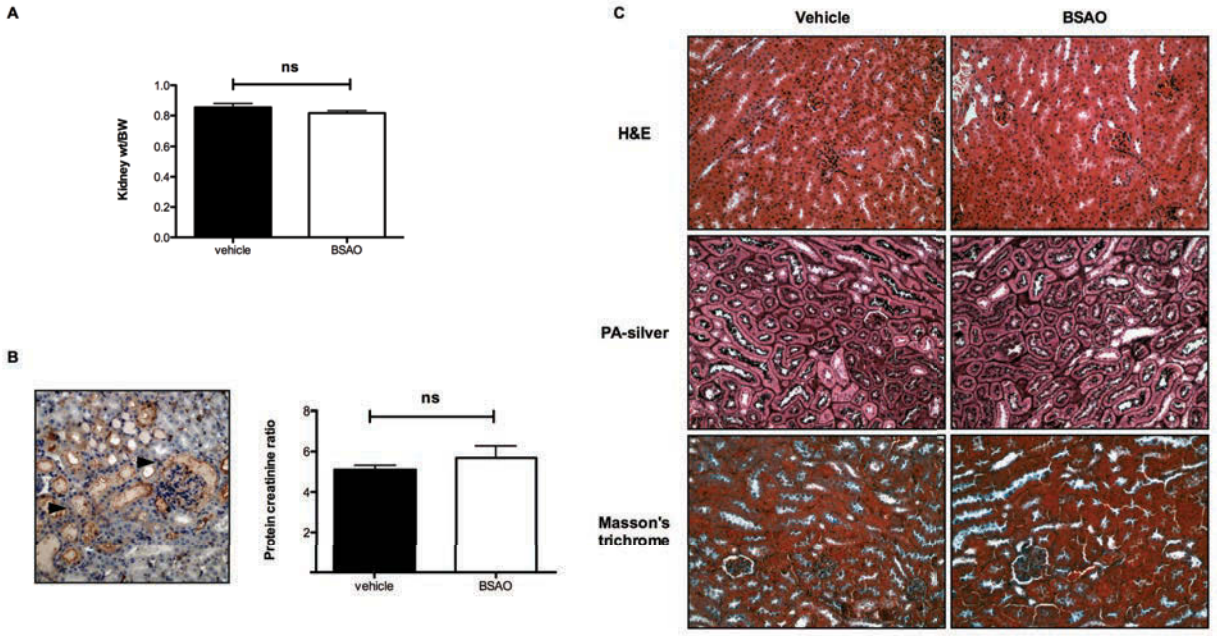

Figure 5.2

Results of the UUO pilot study

(A) Kidney weight corrected for body weight.

(B) Tissue histology

Following UUO marked interstitial inflammation, tubular atrophy and renal fibrosis developed in the injured kidney. Renal mass, relative to body weight was also significantly reduced after 14 days of injury (students t-test, $p<0.001$, $n=3$).

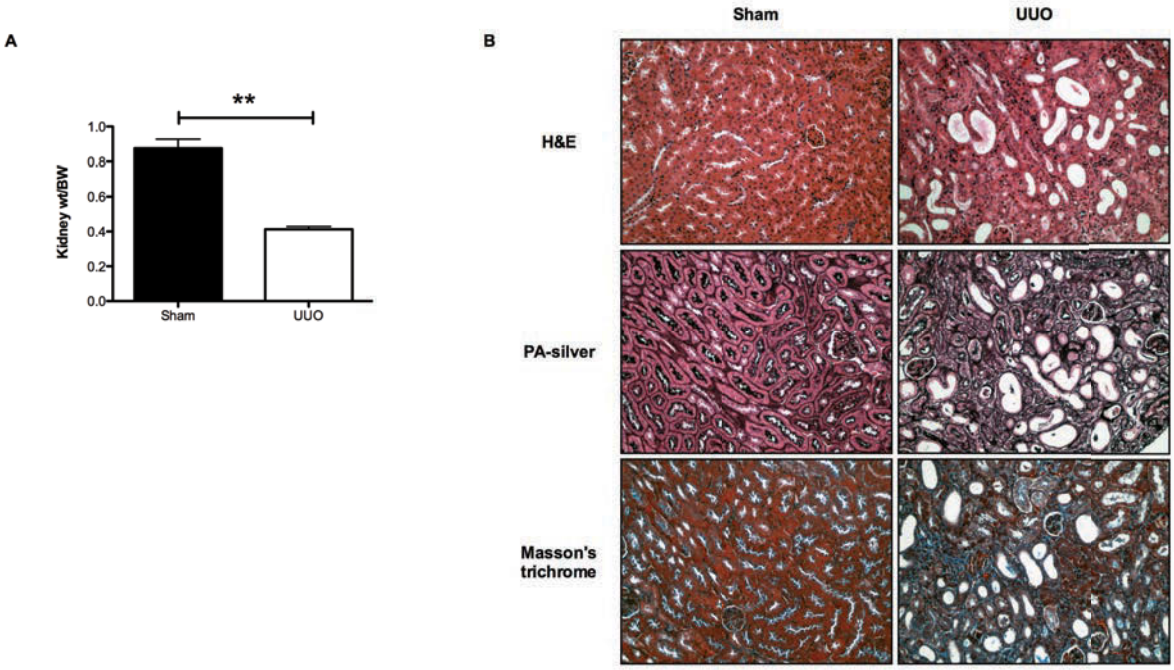

5.3.2 CD248 expression is upregulated following injury

In human kidney disease CD248 expression in the interstitium increased with the development of interstitial fibrosis and damage; I therefore assessed if CD248 expression in the murine kidney increased in response to the induction of renal injury using the UUO model.

CD248 expression progressively increased in the tubulointerstitial compartment following renal injury compared to sham-operated control animals (Figure 5.3 A). The development of renal fibrosis correlated with a reduction in the kidney weight/body weight ratio (Figure 5.3 B) together with histological analysis that demonstrated an inflammatory infiltrate, tubular atrophy and interstitial expansion. Expression of CD248 mRNA in the injured kidney was significantly increased at 7 days post renal injury compared to sham operated control animals. This trend was maintained and increased at day 14 (Figure 5.3 C). Confirmation of CD248 protein expression was established by western blot analysis (Figure 5.3 D).

Figure 5.3

CD248 expression is increased following UUO

(Ai) In sham operated kidney tissue CD248 was expressed by mesangial pericytes of the glomerulus (arrow) and by peri-tubular stromal cells (**). (Aii) At 14 days following UUO tubular dilatation and interstitial expansion accompany increased CD248 (brown) expression in the interstitial space (arrows). Magnification x200. (B) Renal inflammation and fibrosis developed as CD248 expression increased as evidenced by an initial increase in the kidney weight/body weight ratio on day 3 after injury followed by a reduction by day 14 compared to sham operated animals. (C) Immunostaining of CD248 expression was confirmed by quantitative polymerase chain reaction on whole kidneys. Results are expressed as mRNA fold change mean +/- SEM relative to the control group (sham operated day 14) (one way ANOVA with bonferroni's post test relative to control *p<0.01, **p<0.001, n=6). (D) Whole kidney lysates were also used to demonstrate CD248 protein expression at baseline (no operation performed), following a sham operation on day 14 and after UUO for 3, 7 and 14 days.

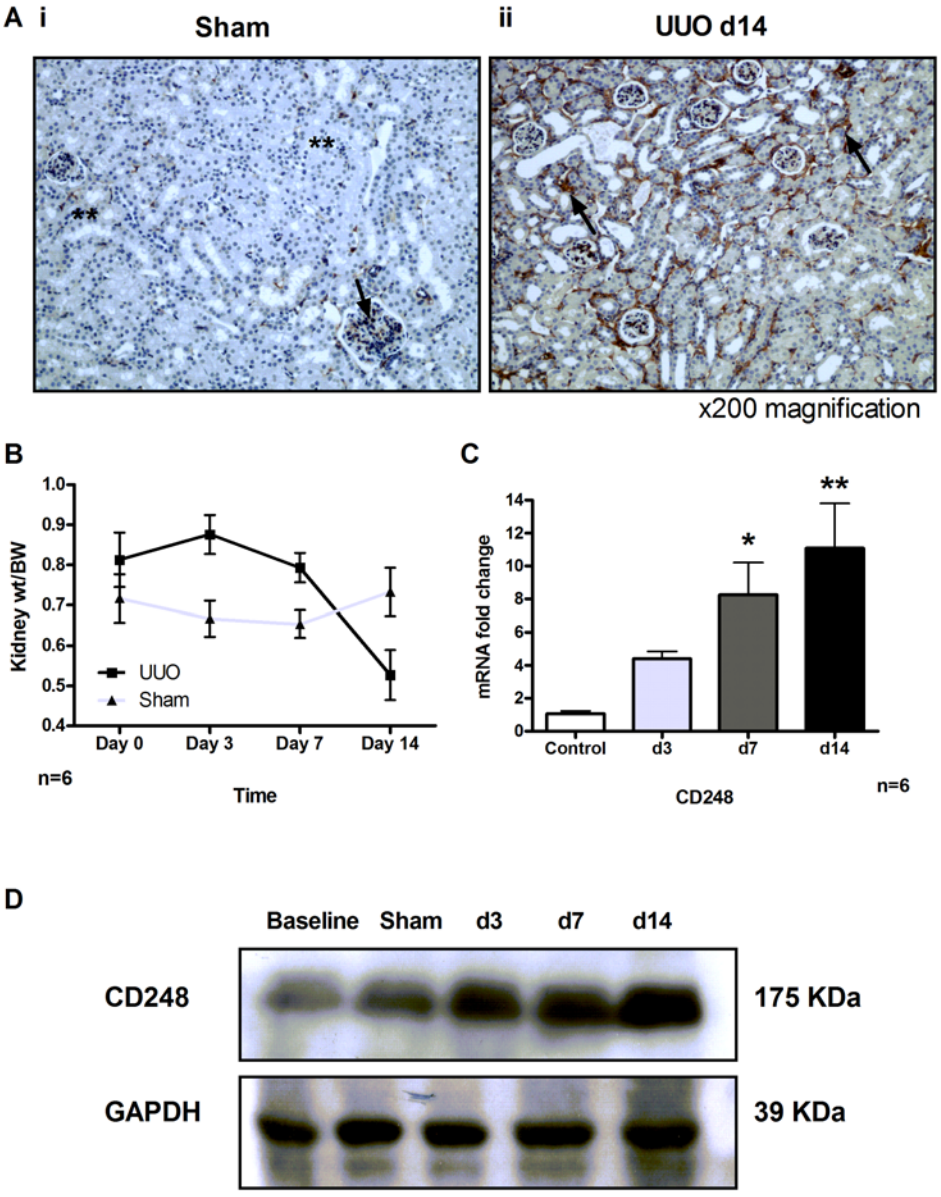

5.3.3 Stromal cell subpopulations following renal injury

In chapter 3, human studies suggest that subpopulations of CD248 stromal cells exist in inflamed renal tissue therefore these populations were also assessed in mice following UUO.

Duffield *et al* have recently suggested that all myofibroblasts are derived from PDGFRβ^+ stromal cell populations (51). Previously it was not possible to assess the expression of this marker by stromal cells in the human studies performed due to technical limitations. The availability of frozen sections here from mice following UUO now made this analysis possible. Tissue from the mice stained for CD248, αSMA and PDGFRβ and was examined using confocal microscopy. Populations of single, double and triple positive stained cells were identified and counted at days 0, 3, 7 and 14 following injury (Figure 5.4 and 5.5).

A small population of CD248$^+$ cells were seen in the interstitium prior to UUO. Glomeruli and blood vessels that stained positive for any of the three markers were excluded from the analysis. Following injury all stromal cell populations expanded in number and this was greatest at day 14 (Figure 5.5). As previously described in human disease, in chapter 3, CD248$^+\alpha$SMA$^+$ myofibroblasts as well as a population of CD248$^+\alpha$SMA$^-$ cells were identified. These subpopulations could further be subdivided using the marker PDGFRβ.

Figure 5.4

Stromal cell subpopulations following UUO day 14

Tissue was stained for CD248 (blue), αSMA (red) and PDGFRβ (green) and was examined using the confocal microscopy. Populations of single (A-C), double (D-F) and triple (G) positive stained cells were identified (arrows). Magnification x630.

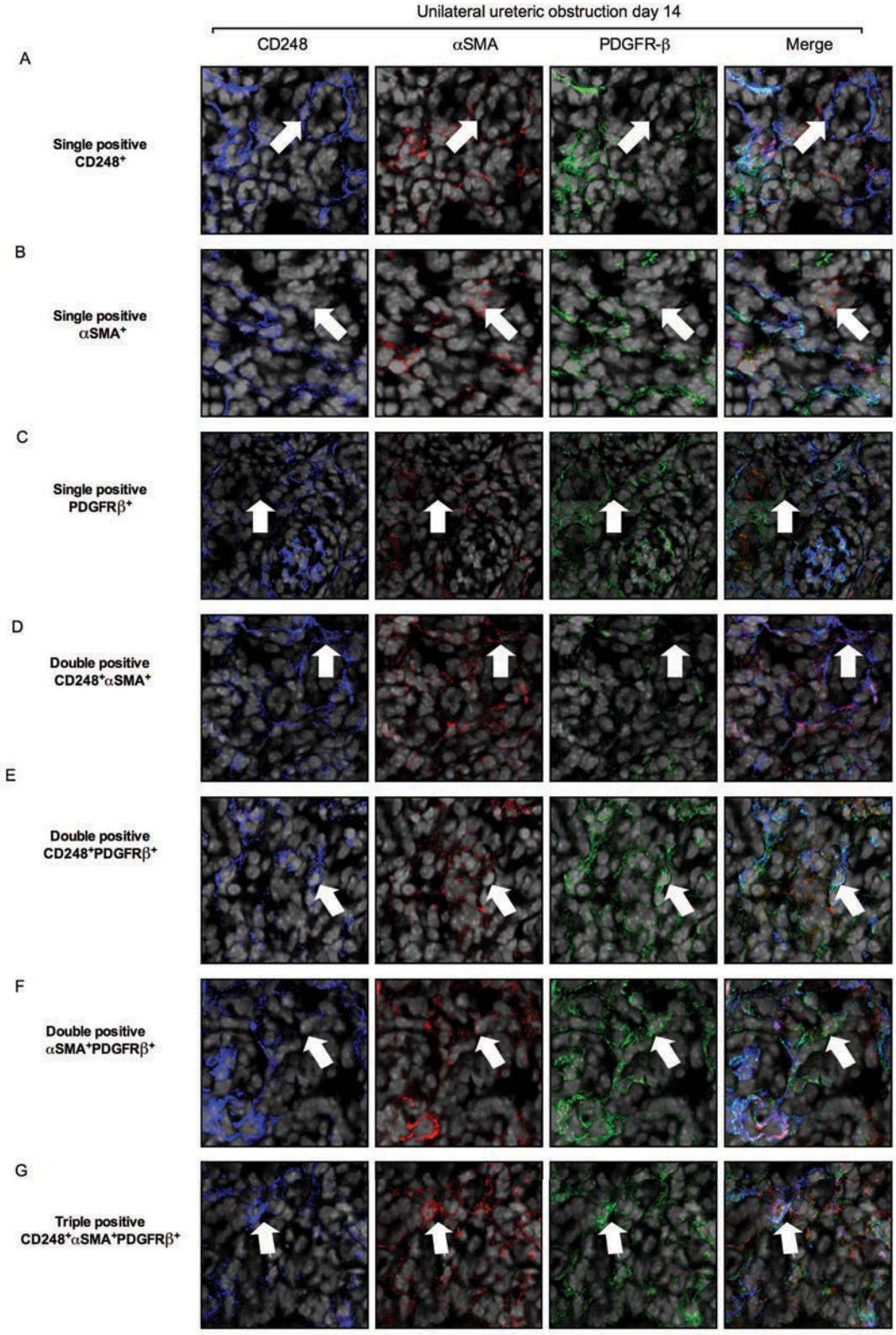

Figure 5.5

Cell counts of stromal cell subpopulations

A small population of CD248^{+} cells were seen in the interstitium prior to injury (A).

Populations of single (A-C), double (D-F) and triple positive (G) stained cells were identified and counted at days 0, 3, 7 and 14 following injury. Following injury all stromal cell populations expanded in number, and this was greatest at day 14. (One-way ANOVA with bonferroni's post test relative to control *p<0.05, **p<0.01, ***p<0.001 n=6)

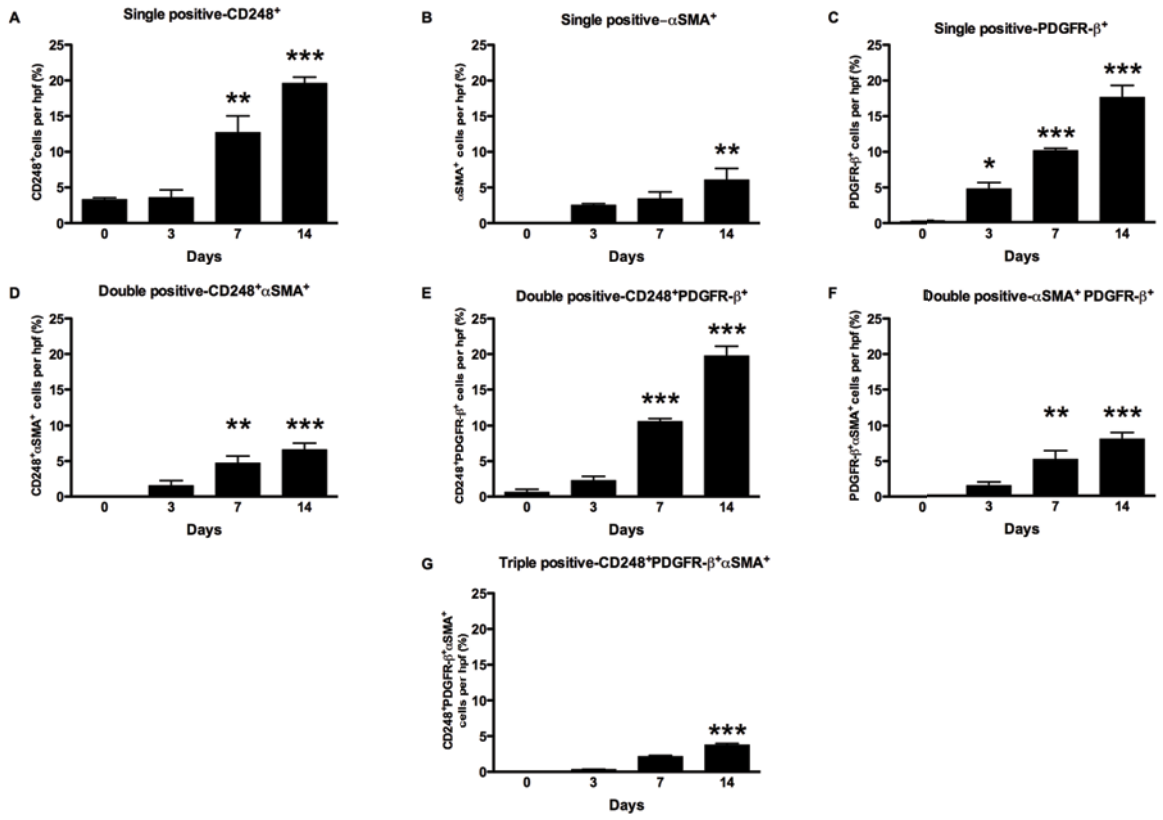

5.3.4 Origin of CD248^{+} stromal cells in the UUO model.

To identify the origin of CD248^{+} stromal cells in the tubulointerstitium in response to renal injury wildtype mice were injected with Bromodeoxyuridine (BrdU). BrdU was observed to be incorporated into proliferating CD248^{+} cells at 7 days following injury (Figure 5.6). BrdU was seen in the cytoplasm of some CD248^{+} cells suggesting that not all of the stromal cells were in S phase of the cell cycle.

To exclude the possibility of a haemopoetic origin for CD248^{+} cell populations, bone marrow chimeras where yellow fluorescent protein (YFP) has been placed under the ubiquitin promoter of all bone marrow derived cells were generated. Renal injury was then performed. CD248 was expressed by resident stromal cells but not by infiltrating (donor) CD45^{+} bone marrow derived cells (Figure 5.7), which suggests that cells expressing CD248 in response to injury originate from the resident stromal cell population.

Figure 5.6

BrdU incorporation into CD248^{+} stromal cells 7 days following UUO

BrdU (green) was seen to be incorporated into the nuclei (blue) of CD248^{+} (red) stromal cells following UUO, appears cyan (arrows). Some CD248+ cells were not in the S phase of cell cycle and consequently BrdU localised to the cytoplasm (n=3). Magnification x 630.

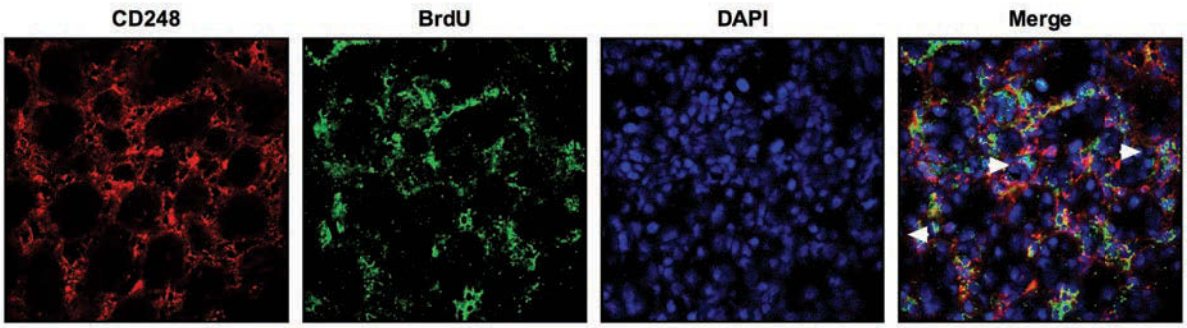

Figure 5.7

CD248^{+} stromal cells are derived from resident cell populations

Bone marrow chimera studies. Tissue from day 14 injured tissues is shown. Yellow fluorescent protein (YFP) (green) co-localises within infiltrating CD45^{+} leucocytes (red) but not within resident CD248^{+} stromal cells (blue). Magnification x400. (n=3)

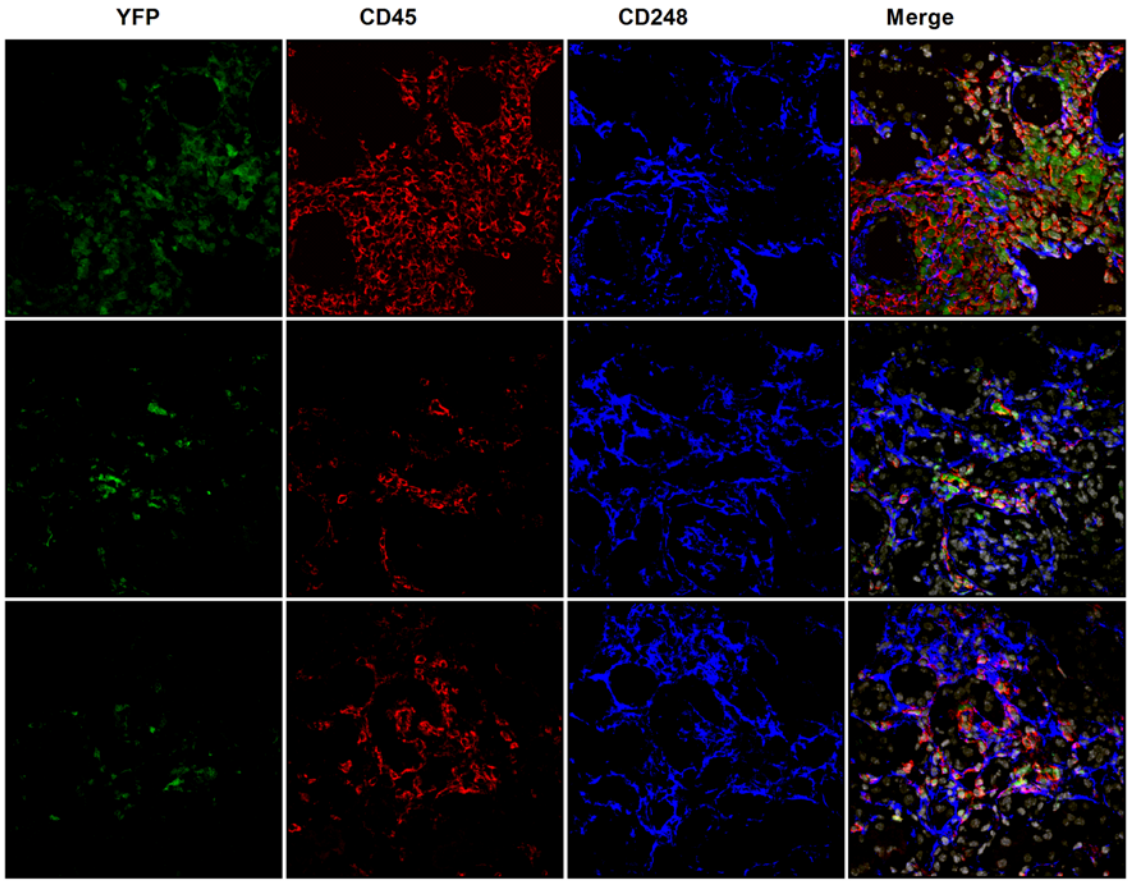

5.3.5 CD248$^{-/-}$ mice are protected against the development of renal fibrosis

The impact of the constitutive removal of CD248 on the evolution of renal injury was assessed. It was established with the use of picosirius red staining that in response to renal injury CD248$^{-/-}$ mice deposited significantly less fibrillary collagen in the tubulointerstitial space by day 14 following the injury. The overall diminishment was measured to be 42% less when compared to wildtype controls (Figure 5.8A). Similarly, Collagen 1a mRNA transcription was significantly increased in wildtype animals following injury but this response was blunted in CD248$^{-/-}$ mice (Figure 5.8B). Interstitial collagen is deposited by myofibroblasts in response to injury. The number of myofibroblasts was, therefore quantified in wildtype and CD248$^{-/-}$ kidney tissue following injury (Figure 5.8D). CD248$^{-/-}$ animals had a significant reduction in the number of interstitial myofibroblasts compared to controls 14 days post UUO.

Leucocyte infiltration was also assessed (Figure 5.9). No significant difference in infiltration by F4/80^{+} macrophages or CD3^{+} T cells was observed in wildtype and CD248$^{-/-}$ mice following injury (Figure 5.9 A and B). As previously observed using chimeric animals CD248 was not co-expressed on infiltrating CD45^{+} cells (Figure 5.9C).

Figure 5.8

Collagen deposition and myofibroblast accumulation

***In vivo* CD248$^{-/-}$ mice accumulate less interstitial collagen and have fewer myofibroblasts than wildtype mice following unilateral ureteric obstruction**

(A) Picosirius red staining of sham operated and UUO day 14 kidney tissue. Magnification x400.

(B) Confocal microscopy images of renal tissue stained for αSMA (red). Nuclei appear grey. Magnification x400

(C) Digital quantification of picosirius red staining expressed as the percentage area of collagen per high power field (hpf). Collagen (red) expression is increased in wildtype and CD248$^{-/-}$ mice following injury. CD248$^{-/-}$ mice deposited significantly less collagen after 14 days of UUO (42% reduction, two way ANOVA, n=6, ***p<0.001, **p<0.01).

(D) Collagen1a (col1a) RNA expression was measured by quantitative polymerase chain reaction on whole kidneys. Results are expressed as mRNA fold change mean +/- SEM relative to the control group (sham operated day 14). In wildtype animals' col1a RNA expression was significantly increased at days 7 and 14 following injury. In CD248$^{-/-}$ mice col1a RNA expression was increased in response to injury but levels were blunted with no significant difference in col1a RNA expression at day 3, 7 and 14. Col1a RNA expression was significantly reduced in CD248$^{-/-}$ mice at day 14 following injury compared expression in wildtype mice (two way ANOVA, n=6, *p<0.05, **p<0.01).

(E) CD248$^{-/-}$ mice had significantly fewer αSMA^{+} myofibroblasts at day 14 following UUO (student t-test, n=6, ***p<0.001)

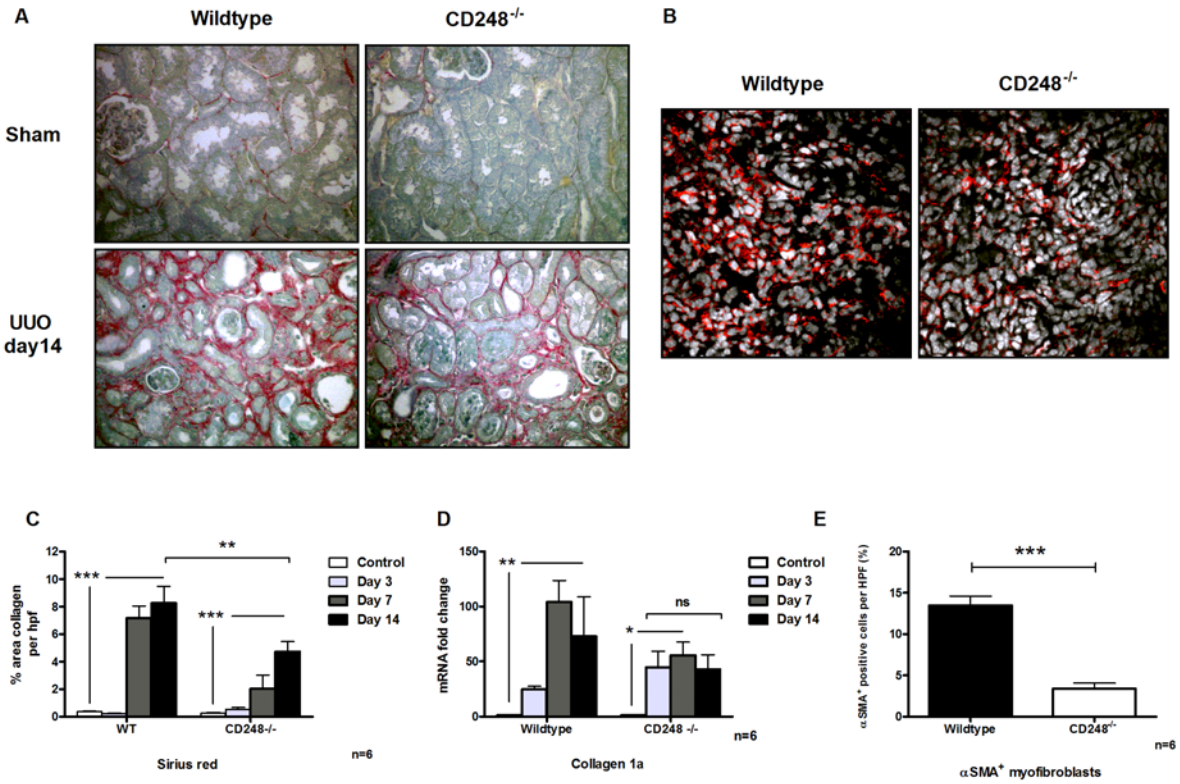

Figure 5.9

Leucocyte infiltration following UUO

No difference in leucocyte infiltration was observed in wildtype and CD248$^{-/-}$ mice following unilateral ureteric obstruction.

(A) F4/80 was used as a marker of murine macrophages. (Ai) F4/80 (brown) expression was increased in the interstitium of wildtype and CD248$^{-/-}$ mice after 14 days UUO when compared to a sham operated day 14 control group. (Aii) F4/80 expression was confirmed by quantitative polymerase chain reaction on whole kidneys. Results are expressed as mRNA fold change mean +/- SEM relative to the control group (sham operated day 14). F4/80 RNA expression in wildtype and CD248$^{-/-}$ was significantly increased following injury but no difference was observed in RNA expression between wildtype and CD248$^{-/-}$ tissue at day 14 (Two way ANOVA, n=6, *p=<0.05, ***p=<0.0001).

(B) CD3 was used as a marker of murine T lymphocytes. (Bi) CD3 (brown) expression was increased in the interstitium of wildtype and CD248$^{-/-}$ mice after 14 days UUO when compared to a sham operated day 14 control group. (Bii) CD3 RNA expression in wildtype and CD248$^{-/-}$ was significantly increased following injury but no difference was observed in RNA expression between wildtype and CD248$^{-/-}$ tissue at day 14.

(C) Confocal microscopy x400 magnification. CD248 (Green) did not co-localise with the pan-leucocyte marker CD45 (red) in wildtype animals following 14 days UUO.

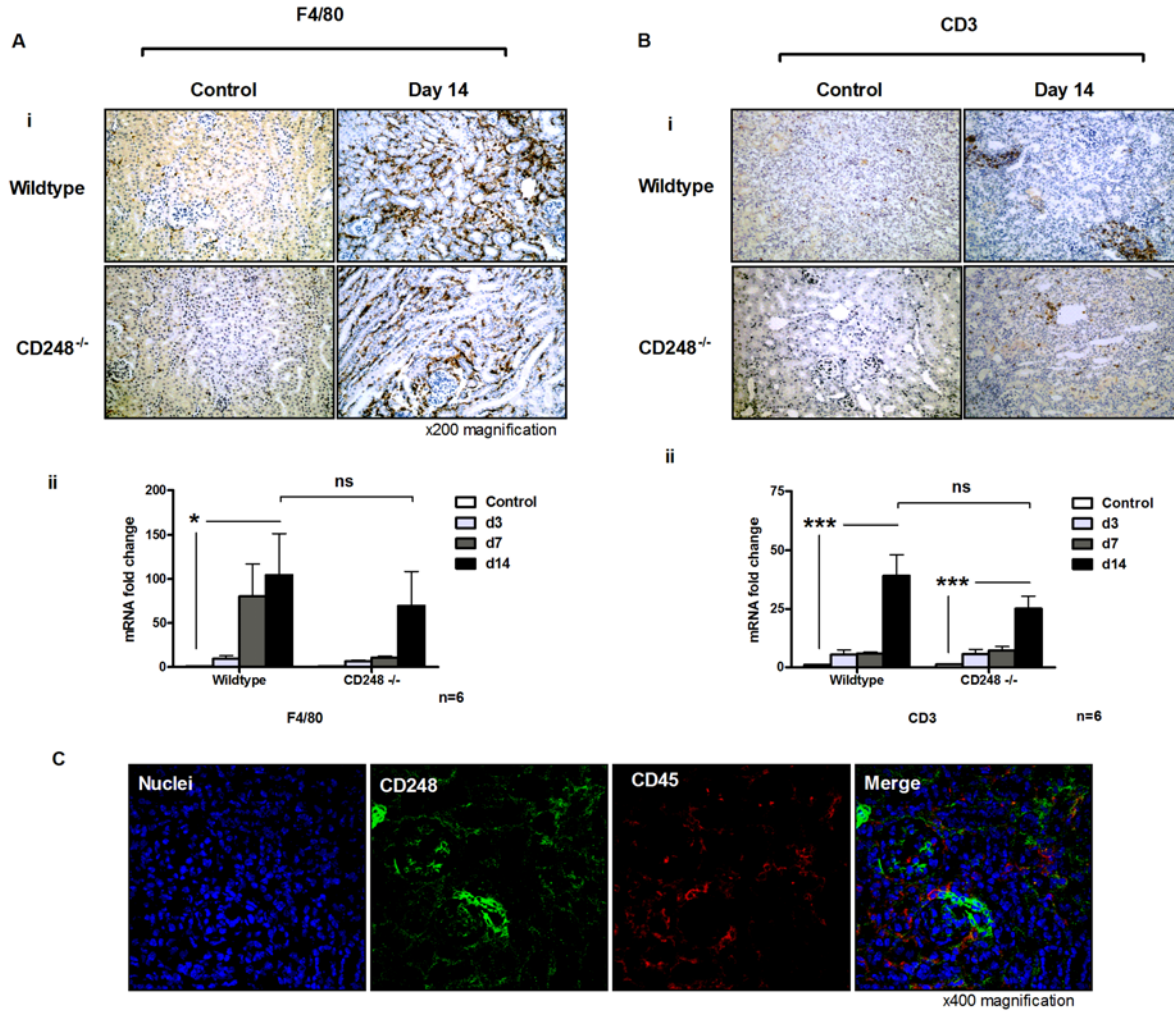

5.3.5 Microvascular rarefaction following injury

Recent work has demonstrated that in response to renal injury pericytes migrate away from the capillary wall into the tubulointerstitium where they differentiate into collagen producing myofibroblasts contributing to fibrotic scar formation (95). The detachment and migration into the tubulointerstitium of pericytes leads to vascular de-stabilisation and ultimately vascular regression (95). These findings directed attention to the architecture of the renal vasculature in $CD248^{-/-}$ mice following injury. Blood vessel area was digitally quantified in wildtype and $CD248^{-/-}$ mice using the endothelial cell marker CD31. Prior to injury no difference could be detected in vessel density between the wildtype and $CD248^{-/-}$ animals (Figure 5.10). Following injury there was an initial increase in vessel density at 3 days post injury followed by progressive vascular regression at 14 days post injury in wildtype animals. These findings were consistent with the vascular regression (microvascular rarefaction) reported by other groups in response to UUO injury (95). In contrast $CD248^{-/-}$ mice were protected from microvascular rarefaction in response to injury and no significant difference in CD31 area could be detected between sham operated animals and day 14 injured animals in the $CD248^{-/-}$ group. In addition to assessing blood vessel area, vessel length was assessed as CD248 has previously been implicated in vessel maturation in response to injury (271). In wildtype animals following day 14 UUO there was evidence of defective vessel maturation and failure of the angiogeneic response to injury. We observed an increase in the number of small vessels (<100μm) but a significant reduction in larger vessels (>200μm) in wildtype animals. In $CD248^{-/-}$ animals this effect was not observed and the vessel lengths seen at day 14 UUO were comparable to those observed in sham-operated animals.

Figure 5.10

Vascular architecture in wildtype and CD248$^{-/-}$ following injury.

Microvascular rarefaction is reduced in CD248$^{-/-}$ mice. CD31^{+} staining in day 14 sham operated or UUO kidney from wildtype (A and B) and CD248$^{-/-}$ mice (C and D). Vessel length was assessed in resting (E) wildtype (F) and CD248$^{-/-}$ mice (G) following sham or UUO at day 14 (two way ANOVA, n=6, **p<0.01, ***p<0.001). Vessel density was assessed at various time points following UUO noted in resting (H) wildtype (I) and CD248$^{-/-}$ mice (J) (one way ANOVA, n=6, *p<0.05 ***p<0.001).

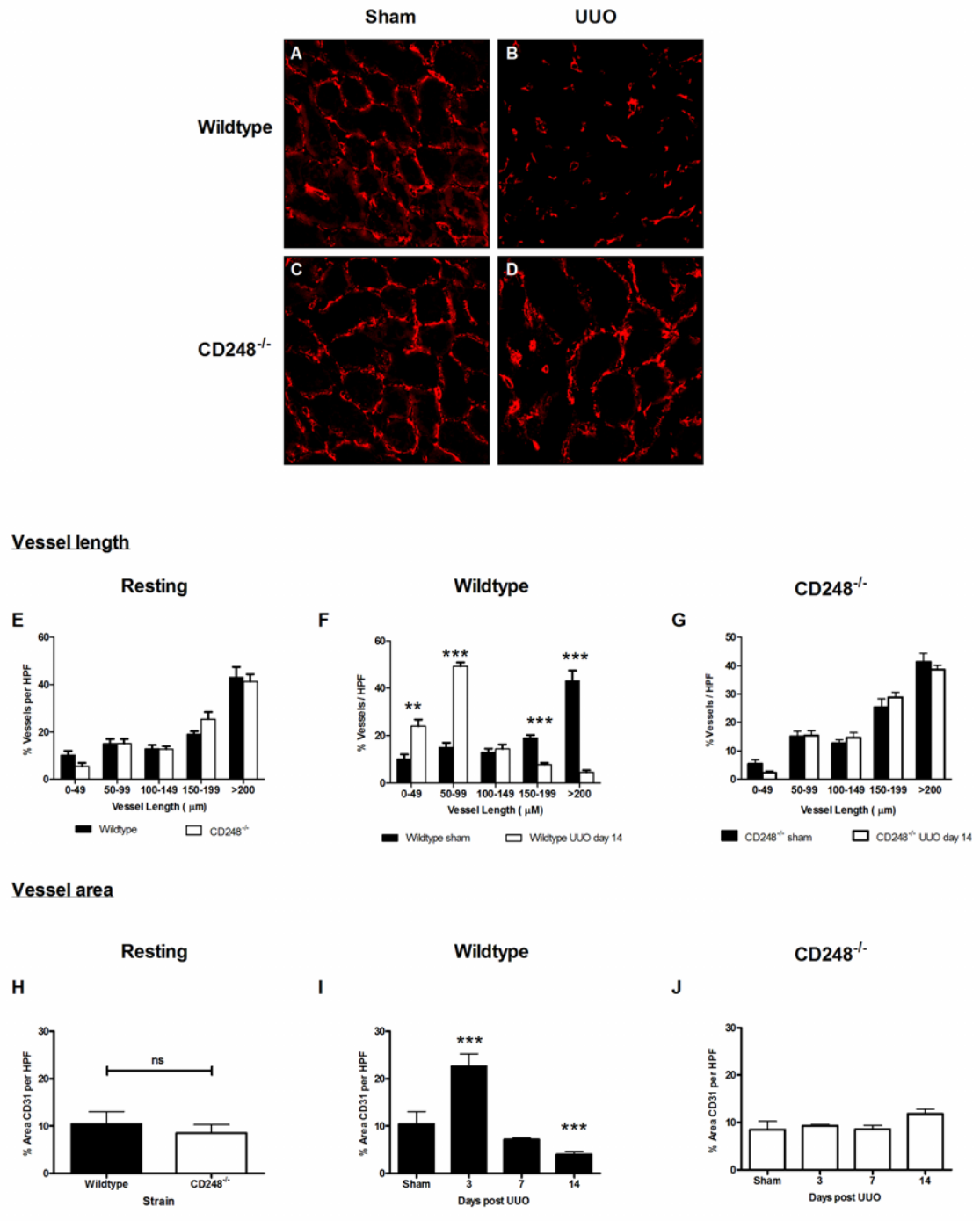

5.4 Discussion

Stromal fibrosis and microvascular rarefaction are reported in both human studies of renal disease and animal models, where they are considered pathomnemonic of progressive CKD (14, 94). In human studies both factors have consistently been reported to associate with a poorer disease outcome (31, 32, 42). Yet until relatively recently the mechanism for these histological associations has remained unclear. Furthermore, there has been significant debate within the literature regarding the origin of activated stromal cells in renal fibrosis with some authors favouring the expansion of resident renal cell populations and others suggesting the infiltration of bone marrow derived cell populations (92, 292). In chapter 3 and 4, I have previously demonstrated that CD248 is expressed on resident renal pericytes in non-inflamed tissue and in inflamed tissue CD248 is seen on αSMA$^+$ myofibroblasts. Here my data shows that the increase in number of CD248$^+$ cells seen in response to renal injury represents the expansion of a resident cell population.

Careful tracking and kinetic modelling studies performed by Lin *et al* have demonstrated that in response to injury, collagen1α1$^+$ pericytes upregulated classical pericyte markers (PDGFRβ, αSMA), upregulated collagen deposition and detached and migrated away from the underlying endothelium to form myofibroblasts. Later studies by the same group using the UUO model have demonstrated that this process is accompanied by microvascular rarefaction as loss of pericytes from the vasculature destabilises the vessel and leads to a failure of reparative angiogenesis (95). A phenotype confirmed here by my studies.

Chen *et al* have also demonstrated that in renal disease, PDGF receptor signalling is involved in pericyte activation, proliferation and differentiation into myofibroblasts(95, 293). The studies reported here mirror the renal phenotype described in the studies by the group of Duffield *et al* targeting PDGF signalling *in vivo.* These demonstrated that both exogenously administered tyrosine kinase inhibitors and endogenously generated soluble PDGFβ receptor ectodomains were protective and stabilised the vasculature(95, 293). Furthermore, blockade of PDGF-BB signalling attenuated microvascular rarefaction and the development of renal fibrosis *in vivo.* CD248 is recognised to be pivotal in pericyte PDGF mediated proliferation (166) and my data in chapter 4 supports this hypothesis.

CD248 is highly expressed in stromal cells found in inflamed tissue but is expressed at low levels in healthy tissue; consequently it is an appealing therapeutic target. Targeting single receptors restricted to pericytes is sufficient in some models to prevent fibrosis(95, 293). Pericyte detachment occurs early in the evolution of renal injury (51); therefore stabilising endothelial/pericyte crosstalk early to prevent proliferation, through the blockade of CD248 may be protective. Maia *et al* have demonstrated using a murine model of arthritis that CD248 contributes to synovial hyperplasia, fibrosis and leukocyte accumulation in inflammatory arthritis and that CD248 may represent a target for the treatment of arthritis (272). In contrast to these reports I did not detect a defect in leucocyte recruitment in the UUO model in CD248-/- mice. CD248 may represent a target for treatment, with the advantage that it may allow modulation of PDGF signalling only on activated stromal cells found in inflamed tissue.

I propose that the constitutive removal of CD248 modulates the stromal renal pericyte functional response to the induction of injury. This serves to stabilise the vasculature and significantly reduces the formation of matrix depositing myofibroblasts. In conclusion, these studies provide further evidence that CD248 expression is increased in response to renal injury by resident renal cell populations and advances our understanding of the functional role CD248 plays in the development of renal fibrosis, thus highlighting CD248 as a novel, stromal cell specific, therapeutic target.

CHAPTER 6

GENERAL DISCUSSION

CHAPTER 6

GENERAL DISCUSSION

6.1 Introduction

The nature of CKD causes it to impact significantly on the quality of life of sufferers and places high demands on the resources of our health care systems. CKD is a significant cause of premature morbidity and mortality. Dominant processes promoting progressive kidney disease, irrespective of the trigger, occur in the renal tubulointerstitial compartment where the deposition of non-functioning fibrotic matrix and microvascular rarefaction are considered hallmarks of progressive disease (5, 94). The stroma plays a key role in the maintenance of normal renal architecture and in the response to injury.

This thesis examined the role of the novel stromal cell marker CD248 in human renal disease and demonstrates that the removal of CD248, at least in an animal model of renal disease, protects against the development of renal fibrosis. In human CKD, CD248 expression increased with disease severity; and expression was linked to known determinants of renal progression. Furthermore, CD248 expression levels can be used to triage patients into those categories that are at the greatest risk of progressing to ESRF. In mice a resident population of stromal cells in the kidney expresses CD248. These cells are pericytes and fibroblasts. In response to injury in mice, as in humans, CD248 expression is increased. *In vitro* the loss of CD248 leads to defects in renal stromal cell function. *In vivo* $CD248^{-/-}$ mice are protected from renal fibrosis and microvascular rarefaction. This phenotype is likely to be due to

stromal cell functional defects in response to growth factor signalling (Figure 6.1). Below the limitations of the current study are examined and discussed and areas for future work are considered.

Figure 6.1

Proposed role of CD248 in the pathogenesis of renal fibrosis

(A) Normal kidney (B) Kidney injury in wildtype mice (C) Kidney injury in CD248$^{-/-}$ mice

In the resting, healthy normal kidney, of wildtype and CD248$^{-/-}$ mice, pericytes are attached to the vasculature where they act to stabilise the endothelium. In response to renal injury (B), resident fibroblasts and pericytes become activated to form matrix-depositing myofibroblasts. Pericytes detach from the endothelium (arrow panel B), destabilising the vasculature causing the vessel to be lost (rarefaction). In CD248$^{-/-}$ mice this process is impaired, and consequently the vasculature is preserved (C) leading to a reduction in myofibroblast numbers and matrix deposition. Resident interstitial fibroblasts also have a reduced proliferative and matrix depositing capacity when CD248 is constitutively removed.

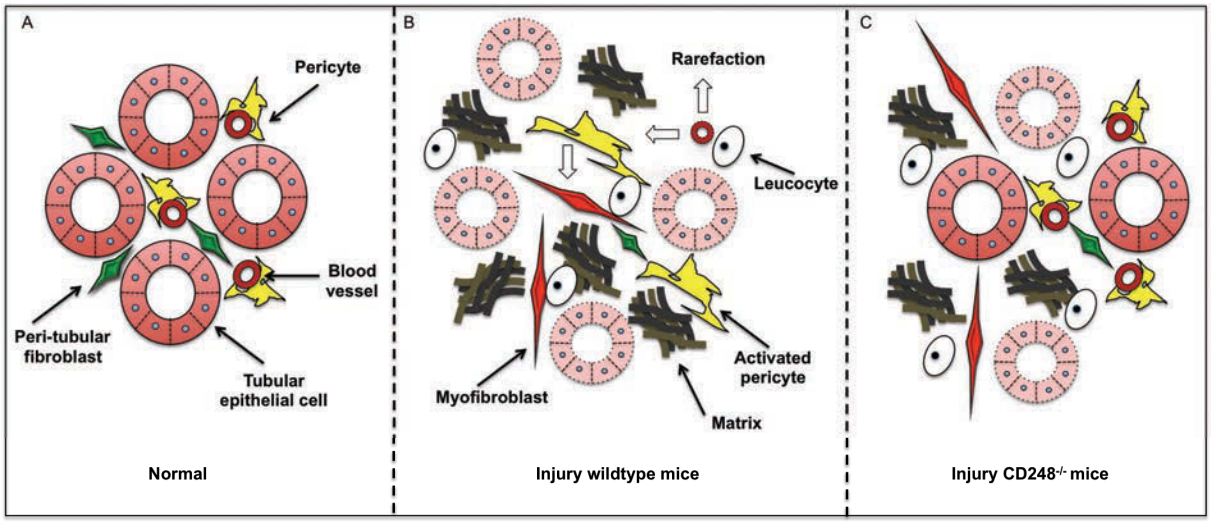

6.2 Limitations and future areas for development

IgA nephropathy has been used as a model of progressive human renal disease in this study. This is because IgA nephropathy has a more predictable clinical time course than many of the other renal diseases; patients are often younger with fewer co-morbidities that could potentially confound data analysis. Other investigators (140) have used this approach previously. CD248 expression was found to increase with

advancing disease, however, as this is only one cause of renal fibrosis this observation needs to be confirmed in a second cohort of patients with progressive renal disease. CD248 expression should also be investigated in non-proteinuric renal disease and in patients who have severely impaired non-progressive renal disease. Blood and urine analysis of CD248 expression could also be explored. Vessel coverage by pericytes using electron microscopy in human disease samples also needs to be performed given the results of the murine studies described here.

In the human tissue samples a number of distinct stromal cell populations were found. These populations were also seen in the murine disease model used in chapter 5. Stromal cell heterogeneity is not a new idea. It has largely been ignored in the renal literature until recently (see chapter 1). The stromal cell subpopulations defined here by CD248 require further study. *In situ* tissue analysis presents difficulties and distinct subpopulations can be hard to describe, especially in inflamed stroma where cells are tightly clustered. Thus these cells need to be isolated and functionally characterised *in vitro.* A detailed understanding of the significance of individual subpopulations is crucial if novel stromal cell targeting therapies are to be developed against renal disease. Indeed, are these distinct cell subpopulations or are the markers used to define them simply markers of cell plasticity or proliferation? It is important to remember that the studies presented here do not remove the cells that express CD248 merely the protein; an important distinction if the results of this work are to be extrapolated to develop treatments for human disease. One approach to isolate $CD248^{+}$ stromal cell populations would be to develop transgenic animals where CD248 is linked to a Cre promoter. These animals could then be bred to

reporter strains of mice that would tag all CD248^{+} cells. This would allow lineage tracing and fate mapping studies to be performed and also facilitate the isolation and identification of CD248^{+} subpopulations. The ultimate aim of these studies would be to modulate, enhance or delete distinct subpopulations of stroma *in vivo* to influence disease outcome.

In Chapter 5 CD248$^{-/-}$ mice were protected against renal fibrosis and microvascular rarefaction following UUO. The results of the UUO model need be repeated in a second model of renal disease preferably in a different mouse strain to validate the observations reported here. It will also be important to know at which stage CD248^{+} stromal cell populations should be targeted for removal in disease models (early versus late disease) as all the studies presented here are in mice that have been born without CD248 and these animals may have adapted to its absence. Therefore, functional blocking and deletion studies of CD248 in wildtype animals are required. Again CD248-Cre mice could be bred to place CD248 under the regulation of the diphtheria toxin receptor (DTR). This would then allow the temporal depletion of CD248 following the induction of renal injury. An alternative approach for consideration would be to inoculate animals with viral vectors capable of generating soluble CD248 ectodomains that block function *in vivo*. These studies would also need to be performed in models that allow the assessment of renal function and possibly death, as simply reducing interstitial collagen and preserving architecture in histological sections may not translate into improvements in disease outcomes and morbidities. The BSAO model piloted in chapter 5 would have allowed these studies to be performed but unfortunately, in my hands, this model failed to induce renal

fibrosis. This could be due to differences in animal strain, dosing schedule or local environmental factors, and further pilot studies are required to optimise this model for use in Birmingham.

The *in vivo* findings shown in Chapter 5 suggest that the renal phenotype seen in $CD248^{-/-}$ mice, following UUO is due to the failure of pericytes to detach from the vasculature in response to injury. This hypothesis is supported by data recently published by Duffield *et al*. However, although I have been able show *in vitro* that loss of CD248 leads to defects in stromal cell function definitive evidence that this is the cause of the *in vivo* phenotype is lacking. Electron micrographs looking at the vasculature to assess pericyte coverage in wildtype and $CD248^{-/-}$ mice following injury may help to resolve this issue. Alternatively, fate mapping of $CD248^{+}$ cells using transgenic mice may help to address this issue further. Additionally, co-culture vascular network forming assays using isolated $CD248^{+}$ stromal cells and endothelial cells would allow CD248 function to be further dissected *in vitro;* and may be more physiologically relevant as it would allow an appreciation of the role CD248 plays in pericyte-endothelial cell crosstalk.

In conclusion, this thesis characterises the role of the stromal cell protein CD248 in healthy and diseased human and murine kidney. A renal phenotype for $CD248^{-/-}$ mice in response to injury has been described and a potential mechanism for this phenotype has been identified. The identification of stromal subsets defined by CD248 *in vivo* is also an intriguing and novel observation. Further work is required to extend the preliminary studies presented here. A greater appreciation of the role

CD248 plays in the evolution of fibrosis may facilitate the development of targeted stromal cell therapies that permit the deletion of activated stromal cell subsets to help prevent or ameliorate the development of CKD and ESRF.

REFERENCE LIST

Reference list

1. Hallan SI, Ritz E, Lydersen S, Romundstad S, Kvenild K, Orth SR. Combining GFR and Albuminuria to Classify CKD Improves Prediction of ESRD. J Am Soc Nephrol. 2009 May 1, 2009;20(5):1069-77.

2. Weiner DE, Tabatabai S, Tighiouart H, Elsayed E, Bansal N, Griffith J, et al. Cardiovascular outcomes and all-cause mortality: exploring the interaction between CKD and cardiovascular disease. Am J Kidney Dis. 2006 Sep;48(3):392-401.

3. Go AS, Chertow GM, Fan D, McCulloch CE, Hsu CY. Chronic kidney disease and the risks of death, cardiovascular events, and hospitalization. N Engl J Med. 2004 Sep 23;351(13):1296-305.

4. El Nahas M. The global challenge of chronic kidney disease. Kidney Int. [Case ReportsClinical Conference]. 2005 Dec;68(6):2918-29.

5. Hewitson TD. Renal tubulointerstitial fibrosis: common but never simple. Am J Physiol Renal Physiol. 2009 Jun;296(6):F1239-44.

6. Lote C. Principles of renal physiology. 4th ed. London: Kluwer Academic publishers; 2000.

7. Schlondorff DO. Overview of factors contributing to the pathophysiology of progressive renal disease. Kidney Int. [Research Support, N.I.H., Extramural

Review]. 2008 Oct;74(7):860-6.

8. Lemley KV, Kriz W. Anatomy of the renal interstitium. Kidney Int. 1991 Mar;39(3):370-81.

9. Madhero88. Physiology of Nephron (public domain). [Wiki] [cited 2011]; Available from: http://en.wikipedia.org/wiki/File:Physiology_of_Nephron.png.

10. Alcorn D, Maric C, McCausland J. Development of the renal interstitium. Pediatr Nephrol. [Research Support, Non-U.S. Gov'tReview]. 1999 May;13(4):347-54.

11. Cullen-McEwen LA, Caruana G, Bertram JF. The where, what and why of the developing renal stroma. Nephron Exp Nephrol. [Review]. 2005;99(1):e1-8.

12. Kaissling B, Hegyi I, Loffing J, Le Hir M. Morphology of interstitial cells in the healthy kidney. Anat Embryol (Berl). 1996 Apr;193(4):303-18.

13. Kaissling B, Le Hir M. The renal cortical interstitium: morphological and functional aspects. Histochem Cell Biol. 2008 Aug;130(2):247-62.

14. Bohle A, Mackensen-Haen S, von Gise H. Significance of tubulointerstitial changes in the renal cortex for the excretory function and concentration ability of the kidney: a morphometric contribution. Am J Nephrol. 1987;7(6):421-33.

15. Nath KA. The tubulointerstitium in progressive renal disease. Kidney Int. [Comment Editorial]. 1998 Sep;54(3):992-4.

16. Taal MW, Omer SA, Nadim MK, Mackenzie HS. Cellular and molecular mediators in common pathway mechanisms of chronic renal disease progression. Curr Opin Nephrol Hypertens. [Research Support, Non-U.S. Gov't Research Support, U.S. Gov't, P.H.S. Review]. 2000 Jul;9(4):323-31.

17. K/DOQI clinical practice guidelines for chronic kidney disease: evaluation, classification, and stratification. Am J Kidney Dis. 2002 Feb;39(2 Suppl 1):S1-266.

18. Atkins RC. The epidemiology of chronic kidney disease. Kidney Int Suppl. [Review]. 2005 Apr(94):S14-8.

19. Tomson CRV, Maggs C. UK Renal Registry 12th Annual Report (December 2009)2010.

20. Lysaght MJ. Maintenance dialysis population dynamics: current trends and long-term implications. Journal of the American Society of Nephrology : JASN. 2002 Jan;13 Suppl 1:S37-40.

21. Hallan SI, Dahl K, Oien CM, Grootendorst DC, Aasberg A, Holmen J, et al. Screening strategies for chronic kidney disease in the general population: follow-up of cross sectional health survey. Bmj. [Research Support, Non-U.S. Gov't]. 2006 Nov 18;333(7577):1047.

22. Mann JF, Gerstein HC, Dulau-Florea I, Lonn E. Cardiovascular risk in patients with mild renal insufficiency. Kidney Int Suppl. [Review]. 2003 May(84):S192-6.

23. Di Angelantonio E, Chowdhury R, Sarwar N, Aspelund T, Danesh J, Gudnason V. Chronic kidney disease and risk of major cardiovascular disease and non-vascular mortality: prospective population based cohort study. Bmj. [Research Support, Non-U.S. Gov't]. 2010;341:c4986.

24. Levey AS, Bosch JP, Lewis JB, Greene T, Rogers N, Roth D, et al. A More Accurate Method To Estimate Glomerular Filtration Rate from Serum Creatinine: A New Prediction Equation. Annals of Internal Medicine. 1999 March 16, 1999;130(6):461-70.

25. Kronenberg F. Emerging risk factors and markers of chronic kidney disease progression. Nat Rev Nephrol. [Research Support, Non-U.S. Gov't Review]. 2009 Dec;5(12):677-89.

26. Taal MW, Brenner BM. Renal risk scores: progress and prospects. Kidney Int. [Review]. 2008 Jun;73(11):1216-9.

27. Peterson JC, Adler S, Burkart JM, Greene T, Hebert LA, Hunsicker LG, et al. Blood pressure control, proteinuria, and the progression of renal disease. The Modification of Diet in Renal Disease Study. Annals of Internal Medicine. [Clinical Trial Randomized Controlled Trial Research Support, U.S. Gov't, P.H.S.]. 1995 Nov 15;123(10):754-62.

28. Randomised placebo-controlled trial of effect of ramipril on decline in glomerular filtration rate and risk of terminal renal failure in proteinuric, non-diabetic nephropathy. The GISEN Group (Gruppo Italiano di Studi Epidemiologici in

Nefrologia). Lancet. [Clinical Trial Randomized Controlled Trial Research Support, Non-U.S. Gov't]. 1997 Jun 28;349(9069):1857-63.

29. Sean Eardley K, Cockwell P. Macrophages and progressive tubulointerstitial disease. Kidney Int. 2005 Aug;68(2):437-55.

30. Abbate M, Zoja C, Remuzzi G. How does proteinuria cause progressive renal damage? J Am Soc Nephrol. 2006 Nov;17(11):2974-84.

31. Eardley KS, Zehnder D, Quinkler M, Lepenies J, Bates RL, Savage CO, et al. The relationship between albuminuria, MCP-1/CCL2, and interstitial macrophages in chronic kidney disease. Kidney Int. 2006 Apr;69(7):1189-97.

32. Eardley KS, Kubal C, Zehnder D, Quinkler M, Lepenies J, Savage CO, et al. The role of capillary density, macrophage infiltration and interstitial scarring in the pathogenesis of human chronic kidney disease. Kidney Int. 2008 Aug;74(4):495-504.

33. Archibald G, Bartlett W, Brown A, Christie B, Elliott A, Griffith K, et al. UK Consensus Conference on Early Chronic Kidney Disease--6 and 7 February 2007. Nephrol Dial Transplant. [Congresses]. 2007 Sep;22(9):2455-7.

34. Gansevoort RT, Matsushita K, van der Velde M, Astor BC, Woodward M, Levey AS, et al. Lower estimated GFR and higher albuminuria are associated with adverse kidney outcomes. A collaborative meta-analysis of general and high-risk

population cohorts. Kidney Int. [Research Support, Non-U.S. Gov't]. 2011 Jul;80(1):93-104.

35. Locatelli F, Marcelli D, Comelli M, Alberti D, Graziani G, Buccianti G, et al. Proteinuria and blood pressure as causal components of progression to end-stage renal failure. Northern Italian Cooperative Study Group. Nephrol Dial Transplant. [Clinical Trial Multicenter Study Randomized Controlled Trial]. 1996 Mar;11(3):461-7.

36. Klag MJ, Whelton PK, Randall BL, Neaton JD, Brancati FL, Ford CE, et al. Blood pressure and end-stage renal disease in men. The New England journal of medicine. [Research Support, Non-U.S. Gov't Research Support, U.S. Gov't, P.H.S.]. 1996 Jan 4;334(1):13-8.

37. Whelton PK, Perneger TV, He J, Klag MJ. The role of blood pressure as a risk factor for renal disease: a review of the epidemiologic evidence. J Hum Hypertens. [Research Support, Non-U.S. Gov't Research Support, U.S. Gov't, P.H.S. Review]. 1996 Oct;10(10):683-9.

38. Vassalotti JA, Stevens LA, Levey AS. Testing for chronic kidney disease: a position statement from the National Kidney Foundation. American journal of kidney diseases : the official journal of the National Kidney Foundation. [Review]. 2007 Aug;50(2):169-80.

39. Tsuboi N, Kawamura T, Ishii T, Utsunomiya Y, Hosoya T. Changes in the glomerular density and size in serial renal biopsies during the progression of IgA

nephropathy. Nephrol Dial Transplant. [Research Support, Non-U.S. Gov't]. 2009 Mar;24(3):892-9.

40. Tsuboi N, Kawamura T, Koike K, Okonogi H, Hirano K, Hamaguchi A, et al. Glomerular density in renal biopsy specimens predicts the long-term prognosis of IgA nephropathy. Clin J Am Soc Nephrol. 2010 Jan;5(1):39-44.

41. Tsuboi N, Kawamura T, Miyazaki Y, Utsunomiya Y, Hosoya T. Low glomerular density is a risk factor for progression in idiopathic membranous nephropathy. Nephrology Dialysis Transplantation. 2011 July 19, 2011.

42. Howie AJ, Ferreira MA, Adu D. Prognostic value of simple measurement of chronic damage in renal biopsy specimens. Nephrol Dial Transplant. 2001 Jun;16(6):1163-9.

43. Fine LG, Bandyopadhay D, Norman JT. Is there a common mechanism for the progression of different types of renal diseases other than proteinuria? Towards the unifying theme of chronic hypoxia. Kidney Int Suppl. [Research Support, Non-U.S. Gov't Review]. 2000 Apr;75:S22-6.

44. Choi YJ, Chakraborty S, Nguyen V, Nguyen C, Kim BK, Shim SI, et al. Peritubular capillary loss is associated with chronic tubulointerstitial injury in human kidney: altered expression of vascular endothelial growth factor. Hum Pathol. [Research Support, Non-U.S. Gov't]. 2000 Dec;31(12):1491-7.

45. Reich HN, Troyanov S, Scholey JW, Cattran DC. Remission of proteinuria improves prognosis in IgA nephropathy. J Am Soc Nephrol. 2007 Dec;18(12):3177-83.

46. Donadio JV, Grande JP. IgA Nephropathy. N Engl J Med. 2002 September 5, 2002;347(10):738-48.

47. Comprehensive clinical nephrology. 4th ed. Floege J, Johnson RJ, Feehally J, editors. London: Mosby; 2011.

48. Lee SB, Kalluri R. Mechanistic connection between inflammation and fibrosis. Kidney Int Suppl. 2010 Dec(119):S22-6.

49. Darby IA, Hewitson TD. Fibroblast differentiation in wound healing and fibrosis. Int Rev Cytol. 2007;257:143-79.

50. Strutz F, Zeisberg M. Renal Fibroblasts and Myofibroblasts in Chronic Kidney Disease. J Am Soc Nephrol. 2006 November 1, 2006;17(11):2992-8.

51. Lin SL, Kisseleva T, Brenner DA, Duffield JS. Pericytes and perivascular fibroblasts are the primary source of collagen-producing cells in obstructive fibrosis of the kidney. Am J Pathol. 2008 Dec;173(6):1617-27.

52. Miller TE, Robinson KB. Experimental pyelonephritis: a new method for inducing pyelonephritis in the rat. J Infect Dis. 1973 Mar;127(3):307-10.

53. Kuncio GS, Neilson EG, Haverty T. Mechanisms of tubulointerstitial fibrosis. Kidney Int. 1991 Mar;39(3):550-6.

54. Duffield JS. Macrophages in kidney repair and regeneration. J Am Soc Nephrol. 2011 Feb;22(2):199-201.

55. Lin SL, Castano AP, Nowlin BT, Lupher ML, Jr., Duffield JS. Bone marrow Ly6Chigh monocytes are selectively recruited to injured kidney and differentiate into functionally distinct populations. J Immunol. 2009 Nov 15;183(10):6733-43.

56. Duffield JS, Tipping PG, Kipari T, Cailhier JF, Clay S, Lang R, et al. Conditional ablation of macrophages halts progression of crescentic glomerulonephritis. Am J Pathol. 2005 Nov;167(5):1207-19.

57. Henderson NC, Mackinnon AC, Farnworth SL, Kipari T, Haslett C, Iredale JP, et al. Galectin-3 expression and secretion links macrophages to the promotion of renal fibrosis. Am J Pathol. 2008 Feb;172(2):288-98.

58. Duffield JS. The inflammatory macrophage: a story of Jekyll and Hyde. Clin Sci (Lond). 2003 Jan;104(1):27-38.

59. Tan TK, Zheng G, Hsu T-T, Wang Y, Lee VWS, Tian X, et al. Macrophage Matrix Metalloproteinase-9 Mediates Epithelial-Mesenchymal Transition in Vitro in Murine Renal Tubular Cells. Am J Pathol. 2010 March 1, 2010;176(3):1256-70.

60. Ricardo SD, van Goor H, Eddy AA. Macrophage diversity in renal injury and repair. J Clin Invest. 2008 Nov;118(11):3522-30.

61. Lee S, Huen S, Nishio H, Nishio S, Lee HK, Choi BS, et al. Distinct macrophage phenotypes contribute to kidney injury and repair. J Am Soc Nephrol. 2011 Feb;22(2):317-26.

62. Duffield JS, Forbes SJ, Constandinou CM, Clay S, Partolina M, Vuthoori S, et al. Selective depletion of macrophages reveals distinct, opposing roles during liver injury and repair. J Clin Invest. 2005 Jan;115(1):56-65.

63. Kurts C, Heymann F, Lukacs-Kornek V, Boor P, Floege J. Role of T cells and dendritic cells in glomerular immunopathology. Semin Immunopathol. 2007 Nov;29(4):317-35.

64. Shappell SB, Gurpinar T, Lechago J, Suki WN, Truong LD. Chronic obstructive uropathy in severe combined immunodeficient (SCID) mice: lymphocyte infiltration is not required for progressive tubulointerstitial injury. J Am Soc Nephrol. 1998 Jun;9(6):1008-17.

65. Lebleu VS, Sugimoto H, Miller CA, Gattone VH, 2nd, Kalluri R. Lymphocytes are dispensable for glomerulonephritis but required for renal interstitial fibrosis in matrix defect-induced Alport renal disease. Lab Invest. 2008 Mar;88(3):284-92.

66. Niedermeier M, Reich B, Rodriguez Gomez M, Denzel A, Schmidbauer K, Gobel N, et al. CD4+ T cells control the differentiation of Gr1+ monocytes into fibrocytes. Proc Natl Acad Sci U S A. 2009 Oct 20;106(42):17892-7.

67. Tapmeier TT, Fearn A, Brown K, Chowdhury P, Sacks SH, Sheerin NS, et al. Pivotal role of CD4+ T cells in renal fibrosis following ureteric obstruction. Kidney Int. 2010 Aug;78(4):351-62.

68. Nikolic-Paterson DJ. CD4+ T cells: a potential player in renal fibrosis. Kidney Int. 2010 Aug;78(4):333-5.

69. Kruger T, Benke D, Eitner F, Lang A, Wirtz M, Hamilton-Williams EE, et al. Identification and functional characterization of dendritic cells in the healthy murine kidney and in experimental glomerulonephritis. J Am Soc Nephrol. 2004 Mar;15(3):613-21.

70. Macconi D, Chiabrando C, Schiarea S, Aiello S, Cassis L, Gagliardini E, et al. Proteasomal processing of albumin by renal dendritic cells generates antigenic peptides. J Am Soc Nephrol. 2009 Jan;20(1):123-30.

71. Kim AH, Markiewicz MA, Shaw AS. New roles revealed for T cells and DCs in glomerulonephritis. J Clin Invest. 2009 May;119(5):1074-6.

72. Heymann F, Meyer-Schwesinger C, Hamilton-Williams EE, Hammerich L, Panzer U, Kaden S, et al. Kidney dendritic cell activation is required for progression

of renal disease in a mouse model of glomerular injury. J Clin Invest. 2009 May;119(5):1286-97.

73. Roberts IS, Brenchley PE. Mast cells: the forgotten cells of renal fibrosis. J Clin Pathol. 2000 Nov;53(11):858-62.

74. Hiromura K, Kurosawa M, Yano S, Naruse T. Tubulointerstitial mast cell infiltration in glomerulonephritis. Am J Kidney Dis. 1998 Oct;32(4):593-9.

75. Sakamoto-Ihara T, Suzuki Y, Kurusu A, Yamashita M, Horikoshi S, Tomino Y. Possible involvement of mast cells in renal fibrosis in patients with IgA nephropathy. Inflamm Res. 2007 Oct;56(10):421-7.

76. Kurusu A, Suzuki Y, Horikoshi S, Shirato I, Tomino Y. Relationship between mast cells in the tubulointerstitium and prognosis of patients with IgA nephropathy. Nephron. 2001 Dec;89(4):391-7.

77. Theoharides TC, Alysandratos KD, Angelidou A, Delivanis DA, Sismanopoulos N, Zhang B, et al. Mast cells and inflammation. Biochim Biophys Acta. 2010 Dec 23.

78. Kondo S, Kagami S, Kido H, Strutz F, Muller GA, Kuroda Y. Role of mast cell tryptase in renal interstitial fibrosis. J Am Soc Nephrol. 2001 Aug;12(8):1668-76.

79. Hochegger K, Siebenhaar F, Vielhauer V, Heininger D, Mayadas TN, Mayer G, et al. Role of mast cells in experimental anti-glomerular basement membrane glomerulonephritis. Eur J Immunol. 2005 Oct;35(10):3074-82.

80. Kanamaru Y, Scandiuzzi L, Essig M, Brochetta C, Guerin-Marchand C, Tomino Y, et al. Mast cell-mediated remodeling and fibrinolytic activity protect against fatal glomerulonephritis. J Immunol. 2006 May 1;176(9):5607-15.

81. Kim DH, Moon SO, Jung YJ, Lee AS, Kang KP, Lee TH, et al. Mast cells decrease renal fibrosis in unilateral ureteral obstruction. Kidney Int. 2009 May;75(10):1031-8.

82. Kanamaru Y, Tamouza H, Pfirsch S, El-Mehdi D, Guerin-Marchand C, Pretolani M, et al. IgA Fc receptor I signals apoptosis through the FcRgamma ITAM and affects tumor growth. Blood. 2007 Jan 1;109(1):203-11.

83. Rodriguez-Iturbe B, Johnson RJ, Herrera-Acosta J. Tubulointerstitial damage and progression of renal failure. Kidney Int Suppl. 2005 Dec(99):S82-6.

84. Burton CJ, Combe C, Walls J, Harris KP. Secretion of chemokines and cytokines by human tubular epithelial cells in response to proteins. Nephrol Dial Transplant. 1999 Nov;14(11):2628-33.

85. Sheerin NS, Sacks SH. Leaked protein and interstitial damage in the kidney: is complement the missing link? Clin Exp Immunol. 2002 Oct;130(1):1-3.

86. Boor P, Konieczny A, Villa L, Schult AL, Bucher E, Rong S, et al. Complement C5 mediates experimental tubulointerstitial fibrosis. J Am Soc Nephrol. 2007 May;18(5):1508-15.

87. Yang L, Besschetnova TY, Brooks CR, Shah JV, Bonventre JV. Epithelial cell cycle arrest in G2/M mediates kidney fibrosis after injury. Nat Med. 2010 May;16(5):535-43, 1p following 143.

88. Li L, Zepeda-Orozco D, Black R, Lin F. Autophagy is a component of epithelial cell fate in obstructive uropathy. Am J Pathol. 2010 Apr;176(4):1767-78.

89. Koesters R, Kaissling B, Lehir M, Picard N, Theilig F, Gebhardt R, et al. Tubular overexpression of transforming growth factor-beta1 induces autophagy and fibrosis but not mesenchymal transition of renal epithelial cells. Am J Pathol. 2010 Aug;177(2):632-43.

90. Docherty NG, O'Sullivan OE, Healy DA, Fitzpatrick JM, Watson RW. Evidence that inhibition of tubular cell apoptosis protects against renal damage and development of fibrosis following ureteric obstruction. Am J Physiol Renal Physiol. 2006 Jan;290(1):F4-13.

91. Strutz FM. EMT and proteinuria as progression factors. Kidney Int. 2009 Mar;75(5):475-81.

92. Kriz W, Kaissling B, Le Hir M. Epithelial-mesenchymal transition (EMT) in kidney fibrosis: fact or fantasy? J Clin Invest. 2011 Feb 1;121(2):468-74.

93. Zeisberg M, Duffield JS. Resolved: EMT produces fibroblasts in the kidney. J Am Soc Nephrol. 2010 Aug;21(8):1247-53.

94. Bohle A, Mackensen-Haen S, Wehrmann M. Significance of postglomerular capillaries in the pathogenesis of chronic renal failure. Kidney Blood Press Res. 1996;19(3-4):191-5.

95. Lin SL, Chang FC, Schrimpf C, Chen YT, Wu CF, Wu VC, et al. Targeting endothelium-pericyte cross talk by inhibiting VEGF receptor signaling attenuates kidney microvascular rarefaction and fibrosis. Am J Pathol. 2011 Feb;178(2):911-23.

96. Ohashi R, Shimizu A, Masuda Y, Kitamura H, Ishizaki M, Sugisaki Y, et al. Peritubular capillary regression during the progression of experimental obstructive nephropathy. J Am Soc Nephrol. 2002 Jul;13(7):1795-805.

97. Nangaku M. Chronic hypoxia and tubulointerstitial injury: a final common pathway to end-stage renal failure. J Am Soc Nephrol. 2006 Jan;17(1):17-25.

98. Rabelink TJ, Wijewickrama DC, de Koning EJ. Peritubular endothelium: the Achilles heel of the kidney? Kidney Int. 2007 Oct;72(8):926-30.

99. Kang DH, Joly AH, Oh SW, Hugo C, Kerjaschki D, Gordon KL, et al. Impaired angiogenesis in the remnant kidney model: I. Potential role of vascular endothelial growth factor and thrombospondin-1. J Am Soc Nephrol. 2001 Jul;12(7):1434-47.

100. Kang DH, Hughes J, Mazzali M, Schreiner GF, Johnson RJ. Impaired angiogenesis in the remnant kidney model: II. Vascular endothelial growth factor administration reduces renal fibrosis and stabilizes renal function. J Am Soc Nephrol. 2001 Jul;12(7):1448-57.

101. Kang DH, Kanellis J, Hugo C, Truong L, Anderson S, Kerjaschki D, et al. Role of the microvascular endothelium in progressive renal disease. J Am Soc Nephrol. 2002 Mar;13(3):806-16.

102. Zeisberg M, Neilson EG. Mechanisms of tubulointerstitial fibrosis. J Am Soc Nephrol. 2010 Nov;21(11):1819-34.

103. Fine LG, Orphanides C, Norman JT. Progressive renal disease: the chronic hypoxia hypothesis. Kidney Int Suppl. 1998 Apr;65:S74-8.

104. Norman JT, Fine LG. Intrarenal oxygenation in chronic renal failure. Clin Exp Pharmacol Physiol. 2006 Oct;33(10):989-96.

105. Kong T, Eltzschig HK, Karhausen J, Colgan SP, Shelley CS. Leukocyte adhesion during hypoxia is mediated by HIF-1-dependent induction of beta2 integrin gene expression. Proc Natl Acad Sci U S A. 2004 Jul 13;101(28):10440-5.

106. Leonard MO, Cottell DC, Godson C, Brady HR, Taylor CT. The role of HIF-1 alpha in transcriptional regulation of the proximal tubular epithelial cell response to hypoxia. J Biol Chem. 2003 Oct 10;278(41):40296-304.

107. Norman JT, Clark IM, Garcia PL. Hypoxia promotes fibrogenesis in human renal fibroblasts. Kidney Int. 2000 Dec;58(6):2351-66.

108. Zeisberg EM, Potenta SE, Sugimoto H, Zeisberg M, Kalluri R. Fibroblasts in kidney fibrosis emerge via endothelial-to-mesenchymal transition. J Am Soc Nephrol. 2008 Dec;19(12):2282-7.

109. Gunaratnam L, Bonventre JV. HIF in kidney disease and development. J Am Soc Nephrol. 2009 Sep;20(9):1877-87.

110. Manotham K, Tanaka T, Matsumoto M, Ohse T, Miyata T, Inagi R, et al. Evidence of tubular hypoxia in the early phase in the remnant kidney model. J Am Soc Nephrol. 2004 May;15(5):1277-88.

111. Higgins DF, Kimura K, Bernhardt WM, Shrimanker N, Akai Y, Hohenstein B, et al. Hypoxia promotes fibrogenesis in vivo via HIF-1 stimulation of epithelial-to-mesenchymal transition. J Clin Invest. 2007 Dec;117(12):3810-20.

112. Kojima I, Tanaka T, Inagi R, Kato H, Yamashita T, Sakiyama A, et al. Protective role of hypoxia-inducible factor-2alpha against ischemic damage and oxidative stress in the kidney. J Am Soc Nephrol. 2007 Apr;18(4):1218-26.

113. Castor CW, Prince RK, Dorstewitz EL. Characteristics of human "fibroblasts" cultivated in vitro from different anatomical sites. Laboratory investigation; a journal of technical methods and pathology. 1962 Sep;11:703-13.

114. Rinn JL, Bondre C, Gladstone HB, Brown PO, Chang HY. Anatomic demarcation by positional variation in fibroblast gene expression programs. PLoS Genet. 2006 Jul;2(7):e119.

115. Chang HY, Chi JT, Dudoit S, Bondre C, van de Rijn M, Botstein D, et al. Diversity, topographic differentiation, and positional memory in human fibroblasts. Proc Natl Acad Sci U S A. 2002 Oct 1;99(20):12877-82.

116. Phipps RP, Penney DP, Keng P, Quill H, Paxhia A, Derdak S, et al. Characterization of two major populations of lung fibroblasts: distinguishing morphology and discordant display of Thy 1 and class II MHC. Am J Respir Cell Mol Biol. 1989 Jul;1(1):65-74.

117. Phipps RP, Borrello MA, Blieden TM. Fibroblast heterogeneity in the periodontium and other tissues. J Periodontal Res. 1997 Jan;32(1 Pt 2):159-65.

118. Okada H, Inoue T, Kanno Y, Kobayashi T, Ban S, Kalluri R, et al. Renal fibroblast-like cells in Goodpasture syndrome rats. Kidney Int. 2001 Aug;60(2):597-606.

119. Qi W, Chen X, Poronnik P, Pollock CA. The renal cortical fibroblast in renal tubulointerstitial fibrosis. Int J Biochem Cell Biol. 2006 Jan;38(1):1-5.

120. Zeisberg M, Strutz F, Muller GA. Role of fibroblast activation in inducing interstitial fibrosis. J Nephrol. 2000 Nov-Dec;13 Suppl 3:S111-20.

121. Wang J, Zohar R, McCulloch CA. Multiple roles of alpha-smooth muscle actin in mechanotransduction. Exp Cell Res. 2006 Feb 1;312(3):205-14.

122. Garin G, Badid C, McGregor B, Vincent M, Guerret S, Zibara K, et al. Ischemia induces early expression of a new transcription factor (6A3-5) in kidney vascular smooth muscle cells: studies in rat and human renal pathology. Am J Pathol. 2003 Dec;163(6):2485-94.

123. Hinz B, Celetta G, Tomasek JJ, Gabbiani G, Chaponnier C. Alpha-smooth muscle actin expression upregulates fibroblast contractile activity. Mol Biol Cell. 2001 Sep;12(9):2730-41.

124. Ronnov-Jessen L, Petersen OW. A function for filamentous alpha-smooth muscle actin: retardation of motility in fibroblasts. J Cell Biol. 1996 Jul;134(1):67-80.

125. Takeji M, Moriyama T, Oseto S, Kawada N, Hori M, Imai E, et al. Smooth Muscle α-Actin Deficiency in Myofibroblasts Leads to Enhanced Renal Tissue Fibrosis. Journal of Biological Chemistry. 2006 December 29, 2006;281(52):40193-200.

126. Iwano M, Plieth D, Danoff TM, Xue C, Okada H, Neilson EG. Evidence that fibroblasts derive from epithelium during tissue fibrosis. J Clin Invest. 2002 Aug;110(3):341-50.

127. Duffield JS, Humphreys BD. Origin of new cells in the adult kidney: results from genetic labeling techniques. Kidney Int. 2011 Mar;79(5):494-501.

128. Bucala R, Spiegel LA, Chesney J, Hogan M, Cerami A. Circulating fibrocytes define a new leukocyte subpopulation that mediates tissue repair. Mol Med. 1994 Nov;1(1):71-81.

129. Wada T, Sakai N, Matsushima K, Kaneko S. Fibrocytes: a new insight into kidney fibrosis. Kidney Int. 2007 Aug;72(3):269-73.

130. Grgic I, Duffield JS, Humphreys BD. The origin of interstitial myofibroblasts in chronic kidney disease. Pediatr Nephrol. 2011 Feb 11.

131. Roufosse C, Bou-Gharios G, Prodromidi E, Alexakis C, Jeffery R, Khan S, et al. Bone marrow-derived cells do not contribute significantly to collagen I synthesis in a murine model of renal fibrosis. J Am Soc Nephrol. 2006 Mar;17(3):775-82.

132. Sakai N, Furuichi K, Shinozaki Y, Yamauchi H, Toyama T, Kitajima S, et al. Fibrocytes are involved in the pathogenesis of human chronic kidney disease. Hum Pathol. 2010;41(5):672-8.

133. Strutz F, Neilson EG. New insights into mechanisms of fibrosis in immune renal injury. Springer Semin Immunopathol. 2003 May;24(4):459-76.

134. Muller GA, Strutz FM. Renal fibroblast heterogeneity. Kidney Int Suppl. 1995 Aug;50:S33-6.

135. Okada H, Inoue T, Suzuki H, Strutz F, Neilson EG. Epithelial-mesenchymal transformation of renal tubular epithelial cells in vitro and in vivo. Nephrol Dial Transplant. 2000;15 Suppl 6:44-6.

136. Strutz F, Okada H, Lo CW, Danoff T, Carone RL, Tomaszewski JE, et al. Identification and characterization of a fibroblast marker: FSP1. J Cell Biol. 1995 Jul;130(2):393-405.

137. Okada H, Danoff TM, Kalluri R, Neilson EG. Early role of Fsp1 in epithelial-mesenchymal transformation. Am J Physiol. 1997 Oct;273(4 Pt 2):F563-74.

138. Inoue T, Plieth D, Venkov CD, Xu C, Neilson EG. Antibodies against macrophages that overlap in specificity with fibroblasts. Kidney Int. [Research Support, N.I.H., Extramural

Research Support, U.S. Gov't, P.H.S.]. 2005 Jun;67(6):2488-93.

139. Iwano M. EMT and TGF-beta in renal fibrosis. Front Biosci (Schol Ed). 2010;2:229-38.

140. Nishitani Y, Iwano M, Yamaguchi Y, Harada K, Nakatani K, Akai Y, et al. Fibroblast-specific protein 1 is a specific prognostic marker for renal survival in patients with IgAN. Kidney Int. 2005 Sep;68(3):1078-85.

141. Kida Y, Duffield JS. Frontiers in Research: Chronic Kidney Diseases: The pivotal role of pericytes in kidney fibrosis. Clin Exp Pharmacol Physiol. 2011 Apr 25.

142. Schrimpf C, Duffield JS. Mechanisms of fibrosis: the role of the pericyte. Curr Opin Nephrol Hypertens. 2011 May;20(3):297-305.

143. Humphreys BD, Lin SL, Kobayashi A, Hudson TE, Nowlin BT, Bonventre JV, et al. Fate tracing reveals the pericyte and not epithelial origin of myofibroblasts in kidney fibrosis. Am J Pathol. 2010 Jan;176(1):85-97.

144. Mayer G. Capillary rarefaction, hypoxia, VEGF and angiogenesis in chronic renal disease. Nephrol Dial Transplant. 2011 Apr;26(4):1132-7.

145. Crisan M, Yap S, Casteilla L, Chen CW, Corselli M, Park TS, et al. A perivascular origin for mesenchymal stem cells in multiple human organs. Cell Stem Cell. 2008 Sep 11;3(3):301-13.

146. Dore-Duffy P, Cleary K. Morphology and properties of pericytes. Methods Mol Biol. 2011;686:49-68.

147. Meyrick B, Reid L. The effect of continued hypoxia on rat pulmonary arterial circulation. An ultrastructural study. Lab Invest. 1978 Feb;38(2):188-200.

148. Courtoy PJ, Boyles J. Fibronectin in the microvasculature: localization in the pericyte-endothelial interstitium. J Ultrastruct Res. 1983 Jun;83(3):258-73.

149. Hughes CC. Endothelial-stromal interactions in angiogenesis. Curr Opin Hematol. 2008 May;15(3):204-9.

150. Diaz-Flores L, Gutierrez R, Madrid JF, Varela H, Valladares F, Acosta E, et al. Pericytes. Morphofunction, interactions and pathology in a quiescent and activated mesenchymal cell niche. Histol Histopathol. 2009 Jul;24(7):909-69.

151. Armulik A, Abramsson A, Betsholtz C. Endothelial/pericyte interactions. Circ Res. 2005 Sep 16;97(6):512-23.

152. Shepro D, Morel NM. Pericyte physiology. FASEB J. 1993 Aug;7(11):1031-8.

153. von Tell D, Armulik A, Betsholtz C. Pericytes and vascular stability. Exp Cell Res. 2006 Mar 10;312(5):623-9.

154. Smith SW, Eardley KS, Croft AP, Nwosu J, Howie AJ, Cockwell P, et al. CD248(+) stromal cells are associated with progressive chronic kidney disease. Kidney Int. 2011 Apr 13.

155. Baluk P, Hashizume H, McDonald DM. Cellular abnormalities of blood vessels as targets in cancer. Curr Opin Genet Dev. 2005 Feb;15(1):102-11.

156. Baluk P, Morikawa S, Haskell A, Mancuso M, McDonald DM. Abnormalities of basement membrane on blood vessels and endothelial sprouts in tumors. Am J Pathol. 2003 Nov;163(5):1801-15.

157. Simonavicius N, Robertson D, Bax DA, Jones C, Huijbers IJ, Isacke CM. Endosialin (CD248) is a marker of tumor-associated pericytes in high-grade glioma. Mod Pathol. 2008 Mar;21(3):308-15.

158. MacFadyen J, Savage K, Wienke D, Isacke CM. Endosialin is expressed on stromal fibroblasts and CNS pericytes in mouse embryos and is downregulated during development. Gene Expr Patterns. 2007 Jan;7(3):363-9.

159. Armulik A, Genove G, Mae M, Nisancioglu MH, Wallgard E, Niaudet C, et al. Pericytes regulate the blood-brain barrier. Nature. 2010 Nov 25;468(7323):557-61.

160. Hellberg C, Ostman A, Heldin CH. PDGF and vessel maturation. Recent Results Cancer Res. 2010;180:103-14.

161. Hirschi KK, D'Amore PA. Pericytes in the microvasculature. Cardiovasc Res. 1996 Oct;32(4):687-98.

162. Synnestvedt K, Furuta GT, Comerford KM, Louis N, Karhausen J, Eltzschig HK, et al. Ecto-5'-nucleotidase (CD73) regulation by hypoxia-inducible factor-1 mediates permeability changes in intestinal epithelia. J Clin Invest. 2002 Oct;110(7):993-1002.

163. MacFadyen JR, Haworth O, Roberston D, Hardie D, Webster MT, Morris HR, et al. Endosialin (TEM1, CD248) is a marker of stromal fibroblasts and is not selectively expressed on tumour endothelium. FEBS Lett. 2005 May 9;579(12):2569-75.

164. Lax S, Hardie DL, Wilson A, Douglas MR, Anderson G, Huso D, et al. The pericyte and stromal cell marker CD248 (endosialin) is required for efficient lymph node expansion. Eur J Immunol. 2010 Jul;40(7):1884-9.

165. Lax S, Hou TZ, Jenkinson E, Salmon M, MacFadyen JR, Isacke CM, et al. CD248/Endosialin is dynamically expressed on a subset of stromal cells during lymphoid tissue development, splenic remodeling and repair. FEBS Lett. 2007 Jul 24;581(18):3550-6.

166. Tomkowicz B, Rybinski K, Sebeck D, Sass P, Nicolaides NC, Grasso L, et al. Endosialin/TEM-1/CD248 regulates pericyte proliferation through PDGF receptor signaling. Cancer Biol Ther. 2010 Jun;9(11):908-15.

167. Demoulin JB. No PDGF receptor signal in pericytes without endosialin? Cancer Biol Ther. 2010 Jun;9(11):916-8.

168. Bergers G, Song S. The role of pericytes in blood-vessel formation and maintenance. Neuro Oncol. 2005 Oct;7(4):452-64.

169. Chan-Ling T, Page MP, Gardiner T, Baxter L, Rosinova E, Hughes S. Desmin Ensheathment Ratio as an Indicator of Vessel Stability: Evidence in Normal Development and in Retinopathy of Prematurity. The American Journal of Pathology. [doi: 10.1016/S0002-9440(10)63389-5]. 2004;165(4):1301-13.

170. Hirschi KK, D'Amore PA. Control of angiogenesis by the pericyte: molecular mechanisms and significance. EXS. 1997;79:419-28.

171. Strutz F, Renziehausen A, Dietrich M, Amin J, Becker V, Heeg M, et al. Cortical fibroblast culture from human biopsies. J Nephrol. 2001 May-Jun;14(3):190-7.

172. Adams RH, Alitalo K. Molecular regulation of angiogenesis and lymphangiogenesis. Nat Rev Mol Cell Biol. 2007 Jun;8(6):464-78.

173. Carmeliet P. Angiogenesis in health and disease. Nat Med. 2003 Jun;9(6):653-60.

174. Zymek P, Bujak M, Chatila K, Cieslak A, Thakker G, Entman ML, et al. The Role of Platelet-Derived Growth Factor Signaling in Healing Myocardial Infarcts. Journal of the American College of Cardiology. [doi: 10.1016/j.jacc.2006.07.060]. 2006;48(11):2315-23.

175. Saunders WB, Bohnsack BL, Faske JB, Anthis NJ, Bayless KJ, Hirschi KK, et al. Coregulation of vascular tube stabilization by endothelial cell TIMP-2 and pericyte TIMP-3. J Cell Biol. 2006 Oct 9;175(1):179-91.

176. Lindblom P, Gerhardt H, Liebner S, Abramsson A, Enge M, Hellstrom M, et al. Endothelial PDGF-B retention is required for proper investment of pericytes in the microvessel wall. Genes Dev. 2003 Aug 1;17(15):1835-40.

177. Hellstrom M, Gerhardt H, Kalen M, Li X, Eriksson U, Wolburg H, et al. Lack of pericytes leads to endothelial hyperplasia and abnormal vascular morphogenesis. J Cell Biol. 2001 Apr 30;153(3):543-53.

178. Hellstrom M, Kalen M, Lindahl P, Abramsson A, Betsholtz C. Role of PDGF-B and PDGFR-beta in recruitment of vascular smooth muscle cells and pericytes during

embryonic blood vessel formation in the mouse. Development. 1999 Jun;126(14):3047-55.

179. Morisada T, Kubota Y, Urano T, Suda T, Oike Y. Angiopoietins and angiopoietin-like proteins in angiogenesis. Endothelium. 2006 Mar-Apr;13(2):71-9.

180. Schlondorff D. The glomerular mesangial cell: an expanding role for a specialized pericyte. FASEB J. 1987 Oct;1(4):272-81.

181. Yamanaka N. Development of the glomerular mesangium. Pediatr Nephrol. 1988 Jan;2(1):85-91.

182. Levéen P, Pekny M, Gebre-Medhin S, Swolin B, Larsson E, Betsholtz C. Mice deficient for PDGF B show renal, cardiovascular, and hematological abnormalities. Genes & Development. 1994 August 15, 1994;8(16):1875-87.

183. Lindahl P, Hellstrom M, Kalen M, Karlsson L, Pekny M, Pekna M, et al. Paracrine PDGF-B/PDGF-Rbeta signaling controls mesangial cell development in kidney glomeruli. Development. 1998 Sep;125(17):3313-22.

184. Stockand JD, Sansom SC. Glomerular mesangial cells: electrophysiology and regulation of contraction. Physiol Rev. 1998 Jul;78(3):723-44.

185. Watanabe S, Yoshimura A, Inui K, Yokota N, Liu Y, Sugenoya Y, et al. Acquisition of the monocyte/macrophage phenotype in human mesangial cells. J Lab Clin Med. 2001 Sep;138(3):193-9.

186. Song B, Niclis JC, Alikhan MA, Sakkal S, Sylvain A, Kerr PG, et al. Generation of Induced Pluripotent Stem Cells from Human Kidney Mesangial Cells. Journal of the American Society of Nephrology. 2011 May 12, 2011.

187. Pallone TL, Silldorff EP. Pericyte regulation of renal medullary blood flow. Exp Nephrol. 2001;9(3):165-70.

188. Crawford C, Kennedy-Lydon TM, Callaghan H, Sprott C, Simmons RL, Sawbridge L, et al. Extracellular nucleotides affect pericyte-mediated regulation of rat in situ vasa recta diameter. Acta Physiol (Oxf). 2011 Jul;202(3):241-51.

189. Little MH. Regrow or repair: potential regenerative therapies for the kidney. J Am Soc Nephrol. 2006 Sep;17(9):2390-401.

190. Grimm PC, Nickerson P, Jeffery J, Savani RC, Gough J, McKenna RM, et al. Neointimal and tubulointerstitial infiltration by recipient mesenchymal cells in chronic renal-allograft rejection. N Engl J Med. 2001 Jul 12;345(2):93-7.

191. Gupta S, Verfaillie C, Chmielewski D, Kim Y, Rosenberg ME. A role for extrarenal cells in the regeneration following acute renal failure. Kidney Int. 2002 Oct;62(4):1285-90.

192. Togel F, Isaac J, Hu Z, Weiss K, Westenfelder C. Renal SDF-1 signals mobilization and homing of CXCR4-positive cells to the kidney after ischemic injury. Kidney Int. 2005 May;67(5):1772-84.

193. Park HC, Yasuda K, Ratliff B, Stoessel A, Sharkovska Y, Yamamoto I, et al. Postobstructive regeneration of kidney is derailed when surge in renal stem cells during course of unilateral ureteral obstruction is halted. Am J Physiol Renal Physiol. 2010 Feb;298(2):F357-64.

194. Tolar J, Le Blanc K, Keating A, Blazar BR. Concise review: hitting the right spot with mesenchymal stromal cells. Stem Cells. 2010 Aug;28(8):1446-55.

195. Semedo P, Correa-Costa M, Antonio Cenedeze M, Maria Avancini Costa Malheiros D, Antonia dos Reis M, Shimizu MH, et al. Mesenchymal stem cells attenuate renal fibrosis through immune modulation and remodeling properties in a rat remnant kidney model. Stem Cells. 2009 Dec;27(12):3063-73.

196. Ninichuk V, Gross O, Segerer S, Hoffmann R, Radomska E, Buchstaller A, et al. Multipotent mesenchymal stem cells reduce interstitial fibrosis but do not delay progression of chronic kidney disease in collagen4A3-deficient mice. Kidney Int. 2006 Jul;70(1):121-9.

197. Sorokin L. The impact of the extracellular matrix on inflammation. Nat Rev Immunol. 2010 Oct;10(10):712-23.

198. Eddy AA. Molecular insights into renal interstitial fibrosis. J Am Soc Nephrol. 1996 Dec;7(12):2495-508.

199. Johnson TS, Skill NJ, El Nahas AM, Oldroyd SD, Thomas GL, Douthwaite JA, et al. Transglutaminase transcription and antigen translocation in experimental renal scarring. J Am Soc Nephrol. 1999 Oct;10(10):2146-57.

200. Johnson TS, El-Koraie AF, Skill NJ, Baddour NM, El Nahas AM, Njloma M, et al. Tissue transglutaminase and the progression of human renal scarring. J Am Soc Nephrol. 2003 Aug;14(8):2052-62.

201. Shweke N, Boulos N, Jouanneau C, Vandermeersch S, Melino G, Dussaule JC, et al. Tissue transglutaminase contributes to interstitial renal fibrosis by favoring accumulation of fibrillar collagen through TGF-beta activation and cell infiltration. Am J Pathol. 2008 Sep;173(3):631-42.

202. Mooradian DL, Lucas RC, Weatherbee JA, Furcht LT. Transforming growth factor-beta 1 binds to immobilized fibronectin. J Cell Biochem. 1989 Dec;41(4):189-200.

203. Weathington NM, van Houwelingen AH, Noerager BD, Jackson PL, Kraneveld AD, Galin FS, et al. A novel peptide CXCR ligand derived from extracellular matrix degradation during airway inflammation. Nat Med. 2006 Mar;12(3):317-23.

204. Ronco P, Lelongt B, Piedagnel R, Chatziantoniou C. Matrix metalloproteinases in kidney disease progression and repair: a case of flipping the coin. Semin Nephrol. 2007 May;27(3):352-62.

205. Catania JM, Chen G, Parrish AR. Role of matrix metalloproteinases in renal pathophysiologies. Am J Physiol Renal Physiol. 2007 Mar;292(3):F905-11.

206. Eddy AA. Plasminogen activator inhibitor-1 and the kidney. Am J Physiol Renal Physiol. 2002 Aug;283(2):F209-20.

207. Eddy AA, Fogo AB. Plasminogen activator inhibitor-1 in chronic kidney disease: evidence and mechanisms of action. J Am Soc Nephrol. 2006 Nov;17(11):2999-3012.

208. Zhang G, Kernan KA, Collins SJ, Cai X, Lopez-Guisa JM, Degen JL, et al. Plasmin(ogen) promotes renal interstitial fibrosis by promoting epithelial-to-mesenchymal transition: role of plasmin-activated signals. J Am Soc Nephrol. 2007 Mar;18(3):846-59.

209. Mott JD, Werb Z. Regulation of matrix biology by matrix metalloproteinases. Curr Opin Cell Biol. 2004 Oct;16(5):558-64.

210. Somerville RP, Oblander SA, Apte SS. Matrix metalloproteinases: old dogs with new tricks. Genome Biol. 2003;4(6):216.

211. Wang X, Zhou Y, Tan R, Xiong M, He W, Fang L, et al. Mice lacking the matrix metalloproteinase-9 gene reduce renal interstitial fibrosis in obstructive nephropathy. Am J Physiol Renal Physiol. 2010 Nov;299(5):F973-82.

212. Nishida M, Okumura Y, Ozawa S, Shiraishi I, Itoi T, Hamaoka K. MMP-2 inhibition reduces renal macrophage infiltration with increased fibrosis in UUO. Biochem Biophys Res Commun. 2007 Mar 2;354(1):133-9.

213. Kassiri Z, Oudit GY, Kandalam V, Awad A, Wang X, Ziou X, et al. Loss of TIMP3 enhances interstitial nephritis and fibrosis. J Am Soc Nephrol. 2009 Jun;20(6):1223-35.

214. Kim H, Oda T, Lopez-Guisa J, Wing D, Edwards DR, Soloway PD, et al. TIMP-1 deficiency does not attenuate interstitial fibrosis in obstructive nephropathy. J Am Soc Nephrol. 2001 Apr;12(4):736-48.

215. Chung AC, Lan HY. Chemokines in renal injury. J Am Soc Nephrol. 2011 May;22(5):802-9.

216. Kitching AR, Holdsworth SR, Hickey MJ. Targeting leukocytes in immune glomerular diseases. Curr Med Chem. 2008;15(5):448-58.

217. Holdsworth SR, Tipping PG. Leukocytes in glomerular injury. Semin Immunopathol. 2007 Nov;29(4):355-74.

218. Eardley KS, Smith SW, Cockwell P. Chemokines in vasculitis. Front Biosci (Elite Ed). 2009;1:26-35.

219. Vielhauer V, Anders HJ. Chemokines and chemokine receptors as therapeutic targets in chronic kidney disease. Front Biosci (Schol Ed). 2009;1:1-12.

220. Anders HJ, Vielhauer V, Schlondorff D. Chemokines and chemokine receptors are involved in the resolution or progression of renal disease. Kidney Int. 2003 Feb;63(2):401-15.

221. Schneider A, Harendza S, Zahner G, Jocks T, Wenzel U, Wolf G, et al. Cyclooxygenase metabolites mediate glomerular monocyte chemoattractant protein-1 formation and monocyte recruitment in experimental glomerulonephritis. Kidney Int. 1999 Feb;55(2):430-41.

222. Shimizu H, Maruyama S, Yuzawa Y, Kato T, Miki Y, Suzuki S, et al. Anti-monocyte chemoattractant protein-1 gene therapy attenuates renal injury induced by protein-overload proteinuria. J Am Soc Nephrol. 2003 Jun;14(6):1496-505.

223. Boor P, Floege J. Special Series: Chronic Kidney Disease Growth Factors in Renal Fibrosis. Clin Exp Pharmacol Physiol. 2011 Jan 29.

224. Patel SR, Dressler GR. BMP7 signaling in renal development and disease. Trends Mol Med. 2005 Nov;11(11):512-8.

225. Chen XM, Qi W, Pollock CA. CTGF and chronic kidney fibrosis. Front Biosci (Schol Ed). 2009;1:132-41.

226. Ostendorf T, Eitner F, Floege J. The PDGF family in renal fibrosis. Pediatr Nephrol. 2011 May 21.

227. Strutz F. The role of FGF-2 in renal fibrogenesis. Front Biosci (Schol Ed). 2009;1:125-31.

228. Liu Y. Hepatocyte growth factor in kidney fibrosis: therapeutic potential and mechanisms of action. Am J Physiol Renal Physiol. 2004 Jul;287(1):F7-16.

229. Boor P, Ostendorf T, Floege J. Renal fibrosis: novel insights into mechanisms and therapeutic targets. Nat Rev Nephrol. 2010 Nov;6(11):643-56.

230. Bottinger EP, Miao J, Schiffer M, Bitzer M, Roberts IS. Transforming growth factor beta signal transduction in the kidney. Kidney Blood Press Res. 1998;21(2-4):259-61.

231. Lim CS, Kim YS, Chae DW, Ahn C, Han JS, Kim S, et al. Association of C-509T and T869C polymorphisms of transforming growth factor-beta1 gene with susceptibility to and progression of IgA nephropathy. Clin Nephrol. 2005 Feb;63(2):61-7.

232. Gagliardini E, Benigni A. Role of anti-TGF-beta antibodies in the treatment of renal injury. Cytokine Growth Factor Rev. 2006 Feb-Apr;17(1-2):89-96.

233. Lee SB, Kanasaki K, Kalluri R. Circulating TGF-beta1 as a reliable biomarker for chronic kidney disease progression in the African-American population. Kidney Int. 2009 Jul;76(1):10-2.

234. Bottinger EP, Bitzer M. TGF-beta signaling in renal disease. J Am Soc Nephrol. 2002 Oct;13(10):2600-10.

235. Yang J, Zhang X, Li Y, Liu Y. Downregulation of Smad transcriptional corepressors SnoN and Ski in the fibrotic kidney: an amplification mechanism for TGF-beta1 signaling. J Am Soc Nephrol. 2003 Dec;14(12):3167-77.

236. Leonard EC, Friedrich JL, Basile DP. VEGF-121 preserves renal microvessel structure and ameliorates secondary renal disease following acute kidney injury. Am J Physiol Renal Physiol. 2008 Dec;295(6):F1648-57.

237. Eremina V, Sood M, Haigh J, Nagy A, Lajoie G, Ferrara N, et al. Glomerular-specific alterations of VEGF-A expression lead to distinct congenital and acquired renal diseases. J Clin Invest. 2003 Mar;111(5):707-16.

238. Zhu X, Wu S, Dahut WL, Parikh CR. Risks of proteinuria and hypertension with bevacizumab, an antibody against vascular endothelial growth factor: systematic review and meta-analysis. Am J Kidney Dis. 2007 Feb;49(2):186-93.

239. Floege J, Eitner F, Alpers CE. A new look at platelet-derived growth factor in renal disease. J Am Soc Nephrol. 2008 Jan;19(1):12-23.

240. Floege J, Johnson RJ. Multiple roles for platelet-derived growth factor in renal disease. Miner Electrolyte Metab. 1995;21(4-5):271-82.

241. Rettig WJ, Garin-Chesa P, Healey JH, Su SL, Jaffe EA, Old LJ. Identification of endosialin, a cell surface glycoprotein of vascular endothelial cells in human cancer. Proc Natl Acad Sci U S A. 1992 Nov 15;89(22):10832-6.

242. St Croix B, Rago C, Velculescu V, Traverso G, Romans KE, Montgomery E, et al. Genes expressed in human tumor endothelium. Science. 2000 Aug 18;289(5482):1197-202.

243. Huber MA, Kraut N, Schweifer N, Dolznig H, Peter RU, Schubert RD, et al. Expression of stromal cell markers in distinct compartments of human skin cancers. Journal of cutaneous pathology. 2006 Feb;33(2):145-55.

244. Rupp C, Dolznig H, Puri C, Schweifer N, Sommergruber W, Kraut N, et al. Laser capture microdissection of epithelial cancers guided by antibodies against fibroblast activation protein and endosialin. Diagn Mol Pathol. 2006 Mar;15(1):35-42.

245. Dolznig H, Schweifer N, Puri C, Kraut N, Rettig WJ, Kerjaschki D, et al. Characterization of cancer stroma markers: in silico analysis of an mRNA expression database for fibroblast activation protein and endosialin. Cancer Immun. 2005;5:10.

246. Brady J, Neal J, Sadakar N, Gasque P. Human endosialin (tumor endothelial marker 1) is abundantly expressed in highly malignant and invasive brain tumors. J Neuropathol Exp Neurol. 2004 Dec;63(12):1274-83.

247. Carson-Walter EB, Watkins DN, Nanda A, Vogelstein B, Kinzler KW, St Croix B. Cell surface tumor endothelial markers are conserved in mice and humans. Cancer Res. 2001 Sep 15;61(18):6649-55.

248. Watkins NA, Gusnanto A, de Bono B, De S, Miranda-Saavedra D, Hardie DL, et al. A HaemAtlas: characterizing gene expression in differentiated human blood cells. Blood. 2009 May 7, 2009;113(19):e1-9.

249. Conejo-Garcia JR, Buckanovich RJ, Benencia F, Courreges MC, Rubin SC, Carroll RG, et al. Vascular leukocytes contribute to tumor vascularization. Blood. 2005 January 15, 2005;105(2):679-81.

250. Shih IM. The role of CD146 (Mel-CAM) in biology and pathology. J Pathol. 1999 Sep;189(1):4-11.

251. Opavsky R, Haviernik P, Jurkovicova D, Garin MT, Copeland NG, Gilbert DJ, et al. Molecular characterization of the mouse Tem1/endosialin gene regulated by cell density in vitro and expressed in normal tissues in vivo. J Biol Chem. 2001 Oct 19;276(42):38795-807.

252. Christian S, Ahorn H, Koehler A, Eisenhaber F, Rodi HP, Garin-Chesa P, et al. Molecular cloning and characterization of endosialin, a C-type lectin-like cell surface receptor of tumor endothelium. J Biol Chem. 2001 Mar 9;276(10):7408-14.

253. MacFadyen JR. Characterisation of endosialin (CD248) in angiogenesis [PhD]. London: Univeristy College London; 2007.

254. Drickamer K. C-type lectin-like domains. Current opinion in structural biology. 1999 Oct;9(5):585-90.

255. Greenlee MC, Sullivan SA, Bohlson SS. CD93 and related family members: their role in innate immunity. Curr Drug Targets. 2008 Feb;9(2):130-8.

256. Isermann B, Hendrickson SB, Zogg M, Wing M, Cummiskey M, Kisanuki YY, et al. Endothelium-specific loss of murine thrombomodulin disrupts the protein C anticoagulant pathway and causes juvenile-onset thrombosis. J Clin Invest. 2001 Aug;108(4):537-46.

257. Conway EM, Van de Wouwer M, Pollefeyt S, Jurk K, Van Aken H, De Vriese A, et al. The lectin-like domain of thrombomodulin confers protection from neutrophil-mediated tissue damage by suppressing adhesion molecule expression via nuclear factor kappaB and mitogen-activated protein kinase pathways. J Exp Med. 2002 Sep 2;196(5):565-77.

258. Van de Wouwer M, Conway EM. Novel functions of thrombomodulin in inflammation. Crit Care Med. 2004 May;32(5 Suppl):S254-61.

259. Kim TS, Park M, Nepomuceno RR, Palmarini G, Winokur S, Cotman CA, et al. Characterization of the murine homolog of C1qR(P): identical cellular expression pattern, chromosomal location and functional activity of the human and murine C1qR(P). Mol Immunol. 2000 May;37(7):377-89.

260. Dean YD, McGreal EP, Akatsu H, Gasque P. Molecular and cellular properties of the rat AA4 antigen, a C-type lectin-like receptor with structural homology to thrombomodulin. J Biol Chem. 2000 Nov 3;275(44):34382-92.

261. Fonseca MI, Carpenter PM, Park M, Palmarini G, Nelson EL, Tenner AJ. C1qR(P), a myeloid cell receptor in blood, is predominantly expressed on endothelial cells in human tissue. Journal of leukocyte biology. 2001 Nov;70(5):793-800.

262. Dean YD, McGreal EP, Gasque P. Endothelial cells, megakaryoblasts, platelets and alveolar epithelial cells express abundant levels of the mouse AA4 antigen, a C-type lectin-like receptor involved in homing activities and innate immune host defense. Eur J Immunol. 2001 May;31(5):1370-81.

263. Nepomuceno RR, Tenner AJ. C1qRP, the C1q receptor that enhances phagocytosis, is detected specifically in human cells of myeloid lineage, endothelial cells, and platelets. J Immunol. 1998 Feb 15;160(4):1929-35.

264. Mura M, Swain RK, Zhuang X, Vorschmitt H, Reynolds G, Durant S, et al. Identification and angiogenic role of the novel tumor endothelial marker CLEC14A. Oncogene. 2011 Jun 27.

265. Rho SS, Choi HJ, Min JK, Lee HW, Park H, Kim YM, et al. Clec14a is specifically expressed in endothelial cells and mediates cell to cell adhesion. Biochem Biophys Res Commun. 2011 Jan 7;404(1):103-8.

266. Christian S, Winkler R, Helfrich I, Boos AM, Besemfelder E, Schadendorf D, et al. Endosialin (Tem1) is a marker of tumor-associated myofibroblasts and tumor vessel-associated mural cells. Am J Pathol. 2008 Feb;172(2):486-94.

267. Ohradanova A, Gradin K, Barathova M, Zatovicova M, Holotnakova T, Kopacek J, et al. Hypoxia upregulates expression of human endosialin gene via hypoxia-inducible factor 2. Br J Cancer. 2008 Oct 21;99(8):1348-56.

268. Tomkowicz B, Rybinski K, Foley B, Ebel W, Kline B, Routhier E, et al. Interaction of endosialin/TEM1 with extracellular matrix proteins mediates cell adhesion and migration. Proc Natl Acad Sci U S A. 2007 Nov 13;104(46):17965-70.

269. Becker R, Lenter MC, Vollkommer T, Boos AM, Pfaff D, Augustin HG, et al. Tumor stroma marker endosialin (Tem1) is a binding partner of metastasis-related protein Mac-2 BP/90K. FASEB J. 2008 Aug;22(8):3059-67.

270. Huang H-P, Hong C-L, Kao C-Y, Lin S-W, Lin S-R, Wu H-L, et al. Gene targeting and expression analysis of mouse Tem1/endosialin using a lacZ reporter. Gene Expression Patterns. [doi: 10.1016/j.gep.2011.03.001].11(5-6):316-26.

271. Nanda A, Karim B, Peng Z, Liu G, Qiu W, Gan C, et al. Tumor endothelial marker 1 (Tem1) functions in the growth and progression of abdominal tumors. Proc Natl Acad Sci U S A. 2006 Feb 28;103(9):3351-6.

272. Maia M, de Vriese A, Janssens T, Moons M, van Landuyt K, Tavernier J, et al. CD248 and its cytoplasmic domain: a therapeutic target for arthritis. Arthritis Rheum. 2010 Dec;62(12):3595-606.

273. Maia M, Devriese A, Janssens T, Moons M, Lories RJ, Tavernier J, et al. CD248 facilitates tumor growth via its cytoplasmic domain. BMC Cancer. 2011;11:162.

274. Carson-Walter EB, Winans BN, Whiteman MC, Liu Y, Jarvela S, Haapasalo H, et al. Characterization of TEM1/endosialin in human and murine brain tumors. BMC Cancer. 2009;9:417.

275. Zhang ZY, Zhang H, Adell G, Sun XF. Endosialin expression in relation to clinicopathological and biological variables in rectal cancers with a Swedish clinical trial of preoperative radiotherapy. BMC Cancer. 2011;11:89.

276. Rouleau C, Smale R, Fu YS, Hui G, Wang F, Hutto E, et al. Endosialin is expressed in high grade and advanced sarcomas: evidence from clinical specimens and preclinical modeling. Int J Oncol. 2011 Jul;39(1):73-89.

277. Davies G, Cunnick GH, Mansel RE, Mason MD, Jiang WG. Levels of expression of endothelial markers specific to tumour-associated endothelial cells and their correlation with prognosis in patients with breast cancer. Clin Exp Metastasis. 2004;21(1):31-7.

278. Watkins NA, Gusnanto A, de Bono B, De S, Miranda-Saavedra D, Hardie DL, et al. A HaemAtlas: characterizing gene expression in differentiated human blood cells. Blood. 2009 May 7;113(19):e1-9.

279. Bagley RG, Rouleau C, St Martin T, Boutin P, Weber W, Ruzek M, et al. Human endothelial precursor cells express tumor endothelial marker 1/endosialin/CD248. Mol Cancer Ther. 2008 Aug;7(8):2536-46.

280. Bagley RG, Weber W, Rouleau C, Yao M, Honma N, Kataoka S, et al. Human mesenchymal stem cells from bone marrow express tumor endothelial and stromal markers. Int J Oncol. 2009 Mar;34(3):619-27.

281. Hardie DL, Baldwin MJ, Naylor A, Haworth OJ, Hou TZ, Lax S, et al. The stromal cell antigen CD248 (endosialin) is expressed on naive CD8(+) human T cells and regulates proliferation. Immunology. 2011 Jul;133(3):288-95.

282. Rouleau C, Curiel M, Weber W, Smale R, Kurtzberg L, Mascarello J, et al. Endosialin protein expression and therapeutic target potential in human solid tumors: sarcoma versus carcinoma. Clin Cancer Res. 2008 Nov 15;14(22):7223-36.

283. Grimwood L, Masterson R. Propagation and Culture of Renal Fibroblasts. In: Becker GJ, Hewitson TD, editors. Kidney Research: Humana Press; 2009. p. 1-13.

284. Bradford MM. A rapid and sensitive method for the quantitation of microgram quantities of protein utilizing the principle of protein-dye binding. Anal Biochem. 1976 May 7;72:248-54.

285. Takemoto M, Asker N, Gerhardt H, Lundkvist A, Johansson BR, Saito Y, et al. A new method for large scale isolation of kidney glomeruli from mice. Am J Pathol. 2002 Sep;161(3):799-805.

286. Heng ECK, Huang Y, Black SA, Trackman PC. CCN2, connective tissue growth factor, stimulates collagen deposition by gingival fibroblasts via module 3 and α6- and β1 integrins. Journal of Cellular Biochemistry. 2006;98(2):409-20.

287. Eddy AA, Kim H, Lopez-Guisa J, Oda T, Soloway PD. Interstitial fibrosis in mice with overload proteinuria: deficiency of TIMP-1 is not protective. Kidney Int. 2000 Aug;58(2):618-28.

288. Eddy AA, Geary DF, Balfe JW, Clark WF, Baumal R. Prolongation of acute renal failure in two patients with hemolytic-uremic syndrome due to excessive plasma infusion therapy. Pediatr Nephrol. [Case Reports

Research Support, Non-U.S. Gov't]. 1989 Oct;3(4):420-3.

289. Chevalier RL, Forbes MS, Thornhill BA. Ureteral obstruction as a model of renal interstitial fibrosis and obstructive nephropathy. Kidney Int. 2009 Jun;75(11):1145-52.

290. Bascands JL, Schanstra JP. Obstructive nephropathy: insights from genetically engineered animals. Kidney Int. 2005 Sep;68(3):925-37.

291. Eddy AA. Interstitial nephritis induced by protein-overload proteinuria. The American Journal of Pathology. [Comparative Study Research Support, Non-U.S. Gov't]. 1989 Oct;135(4):719-33.

292. Quaggin SE, Kapus A. Scar wars: mapping the fate of epithelial-mesenchymal-myofibroblast transition. Kidney Int. 2011 Jul;80(1):41-50.

293. Chen YT, Chang FC, Wu CF, Chou YH, Hsu HL, Chiang WC, et al. Platelet-derived growth factor receptor signaling activates pericyte-myofibroblast transition in obstructive and post-ischemic kidney fibrosis. Kidney Int. 2011 Jun 29.

APPENDIX

MANUSCRIPTS ARISING FROM THIS THESIS

Original manuscripts

Smith, S.W., A.P. Croft, H.L. Morris, A. Naylor, C.M. Isacke, C.O. Savage, and C.D. Buckley. Mice deficient in CD248 are protected against renal fibrosis and microvascular rarefaction following unilateral ureteric obstruction. **(Submitted)**

Smith, S.W., K.S. Eardley, A.P. Croft, J. Nwosu, A.J. Howie, P. Cockwell, C.M. Isacke, C.D. Buckley, and C.O. Savage. 2011. CD248+ stromal cells are associated with progressive chronic kidney disease. *Kidney Int* 80:199-207.

Review articles

Smith, S.W., S. Chand, and C.O. Savage. The biology of the renal pericyte. *Nephrology Dialysis Transplantation* 2012 (**In press)**

Smith, S.W., and J.S. Duffield. The renal pericyte: A novel therapeutic target in tubulointerstitial fibrosis. *Histology and histopathology.* 2012 **(In press)**

Book chapters

Smith, SW. 2012. Progressive renal fibrosis in chronic kidney disease. In: Renal Failure: Prevention, Causes and Treatment. C. Hutchison, editor. Nova, **(In press)**

Abstracts and presentations at scientific meetings

Smith, S.W., A.P. Croft, H. Morris, A. Naylor, D. Huso, C.M. Isacke, C.O. Savage, and C.D. Buckley. 2011a. $CD248^{-/-}$ mice are protected against renal fibrosis following unilateral ureteric obstruction. In BRS/RA Conference 2011. Birmingham. **(Oral presentation)**

Smith, S.W., J. Nwosu, P. Cockwell, C.M. Isacke, C.D. Buckley, and C.O. Savage. 2010. Renal fibroblasts that are linked to albumninuria and tubulointerstitial damage in IgA nephropathy are defined by CD248. In BRS / RA Conference 2010 Manchester.

Smith, S.W., K.S. Eardley, A.P. Croft, J. Nwosu, A.J. Howie, P. Cockwell, C.M. Isacke, C.D. Buckley, and C.O. Savage. 2010. CD248 Positive Stromal Cells Are Linked to Determinants of Progressive Chronic Kidney Disease in IgA Nephropathy In ASN renal week 2010. Denver, Colorado, USA.